Clarkson University

A Nonequilibrium Model for Reactive Distillation

A Dissertation

by

Arnoud Peter Higler

Department of Chemical Engineering

Submitted in partial fulfillment of the requirements

for the degree of

Doctor of Philosophy

(Chemical Engineering)

September 3, 1999

Accepted by the Graduate School

Date	Dean

The undersigned have examined the thesis/dissertation entitled "A Nonequilibrium Model for Reactive Distillation" presented by Arnoud P. Higler, a candidate for the degree of Doctor of Philosophy in Chemical Engineering, and hereby certify that it is worthy of acceptance.

Date

Prof. R. Taylor, Advisor

Prof. G. A. Campbell

Prof. L. Eno

Prof. R. S. Subramanian

Prof. T. J. Ward

Abstract

A nonequilibrium cell model for reactive distillation is developed. In the new model, trays or packed sections are divided into stages that are subsequently split up into nonequilibrium cells. This approach allows for easy modeling of flow patterns on distillation trays and maldistribution in packed columns, by adoption of appropriate cell linking patterns.

In the nonequilibrium cell, thermodynamic equilibrium is assumed only at the vapor-liquid interface. The bulk phases of both vapor and liquid are assumed to be perfectly mixed, and the resistance to mass transfer is located in two films next to the phase boundary. Mass transfer rates are calculated from the Maxwell-Stefan equations.

The Dusty Fluid Model is used for description of mass transfer and reaction in systems with heterogeneous catalysts.

Using the nonequilibrium model for several example problems, it is shown that effi-

ciencies in the reactive distillation process can be influenced by the reaction. Thus, the prediction of efficiencies becomes problematic, and the use of efficiencies and equilibrium models should be avoided.

In addition, it is shown that the reactive distillation process is much more sensitive to the design than normal distillation processes, emphasizing the need to take column design into account in the model calculations.

Furthermore multiple steady states have been found with both NEQ and EQ models, but not all of these may be realizable due to flooding. In addition, the realizable window of multiple steady states is smaller if transfer resistances are accounted for.

For packed columns with systems with highly nonlinear interactions between the reaction rate and the temperature, it is very important to approximate the column concentration and temperature profiles as accurately as possible. Failure to do so may lead to significant deviations in column performance.

The influence of maldistribution in packed columns is often ambiguous. In some cases, choosing a different maldistribution pattern may lead to substantially different column behavior. For reactive systems, maldistribution is found to influence the process through both the loss of interfacial area and changes in residence times and residence time distribution.

Acknowledgements

You are about to read the result of three years of research on modeling of reactive distillation. In the course of these three years, many people have made contributions to this work, or to my working environment, to help shape the results as they are presented here.

The most important of these people has been my advisor, Prof. Ross Taylor. First of all for providing me with the opportunity of doing a Ph.D., and secondly for the way in which he has supervised my studies. It has really been a great pleasure. I would also like to thank Dr. H.A. Kooijman for his valuable comments and discussions on various issues treated in this thesis. And, of course, my two labmates at Clarkson, Richard and Rohit, who had to suffer through my moaning and groaning when things didn't move along as smoothly as I would like them to.

In addition, I would like to express my gratitude to my second advisor, Prof. R.

Krishna, who gave me the opportunity to work in his group at the University of Amsterdam. There, I have been able to get a taste of CFD modeling and experimental work on flow and flow maldistribution on distillation trays and in packed columns. I would also like to thank Dr. J. Ellenberger and Ir. J. van Baten with their help in the experimental and CFD work.

BP-Amoco Chemicals are gratefully acknowledged for their support for our research and Hyprotech Inc. for their partial support.

Contents

Nomenclature

a	interfacial area	m^2
a^C	Catalyst surface area	m^2
a^i	Inside cylindrical area of annular cell	m^2
a^o	Outside cylindrical area of annular cell	m^2
a_i	activity of component i	$-$
$a_{i,j}$	binary interaction parameters	$J \cdot mol^{-1}$
A_t	Total cross sectional area	m^2
B_0	Permeability of porous medium	m^2
C_m	Coefficient of variation	$-$
C_v	Coefficient of variation	$-$
c	number of components	$-$
c_i	Molar concentration of component i	$mol \cdot m^{-3}$
c_t	total concentration	$mol \cdot m^{-3}$

$\mathbb{D}_{i,l}$	Maxwell-Stefan diffusion coefficient	$m^2 \cdot s^{-1}$
$\mathbb{D}^e_{i,l}$	Maxwell-Stefan diffusion coefficient inside catalyst	$m^2 \cdot s^{-1}$
D^e_i	Knudsen diffusion coefficient of component i	$m^2 \cdot s^{-1}$
D_e	Eddy diffusion coefficient	$m^2 \cdot s^{-1}$
D_r	Radial liquid spreading coefficient	m
d_i	Generalized driving force	m^{-1}
d_p	Particle diameter	m
d_p	nominal packing size	m
E^{MV}	Murphree vapor phase efficiency	$-$
e	Energy flux	$J \cdot m^{-2} \cdot s^{-1}$
$\mathcal{E}^L$	Liquid phase energy transfer rate	$J \cdot s^{-1}$
$\mathcal{E}^S$	Liquid phase energy transfer rate to catalyst	$J \cdot s^{-1}$
$\mathcal{E}^V$	Vapor phase energy transfer rate	$J \cdot s^{-1}$
F_i	External force acting per mole on species i	$N \cdot mol^{-1}$
F^L	Liquid feed rate	$mol \cdot s^{-1}$
F^V	Vapor feed rate	$mol \cdot s^{-1}$
$\bar{F}$	Function vector	$-$
f^L_i	Liquid feed rate of component i	$mol \cdot s^{-1}$

f_i^V	Vapor feed rate of component i	$mol \cdot s^{-1}$
$\bar{G}$	Starting function vector	–
H^L	Liquid phase enthalpy	$J \cdot mol^{-1}$
H^V	Vapor phase enthalpy	$J \cdot mol^{-1}$
$\mathcal{H}_i$	Partial molar enthalpy of component i	$J \cdot mol^{-1}$
$\bar{H}$	Homotopy function vector	
$HETP$	Height equivalent of a theoretical plate	m
h	Heat transfer coefficient	$J \cdot K^{-1} \cdot m^{-2} \cdot s^{-1}$
h_r	Cell width	–
h_z	Cell height	–
J	Jacobian	–
K_i	Vapor/liquid equilibrium constant component i	–
K_1, K_2, K_3	Chemical equilibrium constants	–
$\mathcal{K}^L$	Liquid splitting factor	–
$\mathcal{K}^V$	Vapor splitting factor	–
$\mathcal{K}_x$	flow splitting factor in x direction	–
$\mathcal{K}_y$	flow splitting factor in y direction	–
k_1, k_2, k_3	reaction rate constants	$mol \cdot m^{-3} \cdot s^{-1}$

k_b	backward reaction rate constant	s^{-1}
k_f	forward reaction rate constant	s^{-1}
L	Liquid molar flowrate	$mol \cdot s^{-1}$
$\mathcal{L}$	Characteristic length for diffusion	m
l	Flow path length	m
M_i	Molar mass of species i	$kg \cdot mol^{-1}$
MI	Maldistribution index	$-$
N	Molar flux	$mol \cdot m^{-2} \cdot s^{-1}$
N	Number of mixing cells	$-$
$\mathcal{N}^L$	Liquid phase mass transfer rate	$mol \cdot s^{-1}$
$\mathcal{N}^S$	Liquid phase mass transfer rate to catalyst	$mol \cdot s^{-1}$
$\mathcal{N}^V$	Vapor phase mass transfer rate	$mol \cdot s^{-1}$
n_1	Number of discretisation points in the liquid film	$-$
n_2	Number of discretisation points in the vapor film	$-$
n_3	Number of discretisation points in the liquid film at the catalyst	$-$

n_4	Number of discretisation points in the catalyst	$-$
n^L	Number of cells in a liquid flowpath	$-$
n^V	Number of cells in a vapor flowpath	$-$
n^Z	Number of zones or cells on a stage	$-$
Pe	Peclet number	$-$
p	Pressure	Pa
Q^L	Liquid phase heat duty	$J \cdot s^{-1}$
Q^V	Vapor phase heat duty	$J \cdot s^{-1}$
q	conductive contribution to energy flux	$mol \cdot m^{-2} \cdot s^{-1}$
R_m	Reaction rate of reaction m	$mol \cdot s^{-1} \cdot m^{-3}$
$\mathcal{R}$	Gas constant	$J \cdot mol^{-1} \cdot K^{-1}$
R	Column radius	m
r	Radius	m
r	number of reactions	$-$
r_a	Area ratio of mass transfer film to catalyst surface area	$-$
r_l	Cell width	m
r_k^{ai}	inside surface area ratio of cell k	$-$

r_k^{ao}	outside surface area ratio of cell k	$-$
r_k^A	Area ratio of cell k to column cross sectional area	$-$
r_j^L	ratio of liquid side stream to stage liquid flow rate	$-$
r_j^V	ratio of vapor side stream to stage vapor flow rate	$-$
s	arclength of homotopy curve	$-$
T	Temperature	K
T^L	Liquid Temperature	K
T^V	Vapor Temperature	K
t	homotopy parameter	$-$
u	Velocity	$m \cdot s^{-1}$
u^L	Superficial liquid velocity	$m \cdot s^{-1}$
$\bar{u}$	Average velocity, averaged over whole cross-sectional area	$m \cdot s^{-1}$
$\bar{u}_i$	Average velocity, averaged over cell i and neighboring cells	$m \cdot s^{-1}$
V	Vapor molar flowrate	$mol \cdot s^{-1}$

$\bar{V}_i$	Molar volume of component i	$m^3 \cdot mol^{-1}$
$\mathcal{V}_n$	volume fraction of the slice of catalyst	$-$
X	Arbitrary variable	$-$
x_i	Liquid phase mole fraction of component i	$-$
y_i	vapor phase mole fraction of component i	$-$
z	Bed depth or bed height	m
z	Catalyst coordinate	m
z_0	Distance from inner film surface to catalyst center	m
z_c	Distance from catalyst surface to catalyst center	m
z_l	Cell height	m
z_δ	Distance outer film surface to catalyst center	m

Greek symbols

$\alpha_{i,j}$	nonrandomness parameter in NRTL equation	$-$
$\alpha_{i,l}$	Multicomponent thermal diffusion factor	$-$

β_i	correction factor for variable i along homotopy curve	$-$
Γ	Thermodynamic factor	$-$
γ_i	activity coefficient of component i	$-$
δ	film thickness	m
$\delta_{i,l}$	Kronecker delta, 1 of $i = k$, 0 if $i \neq k$	$-$
ϵ	reaction volume	m^3
ϵ^C	catalyst porosity	$-$
η	Dimensionless film coordinate	$-$
η	viscosity	$Pa.s$
$\kappa_{i,l}$	Binary pair mass transfer coefficient for pair (i, l)	$m \cdot s^{-1}$
λ	Thermal conductivity	$J \cdot K^{-1} \cdot m^{-1} \cdot s^{-1}$
μ_i	chemical potential of component i	$J \cdot mol^{-1}$
$\nu_{i,m}$	Stoichiometric factor of component i in reaction m	$-$
ρ	density	$kg \cdot m^{-3}$
τ	Catalyst tortuosity	$-$
ϕ_i	Volume fraction of component i	$-$

ω_i	mass fraction of component i	–

superscripts

$*$	Equilibrium
C	Catalyst quantity of property
D	Diffusive contribution
e	effective
F	Feed quantity or property
I	Interface quantity or property
L	Liquid phase
M	Indicating mixing flow
MV	Murphree vapor phase
S	Property or Qantity related to *liquid film* at catalyst interface
S	Stage quantity or porperty
V	Vapor phase quantity or property
V	Viscous contribution

subscripts

$2M1B$	2 - methyl - 1 - butene	
$2M2B$	2 - methyl - 2 - butene	
$c4$	butene	
$c5$	pentene	
$c6$	hexene	
i	component index	
j	stage index	
k	Cell index	
l	alternative component index	
m	reaction index	
$MeOH$	Methanol	
n	discretisation index	
spec	specification	
t	total	
$TAME$	*tert*-amyl-methyl-ether	

Other

Δ	Difference	
$\bigtriangledown$	Gradient	m^{-1}

$\Big\vert_I$	Evaluated at interface
$\tilde{}$	Pseudo property in dusty gas mixture
$\bar{}$	averaged value
$\underline{}$	vector
$(X)_T$	Quantity X at constant temperature
$(X)_p$	Quantity X at constant pressure
[ ]	Matrix
$\|\|\ \|\|$	Maximum norm

List of Figures

List of Tables

Publications that resulted from this work

- Higler, A., Taylor, R., and Krishna, R., (1998) Modeling of a reactive separation process using a nonequilibrium stage model, *Comput. Chem. Engng* **20**, S111-S118

- Higler, A., Taylor, R., and Krishna, R., (1999) Nonequilibrium modelling of reactive distillation: Multiple steady states in MTBE synthesis, *Chem. Eng. Sci.* **54**, 1389 - 1395

- Higler, A., Taylor, R., and Krishna, R., (1999) The influence of mass transfer and mixing on the performance of a tray column for reactive distillation, *Chem. Eng. Sci.* **54**, 2873 - 2881

- Higler, A., Krishna, R., and Taylor, R., (1999) A Nonequilibrium Cell model for packed distillation columns, *Ind. Eng. Chem. Res.* in press

- Higler, A., Krishna, R., and Taylor, R., (1999) A Nonequilibrium Cell Model for Multicomponent (Reactive) Separation Processes, *accepted, AIChE Journal*

- Higler, A., Krishna, R., and Taylor, R., (1999) The Influence of Maldistribution on Reactive Distillation in Packed Columns, *in preparation.*

- Higler, A., Krishna, R., and Taylor, R., (1999) Nonequilibrium Modelling of Reactive Distillation: A Dusty Fluid Model for Heterogeneously Catalysed Processes, *submitted*

- Baur, R., Higler, A.P., Taylor, R., and Krishna, R. (1999) Comparison of Equilibrium Stage and Nonequilibrium Stage Models for Reactive Distillation *accepted, Chem. Eng. J.*

- Higler, A., Krishna, R., Ellenberger, J. and Taylor, R., (1999) Counter-current operation of a structured Catalytically Packed Bed Reactor: Liquid phase mixing and mass transfer, *Chem. Eng. Sci.* **54** 5145 - 5152

Chapter 1

Introduction and Motivation

In this chapter, the reader is introduced to computer modeling of reactive distillation. The shortcomings of existing methods are discussed, and a list of requirements for an improved nonequilibrium model for reactive distillation are identified.

1.1 Introduction

An important part of process design and process development in chemical engineering is nowadays done with computers. This should not be a surprise. Design of, for instance, a distillation column involves a considerable amount of equation solving, and, generally speaking, computers are much better at handling these, sometimes, absurdly large systems of equations than the average, or even the well trained, chemical engineer. The fact that we can now leave most of the mathematics to the computer, has given us access to a set of very valuable tools for plant design, optimization, and operation. In many cases, expensive plant trials can be replaced by cheap simulations, and feasibility studies are nowadays mostly based on computer calculations.

In the field of chemical engineering, computer modeling of distillation has found wide application. One of the reasons is that distillation is, in the chemical industry, still the most commonly used separation process. But also because in distillation modeling, one routinely has to deal with large systems of nonlinear algebraic equations involving mathematically complicated thermodynamic models. Once the equations have been programmed one can very easily change the operating conditions, thermodynamic model, feed conditions, and so on and see the result of the changes in the blink of an eye.

However, the quality and reliability of the calculated results hinge strongly on the quality of the model. Good and sound physical models are, therefore, essential. In addition, a model is only useful if the numerical method used to solve the model equations is able to do so without too many difficulties.

1.1.1 Distillation Modeling

Almost all distillation models are based on the concept of 'stages'. The simpler models are based on the assumption that in every stage, the chemical potential and the temperature of both vapor and liquid phases are equal. This is commonly referred to as an equilibrium stage model. Of course, in real columns, where we are dealing with either trays or packing, this equilibrium stage does not really exist. Due to the presence of mass transfer resistances we can hardly expect the vapor and liquid phases to be at equilibrium. This point was recognized a long time ago, and led to the introduction of the efficiency factor. The efficiency may be defined as the extent to which equilibrium has been reached on a tray, and, seemingly, provides a link between the equilibrium stage and a real tray. For simple binary systems, this concept works quite well, and efficiencies may easily be predicted. However, using efficiencies in simulations will lead to subcooled vapor and superheated liquid

phases. Furthermore, in multicomponent systems, efficiencies will be different for all components and may vary strongly over the height of the column. This makes estimation of efficiencies problematic.

For the packed columns we use the HETP (Height Equivalent of a Theoretical Plate). The HETP is the height of a section of packing needed to establish the separation obtained in a single equilibrium stage. As is the case with efficiencies, the HETP has a physical meaning only in binary systems. For multicomponent systems they are as confusing as efficiencies. It, therefore, strikes the author as strange that, in distillation modeling many engineers tend to go through great trouble to get the thermodynamics of a system right, however, they are quite willing to pick an efficiency factor without further thought.

The problems attached to the equilibrium-stage-efficiency approach are circumvented by the nonequilibrium stage models. In these models, each stage describes a 'real' tray or a real section of packing. A nonequilibrium model splits the stage material and energy balances into balances for each phase, and the mass and energy transfer process is modeled directly by means of rate equations. The first such model was presented by Krishnamurthy and Taylor (1985a) and used for simulation of both stagewise (conventional distillation in tray columns, extractive distillation, tray absorber) and continuous (packed distillation and absorption columns) processes (Krishnamurthy

and Taylor, 1985b-d, 1986; Taylor *et al.*, 1987). In this nonequilibrium model, the pressure was specified on all stages. However, the column pressure drop is a function of tray (or packing) type and design and the hydrodynamic conditions. In a second generation model, developed by Taylor *et al.* (1994), only the pressures of the condenser and top tray are specified. The pressures on the stages are subsequently calculated by means of a stage pressure drop and the pressure of the stage above.

Taylor *et al.* (1992) present the results of simulations of industrial scale columns and conclude that nonequilibrium models have significant advantages over equilibrium models. First of all, there is no need to guess a number of equilibrium stages, or the location of side and feedstreams when simulating an existing column. Secondly, the use of stage efficiencies and HETP is entirely avoided. This was found to be especially useful for (1) Packed columns, (2) Strongly nonideal systems, (3) Systems involving trace components, (4) Columns with profiles that contain maxima or change rapidly over a small section of the column, (5) Columns with multiple feed and or sidestreams, (6) Any column with unknown efficiencies. In addition, nonequilibrium models can be used in analysis of operating and design problems, since they require the equipment design parameters to be available. As a consequence nonequilibrium models may also be used to identify equipment design parameters that may be altered to improve column performance.

The nonequilibrium model requires information about the column configuration for calculation of parameters such as mass and heat transfer coefficients and interfacial areas. These parameters are usually obtained from semi-empirical correlations. The computed solution of the model equations, therefore, depends to a certain extent on the quality of the correlations. Much of the opposition to nonequilibrium models was, and still is based on this issue. Nevertheless, nonequilibrium models have been gaining more and more ground at the expense of the conventional equilibrium stage models. And although it may be true that the quality of our current day mass transfer models leaves something to be desired, the author believes that there is much more potential for development of better mass transfer models than there is for better efficiency prediction models. Efficiencies will, in multicomponent systems, be confusing no matter what method is used for their prediction.

Therefore, a sound model for distillation should be based on a nonequilibrium approach. For modeling of reactive distillation this will be even more important since the introduction of a reaction also introduces an additional number of interactions between mass transfer rates, composition and temperatures. In many cases it is not in advance clear which ones are important, and which ones are not. And in some cases, the importance of the interactions will vary from stage to stage. Furthermore, it will become clear that knowledge of normal distillation operations may not always

be applied to reactive distillation. For example, a higher reflux ratio does not always give a better performance, and adding more catalyst can in some cases have a detrimental effect on the process. The exact influence of operational and model parameters, and a valid explanation of why a column behaves the way it does, may only be determined with physically realistic models.

The need for these models is not merely academic: There is a large number of processes that has been proposed for reactive distillation (Doherty and Buzad, 1992), but only very few have found industrial application. There are various reasons for the lack of application, the most important of which is that most companies are reluctant to try something that has never been done before and will rather use proven technology. In addition, since in reactive distillation all is done in one vessel, the possibilities for control are fairly limited. If a design is, therefore, not optimized before it is built, it will be very hard to improve its performance afterwards, simply because there are not that many things to manipulate. Therefore, if a new reactive distillation process wants to have any chance, the promise of a much lower capital investment, combined with a guaranteed performance is practically mandatory. Good and sound models will be a vital factor here. The same can be said for optimization of existing processes. Expensive plant trials may be avoided by computer modeling, but only if a model is realistic.

Before formulating the requirements for a nonequilibrium model for reactive distillation we will briefly introduce the concept of distillation with reaction, and discuss the models that have been presented in literature so far.

1.2 Distillation with Reaction

The fact that combination of reaction and distillation into one piece of process equipment can have considerable advantages over more conventional setups has long been recognized. The first patents date back to the mid twenties (Backhaus, 1921, 1922, 1923a, 1923b) on homogeneously catalyzed esterification reactions. A first article on the subject was presented as early as 1932 by Keyes. Publications from this period mainly deal with homogeneous self catalyzed reactions, such as esterifications, trans-esterifications and hydrolysis reactions. Heterogeneous catalysis in reactive distillation was developed more recently and was first described by Spes (1966). A literature survey on articles from this period is given by Doherty and Buzad (1992).

However it is only since the mid eighties that scientific interest in the subject really has boomed with the industrial application of reactive distillation in two processes: The production of methyl acetate (Agreda *et al.*, 1990; Siirola, 1995) and the production of Methyl-*tert*-butyl-ether (MTBE) (DeGarmo *et al.*, 1992). The methyl acetate

process has now turned it into a schoolbook example of the potential of reactive distillation. The conventional process exists of one reactor, eight distillation columns, one extractor, and requires two additional extractive agents, to obtain high purity methyl acetate. This level of complexity is required because of the presence of various azeotropes in the reactor product. The new reactive distillation process, however, requires only one reactive distillation column, two small side-strippers and one column for the recovery of methanol. The overall reduction in capital investment is, therefore, substantial.

The success of the MTBE process was boosted by the phase-out of lead based anti-knock agents in gasolines. These octane enhancers are nowadays mainly replaced by MTBE or similar oxygenates like ethyl-*tert*-butyl-ether (ETBE) and *tert*-amyl-methyl-ether (TAME). For some time, MTBE has been the fastest growing chemical (Ainsworth, 1991), and over the last decade a considerable number of plants for production of these oxygenates were built, many based on reactive distillation technology.

Both the MTBE and the Methyl Acetate processes are illustrative of the power of process integration and intensification, and the synergetic effects that may arise when using simultaneous reaction and product separation. These principles may be illustrated when we look at an example process for the production of chemical C out of

A and B according to the following reaction scheme:

$$A + B \rightleftharpoons C + D \tag{1.1}$$

In addition we assume that there are some undesired side reactions, such as for example:

$$A + C \rightarrow E \tag{1.2}$$

and

$$2C \rightarrow F \tag{1.3}$$

This reaction can be carried out in a conventional process setup as sketched on the left side in Fig. 1.1. The objective is to produce C out of reactants A and B, thereby making byproduct D. In addition, there are undesired side and consecutive reactions, so that the exit stream of the reactor will be a mixture of all components. Of these, A and B have to be separated and recycled, C has to be separated and purified to specification, and D, E and F have to be disposed of. Normally, this will require more than the single distillation column that is given in Fig. 1.1.

Shown on the right hand side of Fig. 1.1 is a typical setup for a reactive distillation column. The reactions will take place in the reactive section. In case of a heterogeneous reaction, this section can consist of reactive packing elements, but also of trays that are covered with a teabag type packing. For homogeneous reactions, the location

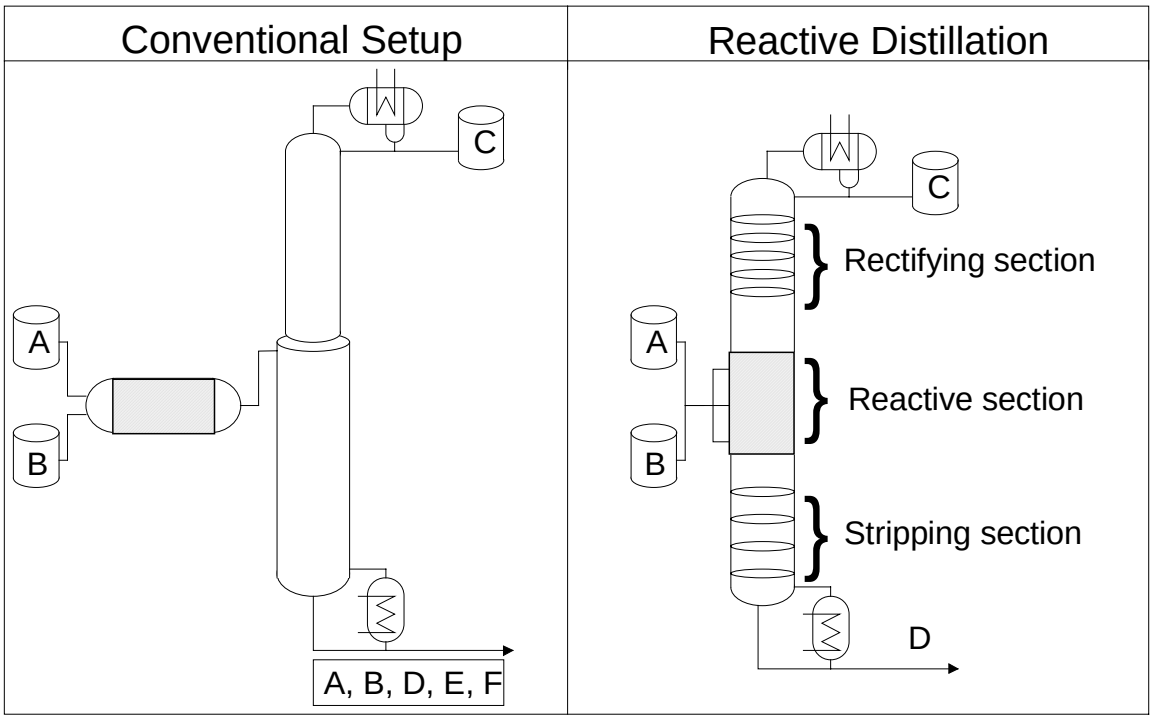

Figure 1.1: Schematic representation of a conventional and reactive distillation process

of the reactive section is usually defined by the feed location of a homogeneous liquid catalyst. The nonreactive rectifying and stripping section take care of additional product purification and waste product separation. In this kind of setup there is in-situ product removal of desired product C, which will pull the equilibrium of the main reaction towards the right hand side, thereby increasing the overall conversion. This way one can overcome a 'bad' equilibrium constant. In addition, lowering the

concentration of C due to the in-situ separation will also reduce the rates of the side reactions. Therefore, there will be less conversion of C to undesired side products, and this illustrates how reactive distillation may also be applied to systems where selectivity is important.

The nonreactive zones in the column play an important role in product separation and reactant recycle. In the ideal case, the nonreactive zones separate the products from the reactants in such a way that the reactants are automatically flushed back into the reactive zone, while pure products may be obtained as product streams. The objective of a reactive distillation column is to minimize the residence time of the products in the reactive zone while maximizing the residence times of the reactants.

The overall advantages of reactive distillation over more conventional process configurations may be summed up as follows:

- Lower capital investment. By carrying out reaction and separation in one piece of process equipment it is possible to eliminate one or more process steps in order to achieve the desired conversion and/or selectivity (Humphrey and Seibert, 1992; DeGarmo, 1992).

- Higher conversion. By in-situ removal of the products, the equilibrium of a reaction may be shifted toward the product side, overcoming a 'bad' equilibrium

constant. Examples for this type of application are MTBE production (Sundmacher and Hoffman, 1994) and methyl-acetate production (Agreda em et al., 1990; Siirola, 1995).

- Better selectivity due to removal of intermediate products from the reactive zone, thereby preventing them to react further to undesired byproducts. Systems for which this is important are, for example, the production of propylene oxide from chloro-hydrins (Carra *et al.*, 1979a, 1979b) and production of cumene from benzene and propene (Shoemaker and Jones, 1987).

- Prevention of hot spot formation. In highly exothermic reactions, the heat of reaction is removed by evaporation of the reactive mixture. This is beneficial in, for example, the hydrolysis of ethylene oxide to ethylene glycol (Ciric and Gu, 1994).

In addition, there may be other advantages, such as breaking of azeotropes, but these depend on the system used.

The combination of reaction and separation also places constraints on the systems for which reactive distillation can be used. Conditions for possible applications are listed by Westerterp (1992).

- Typical temperature ranges for distillation and reaction have to coincide.
- Reactions have to be fast, so that chemical conversion can be obtained within the average residence time for a distillation column.
- The reaction cannot be too fast in order to insure an evenly distributed use of the catalyst for chemical conversion.
- Reactive distillation is unsuitable for reactions with extreme heat effects. Because of excessive evaporation of liquid phase components inside the column, controlability of the apparatus then becomes doubtful.
- The desired product has to be the highest or lowest boiling component in the system.
- A very stable catalyst is required for heterogeneous systems. Catalyst deactivation may have a marked effect on column performance and is not easily overcome.

Some of the above limitations may be circumvented by using reactive extraction instead of reactive distillation.

1.2.1 Modeling of Reactive Distillation

The increased industrial interest in Reactive Distillation has led to an increasing number of publications on this subject in the last decade, many of which have dealt with the modeling of reactive distillation. Models for reactive distillation may be split into two categories: The equilibrium stage models and the nonequilibrium stage models. A further subdivision may be made on the way the reaction is implemented, which may be either equilibrium based or rate based. In the equilibrium based approach one assumes that the liquid phase is in chemical equilibrium. In the rate based approach, the reaction is implemented by means of a kinetic expression. The most recent literature review on reactive distillation modeling is presented by Sundmacher (1995).

Few papers have been written on models based on the assumption of simultaneous physical and chemical equilibrium. One of the first papers on this subject was presented by Davies *et al.* (1979). In their model each stage is described as a conventional equilibrium stage. The outgoing liquid stream is then at thermodynamic equilibrium with the vapor stream, but in itself not necessarily at chemical equilibrium. This stream is subsequently supplied to a theoretical reactor, where chemical equilibrium is established. The outgoing stream of the reactor is then supplied to

the next vapor/liquid equilibrium stage. This method allows for using a conventional equilibrium stage model for distillation, however any effects of the chemical reaction on vapor/liquid equilibrium cannot be taken into account.

A more elegant method is presented by Barbosa and Doherty (1988a, 1988b), which is based on a set of transformed composition variables. These can be derived when one considers that the requirement of chemical equilibrium results in the loss of a degree of freedom for the liquid phase. These models are of particular value in the conceptual design of reactive distillation operations.

Much more popular have been the models incorporating phase equilibrium, while taking into account finite reaction rates. (e.g. Nelson, 1971; Suzuki *et al.*, 1971; Carra *et al.*, 1979; Alejski *et al.*, 1988; Chang and Seader, 1988; Alejski, 1991; Simandl and Svrcek, 1991; Ciric and Gu, 1994; Abufares and Douglas, (1995); Perez-Cisneros *et al.*, 1997). The models presented in all of these papers are more or less the same. They incorporate a set of liquid and vapor mass balances along with equilibrium correlations for the Vapor/Liquid equilibrium calculation. The reaction is normally tackled by implementing a kinetics expression into the liquid phase overall mass balance and the liquid phase composition balances. The above models vary mainly in the way the equations are solved, or the objectives of the model.

The models presented by Nelson (1971) and Suzuki *et al.*, (1971) are extensions of numerical methods originally developed for normal distillation. Nelson uses a Newton-Raphson method for solving the model equations. Suzuki uses Mullers' method. Carra *et al.*, (1979) also use a Newton method for solving the model equations. They use their model for steady state simulation of an experimental column for the production of propylene oxide from chloro-hydrins.

Alejski *et al.*, (1988) present a model along with an inside out type algorithm, combined with Powell's method (Powell, 1965) for finding the minimum of the norm of the residual function vector. The method is claimed to be highly convergent but slow. In a second paper, Alejski (1991) presents a model for taking into account liquid phase plug flow on a distillation tray. This was done by modeling the liquid phase on a tray as a cascade of mixing cells. Local mass transfer effects are taken into account by estimated point efficiencies. The model was solved with a Newton-Raphson algorithm.

Chang and Seader (1988) present a model along with a homotopy method for solving the model equations. Homotopy methods are generally speaking more robust and have a much wider range of convergence than Newton's method, as was illustrated by means of some examples. Calculation times for the homotopy method are, however, much higher than for Newton's method.

Simandl and Svrcek (1991) present a model along with two different solution methods. The first method is a simultaneous solution method after linearization of the equations. The second one is an inside-outside algorithm. The latter was found to converge much faster than the simultaneous solution method, and the robustness was found to be similar.

Ciric and Gu (1994) present a somewhat different approach. They directly implemented the equations for capitalized and variable cost into the model equations. The resulting mixed integer nonlinear programming (MINLP) model determines the optimal configuration and operating conditions, while minimizing the annual.

Abufares and Douglas (1995) present a steady state and a dynamic model describing a reactive distillation column for the production of MTBE. They used the AspenPlus Radfrac routine for the steady state model and SpeedUp was used for the dynamic model calculations. The AspenPlus routine Radfrac is a standard equilibrium stage column model that may be extended to take into account chemical reactions (Venkataraman *et al*, 1990). Radfrac is used by, among others, Jacobs and Krishna (1993), Nijhuis *et al.*, (1993) and Hauan *et al.*, (1995)

Sneesby *et al.* (1997a) used both Pro/II and AspenPlus for steady state modeling of a column for the production of ETBE. In their second paper (Sneesby *et al.*,

1997b) they present a dynamic model, which they solve with the SpeedUp dynamic simulator.

A somewhat different approach to the equilibrium model is presented by Perez-Cisneros *et al.*, (1997). Their model uses so called chemical 'elements' rather than the actual components. The chemical elements are the molecule parts that remain invariant during the reaction, and the actual molecules may be formed by different combinations of elements. The benefit of this approach is that the chemical and physical equilibrium problem in the reactive mixture are the same as a strictly physical equilibrium model. The method is however unsuitable for extension to nonequilibrium models because the real components are required for the transfer rate calculations rather than the chemical elements.

1.2.2 Nonequilibrium Models

Nonequilibrium models belong to more recent times. The first work in this field was presented by Sawistowski *et al.*, (1979) who modeled a packed reactive distillation column for esterification of methanol and acetic acid to methyl acetate. They used an effective diffusivity method for their mass transfer model. Fourier's law was used for heat transfer modeling. The resulting system of differential equations was solved

using a Runge-Kutta method.

In 1990 ASPEN presented the RATEFRAC model for rate based stagewise multicomponent separation modeling. This model can also be used for nonequilibrium reactive distillation modeling, by implementing the appropriate kinetics.

Zheng and Xu, (1992a, 1992b) present a rate based model for stationary simulation of MTBE production in a packed column. Gas-liquid mass transfer is described using the Maxwell-Stefan theory, based on a two-film model. The reaction is treated pseudo-homogeneously where the effects of reaction on mass transfer in the catalyst are lumped into a bulk reaction term. Liquid phase nonidealities are described with the UNIFAC model and vapor phase fugacities are calculated with the virial equation. The resulting model of algebraic equations was solved using a Newton-Raphson method. In a later paper Xu *et al.*, (1999), the model was extended to take into account axial dispersion in a packed column.

Sundmacher and Hoffman (1994) have conducted a very extensive study on the production of MTBE by reactive distillation. The work done included building and testing an experimental column, manufacturing of catalysts, process analysis by means of dimensionless numbers, numerical modeling and experimental validation of their model. Here we will focus mainly on the modeling part of their research. Sundmacher

and Hoffman present a nonequilibrium model using the Maxwell-Stefan theory as a basis for their two-film mass transfer model. The liquid phase heterogeneous reaction kinetics are modeled by an activity based Langmuir-Hinshelwood expression, which is derived from an extensive experimental study (Rehfinger and Hoffmann, 1990a, 1990b). In the mass transfer model for a nonequilibrium stage, mass transfer to and from the catalyst is not taken into account explicitly. The reaction equation is lumped into a component consumption term, corrected with a catalyst efficiency. The reaction term is evaluated at liquid bulk conditions. Nonidealities in the liquid phase were described with the UNIQUAC equations, The SRK equation of state was used for nonideal gas phase behavior. For numerical solution of the system of algebraic equations, the mass balances were extended by introducing so called 'artificial inertia terms'. These accumulation terms were entered to allow for convenient application of a relaxation technique which is based on the method of false transients. The resulting set of differential and algebraic equations was then solved with the DAE solver LIMEX (Deufelhard *et al.*, 1987). The model was used for steady state simulation of an experimental etherification column.

A similar model was presented by Landschützer and Bart (1996). They studied the esterification reaction of acetic acid and propanol to propyl acetate, catalyzed by an exchange resin in a packed column. Mass transfer across the vapor - liquid

interface and between liquid bulk and catalyst surface is described with the Maxwell-Stefan theory. The reaction is assumed to take place only at the catalyst surface and is modeled with an Eley-Rideal kinetic expression. Landschützer and Bart (1996) present a model for an axially dispersed column, which is tackled by implementing an axial dispersion term in the mass balance for a differential control volume. The axial dispersion coefficient is determined by a Bodenstein relation, which was determined experimentally for their model column.

Podrebarac *et al.* (1998) present a nonequilibrium model for their experimental column for the hetrogeneously catalyzed aldol condensation of acetone to diacetone alcohol. The reactive packed section is described by means of a set of differential equations for the individual components. Overall mass transfer coefficients are used in the description of interphase mass transfer. The reaction takes place only at the catalyst surface. The reaction zone is assumed to be isothermal, and the enthalpy balance is discarded from the model equations. The resulting set of equations is solved with the gPROMS package. It should be noted that most of the assumptions made here are not recommended for nonequilibrium modeling of reactive distillation operations (see Kooijman, 1995). This model has an interesting feature in the fact that the authors make a clear distinction between liquid flowing inside a catalyst bale, and liquid flowing outside of the bale. Reaction takes place only inside the bale, and

only the liquid outside of the bale is assumed to be in contact with the vapor. This offers a way to study the influence of wall flow on the reactive distillation process.

A nonequilibrium model for the same aldol condensation process is presented by Huang *et al.* (1998). However, in this case a stagewise approach is used for description of the distillation column. Their model is uses weight fractions rather than mole fractions that are normally used in distillation modeling. The model also employs overall mass transfer coefficients in the evaluation of mass transfer.

Kreul *et al.* (1999), present a nonequilibrium model for homogeneous reactive distillation in packed columns. They use their model for simulation of four test systems, in which they studied differences caused by basic model assumptions, such as equilibrium and kinetic concepts. They conclude that the additional effort of the more complicated nonequilibrium approach is justified, because prediction of HETPs for reactive systems is not always straightforward.

Comparative studies of the above model types are presented by Lee and Dudukovic (1998) and Baur *et al.* (1999). Lee and Dudukovic (1998) state that a close agreement in the prediction of equilibrium and nonequilibrium models arises only when the tray efficiency can be correctly predicted for the equilibrium model. Baur *et al.* (1999) reported large discrepancies between the equilibrium and nonequilibrium models for

an MTBE process. Both papers state that nonequilibrium models should be preferred for the simulation of reactive distillation columns.

1.3 Objective

It has already been stated that the use of efficiencies in distillation modeling is problematic. In reactive distillation this will be no different. Although there are various definitions of the stage efficiencies, the most commonly used is the Murphree (1925) stage efficiency:

$$E_i^{MV} = \frac{y_{i,j} - y_{i,j+1}}{y_{i,j}^* - y_{i,j+1}} \tag{1.4}$$

Here $y_{i,j}$ is the vapor phase mole fraction of component i on stage j. $j+1$ refers to the tray below the tray under consideration. $y_{i,j}^*$ is the mole fraction of component i in a vapor phase that would be in equilibrium with the liquid bulk on the tray. The latter can be determined from a bubble point calculation. In reactive distillation however, the liquid phase composition is subject to changes due, not only to mass transfer, but also due to the reaction. This means that $y_{i,j}^*$, and therefore the efficiency itself, will be dependent on the reaction. This makes the prediction of efficiencies difficult.

To eliminate the problems related to efficiencies we will have to construct a new nonequilibrium model for reactive distillation. In many ways this will be the same as

for normal distillation, but the presence of a reaction leads to additional requirements. First of all, for homogeneous systems, the liquid phase reaction could significantly influence interphase mass transfers. None of the available models for reactive distillation takes into account the coupling between chemical reaction and mass transfer.

Another important limitation in the existing models is that in all models liquid and vapor phases are considered to be well mixed on every stage. The assumption of a well mixed liquid phase is a reasonable one for laboratory scale equipment and commercial tray columns in which short flow paths with multiple downcomers are used. However, for large diameter tray columns with longer flow path lengths there would be a considerable degree of staging of the liquid phase (Bennett and Grimm, 1991; Lockett, 1996), and this can be expected to have an important effect on conversion and selectivity. The vapor phase is normally assumed to rise in plug flow through the layer of froth.

In modeling of packed columns the assumption of perfect mixing in both vapor and liquid phases is often made, but may be considered questionable. In addition, the existing nonequilibrium models implicitly assume a flat flow profile of the liquid trickling down the packing and the vapor rising in the packing. This may be an adequate assumption for short and small diameter lab scale columns, however for industrial columns this is less likely. Flow profiles usually are not flat due to the influence of the

wall. And in some cases, maldistribution of the vapor and the liquid phase will arise due to maldistributed feed streams or structural deficiencies in the packing. Even for normal distillation, there is no good model to describe this kind of behavior, although there is a general understanding that maldistribution is detrimental to column performance.

Another issue that is relevant to heterogeneous systems is that of reaction and mass transfer in porous catalysts. The current models all use a pseudo-homogeneous approach, in which catalyst mass transfer effects are lumped into an efficiency factor. Particularly in systems where one is dealing with more than one reaction, or for non-equistoichiometric reactions, these interactions between multicomponent mass transfer and reaction inside the catalyst may be expected to be important.

In addition a realistic nonequilibrium model requires information about the column internals used. The inevitable link between the design and the model equations is discussed extensively by Taylor *et al.* (1994) and they point out that seemingly, a nonequilibrium model can only be used in case a design is already known. To alleviate this problem they proposed the integration of a design procedure together with the model equations. During the calculations, a design is evaluated based on calculated liquid and vapor flows and physical properties. After the calculations have converged, a design is obtained that is consistent with the numerical solution of the model. A

similar design mode strategy will have to be implemented in the new nonequilibrium model.

Finally, there is a need for a robust numerical technique with a wide radius of convergence. The reaction complicates the generation of a starting point for the calculations, due to formation and disappearance of components. In addition, the reaction adds several nonlinear interactions in the equation system, as compared to a system without reaction.

From the above considerations we can summarize the following model requirements. The model should incorporate

- Interaction between vapor/liquid mass transfer and reaction in homogeneous systems.
- Influence of flow models on the reactive distillation process for tray columns.
- Influence of maldistribution and radial spreading for (reactive) packed columns.
- Interaction between mass transfer and reaction in a porous catalyst.
- A design mode.
- A robust numerical solution method.

The model should be structured in such a way that it allows for an easy switch between models of various levels of complexity. The model is to be used in a study on the effects on multicomponent mass transfer in reactive distillation, in which a comparison will be made between, for example, equilibrium and nonequilibrium models, pseudo-homogeneous and heterogeneous models, etc.

Chapter 2

The Nonequilibrium Cell Model

Presented in this chapter is the mathematical description of the nonequilibrium cell model. Subsequently it is shown how the cell model may be used for modeling of flow patterns on distillation trays and maldistribution in packed columns. A degrees of freedom analysis is given, and additional model requirements are discussed. Finally, an outline is given of the methods used for solving the model equations.

2.1 Introduction

As stated before, most distillation models are based on the concept of stages, and this model will, in that respect, not be different. This is illustrated in Figure 2.1. Given on the right hand side is an example column, with trays in the top section and packing in the bottom section. In the top section, a nonequilibrium stage represents a real tray, in the bottom section a nonequilibrium stage corresponds to a thin slice of packing. L and V represent the column internal liquid and vapor flows.

The first nonequilibrium model for normal distillation, presented by Krishnamurthy and Taylor (1985), consists of a set of mass and energy balances for the vapor and liquid phases on a tray, along with rate equations for the evaluation of mass and heat transfer rates. The assumption of phase equilibrium is made only at the vapor-liquid interface. The method proposed by Krishnamurthy and Taylor requires the evaluation of the mass transfer processes for both phases separately. These mass transfer processes are linked together by the fact that the mass transfer rates at the vapor liquid interface should be the same for both phases. This suggests that one could also write one mass transfer relation, using an overall mass transfer coefficient and the average concentration gradient between bulk liquid and bulk vapor phase. This approach is not recommended by Kooijman and Taylor (1995), who found cases

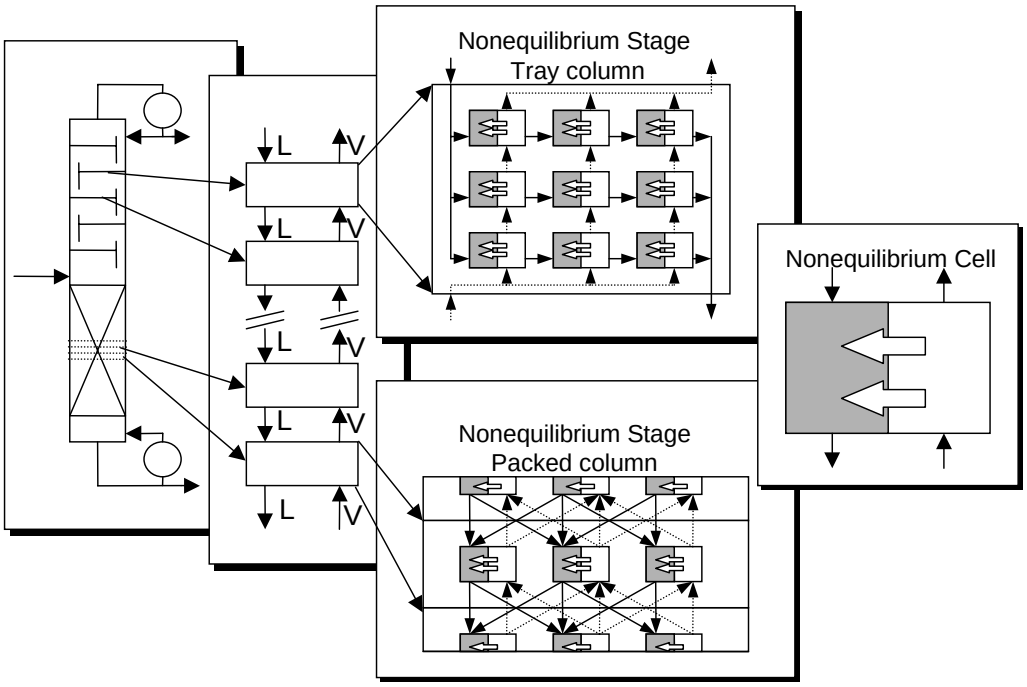

Figure 2.1: Schematic representation of the nonequilibrium cell model

in which the use of overall mass transfer coefficients will result in components moving in the 'wrong' direction. This is because the use of overall mass transfer coefficients is only justified if the partial molar enthalpies are all equal (equimolar overflow), *and* if there is no sensible heat transfer between the two phases.

2.1.1 Flow on Distillation Trays

An issue that is not addressed by the simplest nonequilibrium models is that of vapor and liquid flow patterns on distillation trays. Normally these models assume the vapor and liquid bulk phases to be ideally mixed. However in reality, vapor will rise in plug flow through a layer of froth. The froth will flow more or less in plug flow, with some axial dispersion due to the vapor jets and bubbles (Lockett, 1986; Bennett and Grimm, 1991).

An attempt was made by Krishnamurthy and Taylor (1985) to take into account flow patterns on distillation trays by imposing particular concentration profiles over the flow path lengths in both phases. Based on the particular assumed concentration profiles an average concentration for both phases can be calculated. The average mass transfer flux can then be evaluated using the binary mass transfer coefficients and the average (arithmetic or logarithmic) composition difference. The overall mass transfer rate is calculated by multiplying the average mass transfer flux by the interfacial area on the stage. Kooijman and Taylor (1995) point out that although the assumption of concentration profiles along the flow paths might lead to seemingly good results, the method itself is fundamentally wrong. They went on to develop a method in which the mass transfer calculations for both phases are done independently. Assuming

various flow models for vapor and liquid flows (plug flow, ideally mixed flow, axially dispersed flow), they derive expressions for the mass transfer rates in the various flow types. This method is more sound than the approach taken by Krishnamurthy and Taylor, but it still requires one to make some assumptions that limit the flexibility of the model and, for the liquid plug flow model, one is required to specify a correction factor for the vapor interface concentration.

For systems with chemical reactions, residence time distribution will be important, as well as a proper description of mass transfer. The reaction rates and chemical equilibrium constants are dependent on the local concentrations and temperature and may, therefore, vary along the flow path of liquid on a tray. In addition, if the reaction is fast enough, there will be an interaction between mass transfer and reaction. This cannot be described correctly when using the method proposed by Kooijman and Taylor (1995).

In this work we will present a different approach to tackling the mass transfer (with and without reaction) and flow problem for distillation trays. This is done by means of a nonequilibrium cell model. The new feature of this model is that the nonequilibrium stages are subdivided by means of a number of contacting cells. These cells describe just a small section of the tray, and by choosing an appropriate connection pattern, one can very easily study the influence of flow patterns and maldistributions on the

distillation process. Typical cell layout patterns for trays are illustrated in the top section of Fig. 2.1. The solid lines represent possible liquid flow patterns, the dotted lines represent vapor flows. Details of flow modeling are discussed in Section 2.4.

2.1.2 Maldistribution in Packed Columns

For packed columns, one has to deal with another type of flow problem. Since, normally, a slice of packing is described by means of a nonequilibrium stage, it is implicitly assumed that the liquid and vapor phases are well mixed and evenly distributed over the cross section of the packing. Whereas this may be a valid assumption in small diameter columns, for industrial size packed columns this cannot be guaranteed.

Maldistribution of internal vapor and liquid flows over the cross sectional area of the column can lead to loss of interfacial area. This is known to be one of the main reasons for inadequate performance of packed columns. Often, vapor and liquid channelling cannot be avoided, since the packing itself usually is one of the main causes for maldistribution. Liquid rivulets will form in any commercial packing, following specific paths. These rivulets will mix with other streams and split up again, thereby introducing small scale irregularities. The formation of rivulets, which mix and later split and mix again, is really the ideal way in which the liquid should flow down a

(random) packed structure. The mechanism of frequent mixing and splitting leads to improvement in mass transfer; this is based on the rivulet model for mass transfer developed by Porter in the sixties (Porter and Jones, 1963). According to Hoek *et al.* (1986) the detrimental effects of this type of maldistribution largely is compensated by radial mixing. More detrimental is the so called large scale maldistribution that may be caused by, among other things, changes in packing isotropy, most notably at the column wall, and a bad initial distribution of either phase. Stoter (1993) presented substantial experimental evidence indicating a strong dependence of the packing HETP on maldistribution. Extensive discussions on the nature of these large scale maldistributions are given by Hoek *et al.* (1986), Stikkelman (1989), Stoter *et al.* (1992), and Stoter (1993).

The knowledge from these works has, however, never been combined with a nonequilibrium model. The nonequilibrium cell model offers an easy way of studying the influence of flow maldistributions on packing performance. This will be discussed in more detail in Section 2.5.

Another issue that needs attention is the use of porous catalysts in heterogeneous reactive distillation. Diffusion and reaction inside porous catalysts often is modelled using simple effective diffusivity models of the diffusion process and an effectiveness factor (a function of the Thiele modulus) to represent the effect of reaction (see,

e.g. Froment and Bischoff, 1990). In a pair of papers Sundmacher and Hoffmann (1992, 1994b) present a nonequilibrium model for heterogeneously catalyzed reactive distillation. For incorporation of the reaction rate, they have developed a mathematical model to analyze the interaction of the internal mass and heat transport with the microkinetics of the heterogeneous reaction. The coupled balance equations for transport and reaction are reduced to a single differential equation, for which solutions, depending on a generalized Thiele modulus and an effectiveness factor are derived for three geometries. This effectiveness factor is used in a pseudo-homogenous reaction rate expression in the liquid phase mass balances. In this work we will use a more rigorous theory of diffusion (and reaction) inside porous catalysts: The Dusty Fluid Model. This is discussed in Section 2.3.2

In this chapter we will first develop the equation system for the new nonequilibrium cell model. Henceforth, we will work Fig. 2.1 from right to left: First, the nonequilibrium cell is treated, and subsequently the arrangement of cells in flow patterns to model trays or packing, is discussed. A degree of freedom analysis, and additional model requirements are discussed, and finally we will discuss the numerical techniques used for solving the equation system.

2.2 The Nonequilibrium Cell

A schematic diagram of the unit cell for a vapor-liquid-porous catalyst system is shown in Fig. 2.2. It is assumed that the bulk of both vapor and liquid phases are ideally mixed and that the mass transfer resistances are located in films near the vapor/liquid and liquid/solid interfaces. The liquid film at the vapor/liquid phase boundary will be denoted by the superscript L, the *liquid* film adjacent to the *solid* catalyst phase will be denoted by a superscript S. To model mass transfer in these films the Maxwell-Stefan Equations are used. Thermodynamic equilibrium is assumed only at the vapor-liquid interface. Mass transfer inside the porous catalyst will be described with the so called Dusty Fluid Model. For homogeneous systems, and for systems without reactions, the catalyst phase is irrelevant and may be removed from the model.

Although the model is derived for reactive vapor/liquid systems (reactive distillation) it may also be used for reactive gas/liquid systems (reactive stripping) and reactive liquid/liquid systems (reactive extraction).

Fig. 2.2 also serves to introduce part of the notation used in formulation of the model equations. L_k and V_k are the liquid and vapor molar flowrates leaving cell k. The subscript k will be reserved for referring to cell quantities or properties. $x_{i,k}$ and $y_{i,k}$

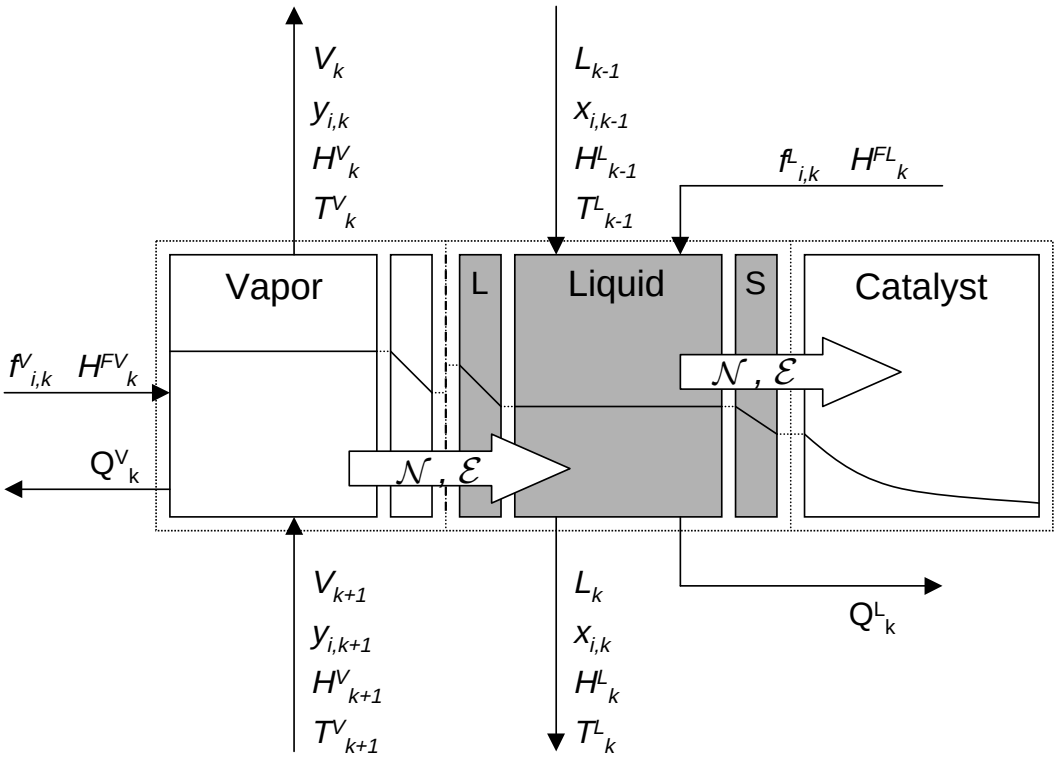

Figure 2.2: Schematic representation of the nonequilibrium cell

are the mole fractions of component i in the liquid and vapor streams leaving cell k. H_k^L and H_k^V are the liquid and vapor phase enthalpies and T_k^L and T_k^V are the liquid and vapor phase temperatures. $\mathcal{N}$ and $\mathcal{E}$ represent mass and energy transfer rates.

$f_{i,k}^V$ and $f_{i,k}^L$ are the vapor and liquid feed rates of component i to cell k. H_k^{FV} and H_k^{FL} are the feed stream enthalpies. And finally, Q_k^V and Q_k^L are external heat duties that may be specified to either vapor and liquid phase of cell k.

2.2.1 Conservation Equations

The overall mole (mass) balances for the liquid and vapor phase are given by.

$$L_k - L_{k-1} - F_k^L - \mathcal{N}_{t,k}^L - \mathcal{N}_{t,k}^S + \sum_{m=1}^{r} \left(\sum_{i=1}^{c} \nu_{i,m} \right) R_{m,k} \epsilon_k = 0 \tag{2.1}$$

$$V_k - V_{k+1} - F_k^V + \mathcal{N}_{t,k}^V = 0 \tag{2.2}$$

$\mathcal{N}_{t,k}^L$ and $\mathcal{N}_{t,k}^V$ are the overall interphase mass transfer rates in vapor and liquid phase, $\mathcal{N}_{t,k}^S$ is the overall mass transfer rate in the liquid film around the catalyst. The overall mass transfer rates are obtained by summing up over the individual component mass transfer rates.

$$\mathcal{N}_{t,k}^L = \sum_{i=1}^{c} \mathcal{N}_{i,k}^L \tag{2.3}$$

$$\mathcal{N}_{t,k}^V = \sum_{i=1}^{c} \mathcal{N}_{i,k}^V \tag{2.4}$$

$$\mathcal{N}_{t,k}^S = \sum_{i=1}^{c} \mathcal{N}_{i,k}^S \tag{2.5}$$

$\mathcal{N}_{t,k}^L$ and $\mathcal{N}_{t,k}^V$ are not the same for a system with homogeneous reactions. This is because for these systems chemical conversion will also take place in the liquid transfer film. The catalyst mass transfer rate $\mathcal{N}_{t,k}^S$ will only be relevant for a heterogeneous reaction, and will be nonzero only for a nonequistoichiometric reaction.

$R_{m,k}$ represents the reaction rate of reaction m in cell k, and is only relevant for homogeneous or pseudo-homogeneous reactions. $\nu_{i,m}$ is the stoichiometric coefficient

of component i in reaction m. ϵ_k is a specific reaction volume. For homogeneous reactions, this is the total liquid inventory in the cell. For pseudo-homogeneous reactions, it is the total catalyst volume present in the cell. For equistoichiometric reactions the reaction term in the overall liquid mass balance term is zero.

The component balances for each component in the vapor and liquid phases are given by:

$$L_k \cdot x_{i,k} - L_{k-1} \cdot x_{i,k-1} - f_{i,k}^L - \mathcal{N}_{i,k}^L - \mathcal{N}_{i,k}^S + \sum_{m=1}^{r} \nu_{i,m} R_{m,k} \epsilon_k = 0 \tag{2.6}$$

$$V_k \cdot y_{i,k} - V_{k+1} \cdot y_{i,k+1} - f_{i,k}^V + \mathcal{N}_{i,k}^V = 0 \tag{2.7}$$

$\mathcal{N}_{i,k}^L$ and $\mathcal{N}_{i,k}^V$ will only be equal if the reaction is not homogeneous. In heterogeneous systems, $\mathcal{N}_{i,k}^S$ is only nonzero if component i is not a reactant.

The energy conservation equation for each phase is given by.

$$L_k \cdot H_k^L - L_{k-1} \cdot H_{k-1}^L - F_k^L H_k^{FL} + Q_k^L - \mathcal{E}_k^L - \mathcal{E}_k^S = 0 \tag{2.8}$$

$$V_k \cdot H_k^V - V_{k+1} \cdot H_{k+1}^V - F_k^V H_k^{FV} + Q_k^V + \mathcal{E}_k^V = 0 \tag{2.9}$$

In these equations, the vapor/liquid energy transfer rates, $\mathcal{E}_k^L$ and $\mathcal{E}_k^V$ are equal. The significance of this will be discussed in a following section. The catalyst energy transfer rate $\mathcal{E}_k^S$ has only been added for completeness, but this term is zero in steady state systems. An extra reaction term is not required in the energy balances, because this is directly accounted for by the individual component enthalpies.

One should keep in mind that the indexing system used here is for a very general cell. As can be seen in Fig. 2.1 in a tray model not all cells receive flow from a cell above or below, and in a packed column, cells will have incoming streams from more than one cell. These issues will be addressed in more detail below.

2.2.2 Transport Relations

The vapor/liquid interphase mass transfer rates in the above conservation equations are evaluated using the Maxwell-Stefan theory (see Krishna and Wesselingh, 1997; Taylor and Krishna, 1993). The Maxwell-Stefan equations for mass transfer in liquid and vapor phase respectively are given by Eq. (2.10) and Eq. (2.11).

$$\frac{x_{i,k}}{\mathcal{R}T_k}\frac{\partial \mu^L_{i,k}}{\partial \eta} = \sum_{l=1}^{c} \frac{x_{i,k}\mathcal{N}^L_{l,k} - x_{l,k}\mathcal{N}^L_{i,k}}{c^L_{t,k}(\kappa^L_{i,l}a)_k} \tag{2.10}$$

$$\frac{y_{i,k}}{\mathcal{R}T_k}\frac{\partial \mu^V_{i,k}}{\partial \eta} = \sum_{l=1}^{c} \frac{y_{i,k}\mathcal{N}^V_{l,k} - y_{l,k}\mathcal{N}^V_{i,k}}{c^V_{t,k}(\kappa^V_{i,l}a)_k} \tag{2.11}$$

In these equations, $\mathcal{R}$ is the gas constant, μ_i is the chemical potential of species i, η is a dimensionless film coordinate, $c^L_{t,k}$ is the total liquid phase concentration and $c^V_{t,k}$ is the total vapor phase concentration. $\kappa^L_{i,l}a$ and $\kappa^V_{i,l}a$ are the liquid and vapor phase binary pair mass transfer coefficients respectively. These are evaluated from (semi)-empirical models (e.g. AIChE, 1958; Chan and Fair, 1984). Only $c-1$ of these

equations are independent. The mole fraction of the *c-th* component is obtained by the summation equations for both phases:

$$\sum_{i=1}^{c} x_{i,k} - 1 = 0 \tag{2.12}$$

$$\sum_{i=1}^{c} y_{i,k} - 1 = 0 \tag{2.13}$$

In addition, for a homogeneous system, the mass transfer rates in the liquid mass transfer film may change due to the chemical reaction:

$$\frac{\partial \mathcal{N}_{i,k}^{L}}{\partial \eta} = a_k \cdot \delta^{L} \sum_{l=1}^{r} \nu_{i,l} R_l \tag{2.14}$$

Here a_k is the total interfacial area in cell k and δ^L is the transfer film thickness. For most systems in reactive distillation this term will not be very important. This is because in most systems the Hatta numbers are very small. However, it will not always be clear in advance in which regime a stage will be operating, and this may even vary from stage to stage.

In their paper, Krishnamurthy and Taylor (1985), and later Kooijman (1995), rewrite the Generalized Maxwell-Stefan (GMS) equations into an expression for a mass transfer coefficient multiplied by a driving force to obtain an expression for the mass transfer rate directly. However, this is not usually possible in systems with liquid film reactions. Eq. (2.10) and Eq. (2.14) form a system of highly nonlinear coupled

differential equations that cannot be solved analytically in general and we will have to rely on numerical techniques. Since concentration gradients within the diffusion layer on either side of the vapor/liquid interface in distillation operations are not usually steep, a finite difference approximation can be used with a reasonably small number of grid points, so that calculation cost should not become too much of a problem. For fast reactions the use of more grid points is advisable.

Finite differencing the Maxwell-Stefan equations is done by dividing the mass transfer film in discrete steps by means of a number of grid points. The differential terms from Eq. (2.10) and Eq. (2.11) are approximated by:

$$\left(\frac{x_{i,k}}{\mathcal{R}T_k}\frac{\partial \mu_{i,k}}{\partial \eta}\right)_n = \sum_{l=1}^{c-1}(\Gamma_{i,l})_n \frac{(x_{i,k})_n - (x_{i,k})_{n-1}}{\Delta\eta} \tag{2.15}$$

In which

$$\Gamma_{i,l} = \delta_{i,l} + x_i \cdot \left(\frac{\partial ln(\gamma_i)}{\partial x_l}\right)_{T,P,x_l,l\neq j=1\ldots c-1} \tag{2.16}$$

Central difference approximations should not be used here, since they have a tendency to generate zigzag-profiles. Using the above discretisation scheme does not give these problems, but results in the introduction of a numerical diffusion term. However in most cases the concentration profiles will be nearly linear, and this term is not expected to have a large impact.

The energy transfer rates consist of convective and conductive contributions. For the

liquid and vapor phases we have:

$$\mathcal{E}_k^L = -h_k^L \cdot a_k \cdot \frac{\partial T^L}{\partial \eta} + \sum_{i=1}^{c} \mathcal{N}_{i,k}^L \mathcal{H}_{i,k}^L \tag{2.17}$$

$$\mathcal{E}_k^V = -h_k^V \cdot a_k \cdot \frac{\partial T^V}{\partial \eta} + \sum_{i=1}^{c} \mathcal{N}_{i,k}^V \mathcal{H}_{i,k}^V \tag{2.18}$$

Here h_k^L and h_k^V are the heat transfer coefficients for liquid and vapor phase. $\mathcal{H}_i^L$ and $\mathcal{H}_i^V$ are the partial molar enthalpies of component i in the liquid and vapor phase. Derivatives in the energy transfer equations are replaced by central difference approximations in the calculation.

2.2.3 Interface Equations

Thermodynamic equilibrium is assumed only at the phase boundary. For each component we have:

$$y_{i,k}^I - K_{i,k} x_{i,k}^I = 0 \tag{2.19}$$

Here $y_{i,k}^I$ is the vapor phase composition at the interface and $x_{i,k}^I$ is the liquid phase composition at the interface. $K_{i,k}$ is the vapor - liquid equilibrium ratio for component i in cell k and is a function of interface temperature, (T_k^I) and concentrations and stage pressure p_j.

$$K_{i,k} = K_{i,k}(x_{i,k}^I, y_{i,k}^I, T_k^I, p_j) \tag{2.20}$$

In addition, it is necessary that all the mole fractions should sum up to one for both phases:

$$\sum_{i=1}^{c} x_{i,k}^{I} - 1 = 0 \tag{2.21}$$

$$\sum_{i=1}^{c} y_{i,k}^{I} - 1 = 0 \tag{2.22}$$

From a mass and energy balance over the interface, we can deduce that the mass and energy transfer rates through the interface should be continuous, which leads to the following equations.

$$\mathcal{N}_{i,k}^{L}\big|_{I} = \mathcal{N}_{i,k}^{V}\big|_{I} \tag{2.23}$$

And for the energy transfer rate:

$$\mathcal{E}_{k}^{L}\big|_{I} = \mathcal{E}_{k}^{V}\big|_{I} \tag{2.24}$$

This equation plays a very important role in determining the mass transfer rates. The Maxwell-Stefan equations by themselves are 'floating equations'. They relate the driving force for mass transfer of a component to the frictional drag between different species in terms of relative velocities and drag coefficients. Eq. (2.24) is, therefore, required to 'tie down' these relative velocities. This equation is commonly referred to as the 'bootstrap' condition (Taylor and Krishna, 1993; Wesselingh and Krishna, 1997).

2.3 Reactions

For the implementation of the reaction equations, we need to make a distinction between heterogeneous and homogeneous systems.

Homogeneous reactions take place in the liquid bulk and liquid transfer film. In case of very fast reactions, a correct description of the combined mass transfer and reaction in the transfer film is very important.

Heterogeneous systems can be tackled by two methods. The most fundamental method takes into account multicomponent mass transfer to, in, and from the catalyst. In addition, it requires a detailed description of concentration gradients and local reaction rates inside the catalyst. Heterogeneous systems may also be tackled by means of a pseudo-homogeneous approach. With this approach, the catalyst mass transfer effects are lumped into the kinetic equation and the reaction is effectively tackled as being homogenous, assuming no reaction in the liquid transfer film. We will now continue with the mathematical description of both reaction models

2.3.1 Homogeneous Reactions

In homogeneous reaction systems, the reaction takes place in the liquid phase only. Composition changes in the bulk liquid reaction are taken into account by the reaction terms in Eq. (2.1) and Eq. (2.6). The composition changes due to the chemical reaction in the liquid transfer film are accounted for by Eq. (2.14).

An important parameter for homogeneous reaction systems is the total liquid inventory on a tray. The change in the total number of moles due to the reaction on a tray is obtained by multiplying the reaction rate with the total liquid inventory on a tray (or in a cell). For tray columns, the liquid inventory follows from the clear liquid height and the active area of a tray. The clear liquid height can be determined from semi-empirical correlations as given by Lockett (1986). One of the observations that needs to be made is that under the same conditions, these methods tend to predict vastly different values. Differences of more than 100 percent are not uncommon. The choice of the liquid holdup model may therefore substantially influence the outcome of the calculations. In our calculations, the method due to Bennett *et al.* (1983) was used for tray columns. This method is recommended by Lockett (1986).

Similar observations can be made for packed columns. Here the liquid holdup is normally obtained from semi empirical expressions for the liquid holdup per unit of

packing volume. A complete listing of the holdup prediction methods for various types of packing, that are available in the model, is given by Kooijman (1995).

2.3.2 Heterogeneous Reactions

The pseudo-homogeneous reaction approach may be easily implemented in the above system of equations. The reaction rate equations, along with the effectiveness factor may be entered into the reaction terms in Eq. (2.1) and Eq. (2.6). The reaction volume ϵ_k is given by the catalyst holdup in a cell. In addition, there will be no reaction in the liquid transfer film at the vapor/liquid interface. The film reaction equation, Eq. (2.14), may, therefore, be removed.

When using this approach, we are, however, losing insight in multicomponent mass transfer interactions in the pores, that may be particularly important in non-equi-stoichiometric reactions. Therefore, we will use a more rigorous theory of diffusion (and reaction) inside porous catalysts: The Dusty Fluid model.

The use of the Dusty Fluid model for heterogeneous reactions leads to the introduction of a liquid mass transfer film and a catalyst phase into the model equations.

The Maxwell-Stefan equations are used for description of mass transport in the liq-

uid/solid mass transfer film:

$$\frac{x_{i,k}}{\mathcal{R}T}\frac{\partial \mu_{i,k}^{S}}{\partial \eta} = \sum_{l=1}^{c} \frac{x_{i,k}\mathcal{N}_{l,k}^{S} - x_{l,k}\mathcal{N}_{i,k}^{S}}{c_t^{S}(\kappa_{i,l}^{S} a^{C})} \tag{2.25}$$

The mass transfer coefficient $\kappa_{i,l}^{S}$ has to be calculated from an appropriate correlation for liquid/solid mass transfer. Only $c-1$ of these equations are independent. The mole fraction of the c-th component follows from the summation equation.

$$\sum_{i=1}^{c} x_i = 1 \tag{2.26}$$

In addition, the energy flux through the liquid film around the catalyst is zero:

$$\mathcal{E}_j^{S} = -h^{S} a^{C}\frac{\partial T}{\partial \eta} + \sum_{i=1}^{c} \mathcal{N}_i^{S}\mathcal{H}_i^{S} = 0 \tag{2.27}$$

The major new problem we have to deal with in this nonequilibrium model involves liquid phase multicomponent mass transfer with reaction in the porous catalyst. For this, there is, however, no complete theory. Even for gases, for which there is a kinetic theory, there are complete and internally consistent theories of multicomponent mass transfer in porous media only for two cases. When the pore size is much smaller than the mean free path length there is the Knudsen diffusion theory, and the kinetic theory applies when the pore size is orders of magnitudes longer than the mean free path length. However, for the intermediate regime there are substantial problems. The molecular velocity distribution varies in a complicated way over the cross section

of the pore and additional problems are posed by catalyst geometry and pore size distribution.

We will, therefore, first describe the theory of gas phase multicomponent mass transfer in porous media, and subsequently discuss a modification of these equations suitable for liquid phase systems.

2.3.3 The Dusty Gas Model

Modeling multicomponent mass transfer in porous media is complicated when the mean free path length of the molecules is of the order of magnitude of the pore diameter. The difficulties posed by this intermediate case may be circumvented by a method originally introduced by Maxwell (1866) and developed further by Mason and various co-workers (1961, 1962, 1963, 1964, 1967). The original idea of Maxwell is as follows:

> "We may suppose the action of the porous material to be similar to that of a number of particles, fixed in space and obstructing the motion of the particles of the moving systems."

In other words, he suggested that the porous material itself be described as a supplementary 'dust' species, consisting of very large molecules that are kept motionless by some unspecified external force. The Chapman-Enskog kinetic theory is then applied to the new pseudo gas mixture, in which the interaction between the dust and gas molecules simulates the interaction between the solid matrix and the gas species. In addition, one is no longer faced with the problem of flux and composition variations across a pore and problems related to catalyst geometry.

The price we have to pay for this simplification is that we 'lose' certain physical features of the porous medium. One of the more important issues is that we are no longer dealing with channels of finite size corresponding to the pores in the real medium. Thus, there is no introduction of the viscous fluxes in the formal development of the equations. These have to be added empirically, although Evans *et al.* (1961) presented arguments to justify the addition of diffusive and viscous fluxes. In what follows, we will first derive the diffusive part of the equations, and subsequently deal with the viscous fluxes.

For diffusion of a gas in 'open space' the Generalized Maxwell-Stefan equations are (see, for example, Jackson, 1977):

$$
\begin{aligned}
d_i &\equiv \frac{x_i}{\mathcal{R}T}(\bigtriangledown \mu_i)_{T,p} + \frac{\phi_i - \omega_i}{c_t \mathcal{R}T} \bigtriangledown p - \frac{1}{c_t \mathcal{R}T}\left(c_i F_i - \omega_i \sum_{l=1}^{c} c_l F_l\right) \\
&+ \sum_{l=1}^{c} x_i x_l \alpha_{i,l} \bigtriangledown ln(T) \\
&= \sum_{l=1}^{c} \frac{x_i N_l - x_l N_i}{c_t \mathcal{D}_{i,l}}
\end{aligned} \tag{2.28}
$$

The left hand side of this equation represents the sum of the driving forces. The first term represents the driving force due to a chemical potential gradient $\bigtriangledown \mu_i$. The second term represents a driving force due to a pressure gradient $\bigtriangledown p$. This term will be important only if the volume fraction ϕ_i and mass fraction ω_i of component i are not the same. The third term is the driving force for forced diffusion. This may be the case for charged particles in an electric field. The last term represents thermal diffusion. In most cases encountered in distillation, extraction, or gas absorption, the thermal diffusion term is very much smaller than the other terms and may safely be neglected. The right hand side of the equation represents the sum of the molecular friction terms.

For an ideal gas the chemical potential gradient term simplifies as follows.

$$
\frac{x_i}{\mathcal{R}T}(\bigtriangledown \mu_i)_{T,p} = \bigtriangledown x_i \tag{2.29}
$$

In addition, the volume fraction and mole fractions will be the same for each component:

$$\phi_i = x_i \tag{2.30}$$

Furthermore, the concentration of the mixture may be expressed in terms of pressure and temperature by means of the ideal gas law.

$$c_t = \frac{p}{\mathcal{R}T} \tag{2.31}$$

To obtain the dusty gas model equations, Eq. (2.28) is applied to a pseudo mixture of $c + 1$ species, in which the extra species represents the catalyst phase. The dust species is subject to the following constraints:

1. The dust must be evenly distributed in space: $\bigtriangledown c_{c+1} = 0$.
2. The dust is kept immobile by an unspecified external force so that $N_{c+1} = 0$.
3. The dust species consists of giant molecules whose molar mass goes to infinity: $M_{c+1} \to \infty$.

The unspecified forces in item 2 prevent the porous medium from moving due to pressure gradients in the gas. This will be the force exerted by the catalyst matrix to

keep everything in place. Furthermore, for the cases considered in this paper, there are no external forces on the gaseous species, so that $F_l = 0$ for l from 1 to c.

When Eq. (2.28) is applied to the pseudo mixture of $c+1$ components, variables such as mole fractions and concentrations will be those of the pseudo mixture, including the dust molecules. In the subsequent derivation of the Dusty Gas Model equations these variables will be marked by a tilde to distinguish them from the true quantities in the mixture. For the species concentrations, partial pressures and component fluxes, there is no difference between the pseudo quantities and the real quantities.

Applying Eq. (2.28) to the pseudo mixture, under the above assumptions lead to:

$$\begin{aligned} d_i &\equiv \bigtriangledown \tilde{x}_i + \frac{\tilde{x}_i - \tilde{\omega}_i}{\tilde{p}} \bigtriangledown \tilde{p} + \frac{\tilde{\omega}_i}{\tilde{p}} c_{c+1} F_{c+1} \\ &= \sum_{l=1}^{c} \frac{\tilde{x}_i N_l - \tilde{x}_l N_i}{\tilde{c}_t \tilde{\mathcal{D}}_{i,l}} - \frac{\tilde{x}_{c+1}}{\tilde{c}_t \tilde{\mathcal{D}}_{i,c+1}} N_i \end{aligned} \tag{2.32}$$

From hydrodynamic considerations it follows that the force exerted by the gas on the porous medium is equal to the physical pressure gradient of the gas over the porous medium:

$$c_{c+1} F_{c+1} = \bigtriangledown p \tag{2.33}$$

We need only relate the variables pertaining to the pseudo mixture to those of the real gas. The complete derivation is given by Jackson (1977). The result is Eq. (2.34):

$$\frac{1}{\mathcal{R}T} \bigtriangledown p_i = \sum_{l=1}^{c} \frac{x_i N_l^D - x_l N_i^D}{\mathcal{D}_{i,l}^{e}} - \frac{N_i^D}{D_i^e} \tag{2.34}$$

D_i^e is the Knudsen diffusion coefficient of component i. The D's have been added as superscripts to emphasize that these are the *diffusive* flux relations associated with the dusty gas model. We also have viscous fluxes that arise from movement of the mixture as a whole. This is related to flow of a pure substance in a cylindrical tube, and is described by the standard Poiseuille flow problem. For a circular tube of diameter d_p, the contribution to the molar flux due to viscous flow is:

$$N^V = -\frac{d_p^2 p}{32\eta\mathcal{R}T}\frac{dp}{dz} \tag{2.35}$$

For a porous medium with a distribution of pore sizes, we may rewrite this equation as (Jackson, 1977).

$$N^V = -\frac{B_0 p}{\eta\mathcal{R}T}\frac{dp}{dz} \tag{2.36}$$

which equation defines the permeability B_0. When all the pore sizes are uniform and of diameter d_p, the permeability is given by

$$B_0 = \frac{d_p^2}{32} \tag{2.37}$$

If we are dealing with a gas mixture instead of a pure gas, and there is no diffusion of the species in the mixture relative to the mixture as a whole, then the total *viscous*

flux for component i (in all directions) is given by:

$$N_i^V = -\frac{x_i B_0 p}{\eta \mathcal{R} T} \bigtriangledown p \tag{2.38}$$

The flux of component i is given by adding the diffusive and convective fluxes

$$N_i = N_i^D + N_i^V \tag{2.39}$$

Eq. (2.34), Eq. (2.38) and Eq. (2.39) may now be combined to give the complete Dusty Gas Model equations.

$$\frac{1}{\mathcal{R}T} \bigtriangledown p_i + \frac{x_i B_0 p}{\eta \mathcal{R} T D_i^e} \bigtriangledown p = \sum_{l=1}^{c} \frac{x_i N_l - x_l N_i}{\mathcal{D}_{i,j}^e} - \frac{N_i}{D_i^e} \tag{2.40}$$

Rearranging once more gives the working form of the Dusty Gas Model equations.

$$\frac{p}{\mathcal{R}T} \bigtriangledown x_i + \frac{x_i}{\mathcal{R}T} \left(1 + \frac{B_0 p}{\eta D_i^e}\right) \bigtriangledown p = \sum_{l=1}^{c} \frac{x_i N_l - x_l N_i}{\mathcal{D}_{i,l}^e} - \frac{N_i}{D_i^e} \tag{2.41}$$

2.3.4 The Dusty Fluid Model

The Dusty Fluid Model as developed by Krishna and Wesselingh (1997) is a modification of the Dusty Gas Model so as to be able to model liquid phase diffusion in porous media. First, all pressure terms are replaced with concentrations by back-substituting the ideal gas law ($p = c_t \mathcal{R} T$). Note that this was done for convenience in the derivation of the Dusty Gas Equations. Eq. (2.41) may be rewritten as:

$$\bigtriangledown x_i + \frac{x_i}{p} \bigtriangledown p + \frac{x_i B_0}{\eta D_i^e} \bigtriangledown p = \sum_{l=1}^{c} \frac{x_i N_l - x_l N_i}{c_t \mathcal{D}_{i,l}^e} - \frac{N_i}{c_t D_i^e} \tag{2.42}$$

The first two terms in this equation correspond to the isothermal chemical potential gradient for an ideal mixture, which may be split up as follows:

$$\bigtriangledown x_i + \frac{x_i}{p} \bigtriangledown p = \bigtriangledown_T \mu_i = \bigtriangledown_{T,p} \mu_i + \bar{V}_i \bigtriangledown p \tag{2.43}$$

For a nonideal mixture we have:

$$\frac{x_i}{\mathcal{R}T} \bigtriangledown_{T,p} \mu_i + \frac{x_i}{\mathcal{R}T} \bar{V}_i \bigtriangledown p + \frac{x_i B_0}{\eta D_i^e} \bigtriangledown p = \sum_{l=1}^{c} \frac{x_i N_l - x_l N_i}{c_t \mathcal{D}_{i,l}^e} - \frac{N_i}{c_t D_i^e} \tag{2.44}$$

Eq. (2.44) is expressed in terms of diffusion coefficients and fluxes, rather than mass transfer coefficients and mass transfer rates as is done for the liquid and vapor film transfer equations. The mass transfer rates are obtained by multiplying the fluxes by the interfacial area of the catalyst particles. This is not as straightforward, as it looks, since, depending on the geometry of the catalyst, the cross sectional area can change along the diffusion path. In addition, one should take the different geometries into account in the derivation of the discretized equations. This will be discussed in detail below.

The Dusty Fluid Model equations do not sum up to zero (unlike the GMS equations), because of the pressure term, leading to an extra equation for the pressure drop. Summing up over the c species gives:

$$\sum_{i=1}^{c} \frac{N_i}{D_i^e} = -\frac{1}{\mathcal{R}T} \left(1 + \frac{c_t B_0 \mathcal{R}T}{\eta} \sum_{i=1}^{c} \frac{x_i}{D_i^e} \right) \bigtriangledown p \tag{2.45}$$

because

$$\sum_{i=1}^{c}\sum_{l=1}^{c}\frac{x_l N_i - x_i N_l}{\mathcal{D}_{i,l}^{e}} = 0 \tag{2.46}$$

and the Gibbs-Duhem equation:

$$\sum_{i=1}^{c}\frac{c_i}{\mathcal{R}T}\bigtriangledown_{T,p}\,\mu_i = 0 \tag{2.47}$$

Not all of the above equations are independent. We can choose either c times Eq. (2.44) while discarding Eq. (2.45), or $c-1$ times Eq. (2.44) together with Eq. (2.45).

Since there can be no accumulation of mass in the catalyst particle at steady state, the following equation has to be satisfied:

$$\sum_{i=1}^{c} M_i N_i = 0 \tag{2.48}$$

This equation provides the 'bootstrap' condition for the dusty fluid equations. The component fluxes will change due to reaction:

$$\frac{\partial N_i}{\partial z} = \sum_{i=1}^{c}\nu_{i,m}R_m \tag{2.49}$$

The total energy flux in a catalyst particle is zero, since at steady state there can be no accumulation inside the catalyst. Therefore:

$$e^C = q + \sum_{i=1}^{c}\mathcal{H}_i^L N_i = 0 \tag{2.50}$$

q represents the conductive contribution to the energy flux.

2.3.5 Boundary Conditions

The boundary conditions at the outer surface of the catalyst are provided by the mass balances around the catalyst particle. In addition, the mass transfer rates at the catalyst interface should be continuous:

$$\mathcal{N}_{i,j}^{S} = \mathcal{N}_{i,j}^{C} \tag{2.51}$$

At the catalyst center, temperature, pressure and composition have zero gradients.

$$\frac{\partial P}{\partial z} = 0, \frac{\partial T}{\partial z} = 0, \frac{\partial x_i}{\partial z} = 0 \tag{2.52}$$

And the flux of species i is zero.

$$N_i = 0 \tag{2.53}$$

This concludes the development of the Dusty Fluid Model for mass transfer in porous media.

2.3.6 Discretisation and Geometry

When discretising the dusty fluid equations, the catalyst shape plays an important role. For Raschig ring type packings, it is possible to use a simple Cartesian coordinate system. However, this approach is not recommended for teabag and sandwich

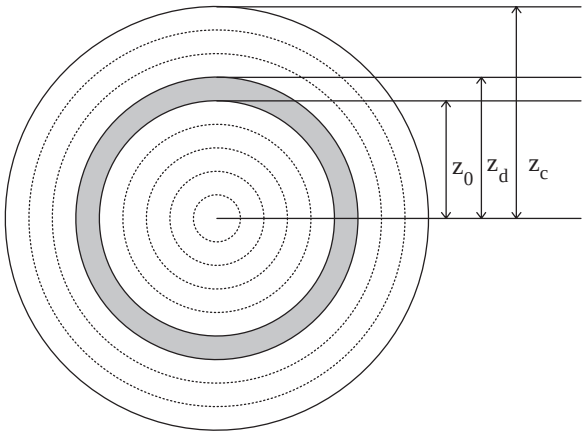

Figure 2.3: Schematic representation of grid for catalyst particle.

type packings, where smaller catalyst particles can be used. First, however, the multi-dimensional problem is simplified by replacing the gradient terms by derivatives with respect to one direction coordinate. In addition, since we prefer to deal with mass transfer rates, the fluxes are multiplied by the interfacial area. Eq. (2.44) becomes:

$$\frac{x_i}{\mathcal{R}T}\frac{\partial \mu_i}{\partial z} + x_i\left(\frac{\bar{V}_i}{\mathcal{R}T} + \frac{B_0}{\eta D_i^e}\right)\frac{\partial p}{\partial z} = \sum_{l=1}^{c}\frac{x_i\mathcal{N}_l - x_l\mathcal{N}_i}{c_t \mathcal{D}_{i,l}^e a^C} - \frac{\mathcal{N}_i}{c_t D_i^e a^C} \tag{2.54}$$

Assuming that we are dealing with a catalyst particle with radius z_c, this particle will be split up in a number of finite volumes, as illustrated in Fig. 2.3. Subsequently, the Dusty Fluid Model equations are applied to each finite volume individually. This has some consequences for the differential terms and interfacial areas in the above

equation. For the differential term of an arbitrary quantity X:

$$\frac{\partial X}{\partial z} = \frac{1}{\mathcal{L}} \frac{\partial X}{\partial \eta} = \frac{X_k - X_{k-1}}{\mathcal{L}} \tag{2.55}$$

where $\mathcal{L}$ is a characteristic length for diffusion in the film under consideration (Taylor and Krishna, 1993):

- For a planar film: $\mathcal{L} = z_d - z_0$
- For a cylindrical film: $\mathcal{L} = r_0 \cdot ln(z_d/z_0)$
- For a spherical film: $\mathcal{L} = z_0 \cdot (1 - z_d/z_0)$

The cross sectional area for cylindrical and spherical catalysts depends on the location in the film as well. This can be accounted for by relating the area ratio of the catalyst area at location k to the outside catalyst area. For the various geometries this ratio can be represented by:

$$r_a = \left(\frac{z_d}{z_c} \right)^{\alpha} \tag{2.56}$$

in which $\alpha = 0$ for a planar film, 1 for a cylindrical film and 2 for a spherical film.

The chemical potential gradient is approximated as follows:

$$\left(\frac{x_i}{\mathcal{R}T} \frac{\partial \mu_i}{\partial \eta} \right)_n = \sum_{l=1}^{c-1} (\Gamma_{i,l})_n \frac{(x_i)_n - (x_i)_{n-1}}{\mathcal{L}_n} \tag{2.57}$$

The definition of $\Gamma_{i,l}$ is given in Eq. (2.16). For the pressure and temperature derivatives central difference approximations will be used. Note that, depending on the geometry, the discretisation step length varies for each discretisation point. Taking everything into account, the discretized Dusty Fluid equations become.

$$\begin{aligned} & \sum_{l=1}^{c-1}(\Gamma_{i,l})_n \frac{(x_i)_n - (x_i)_{n-1}}{\mathcal{L}_n} + (x_i)_n \left(\frac{\bar{V}_i}{\mathcal{R}T}\frac{B_0}{\eta D_i^e}\right)\left(\frac{p_{n+1}-p_{n-1}}{\mathcal{L}_n + \mathcal{L}_{n-1}}\right) \\ = & \sum_{l=1}^{c} \frac{(x_i)_n N_l - (x_l)_n N_i}{c_t \mathcal{D}_{i,l}^e a^C r_a} - \frac{N_i}{c_t D_i^e a^C r_a} \end{aligned} \tag{2.58}$$

The catalyst shape also influences the reaction equation. In effect, Eq. (2.49) is a conservation equation, the expressions for the different catalyst shapes may be derived by writing a mass balance for a finite volume of the catalyst:

$$(N_i a)_n - (N_i a)_{n+1} = \sum_{m=1}^{r} \nu_{i,m} R_m \epsilon_k \mathcal{V}_n \tag{2.59}$$

where ϵ_k is the total catalyst volume available in the contacting cell, and $\mathcal{V}_n$ is the volume fraction of the slice of catalyst (see Fig. 2.3) under consideration. The fluxes may be replaced by mass transfer rates, taking into account the interfacial area ratio. The volume fraction of catalyst is obtained by taking the volume fraction under consideration, divided by the total catalyst volume. A general expression for the

volume fraction is given by:

$$\mathcal{V}_n = \frac{r_\delta^\beta - r_0^\beta}{r_c^\beta} \tag{2.60}$$

In which β =1 for a planar catalyst, β=2 for a cylindrical catalyst and β=3 for a spherical catalyst. The resulting discretized conservation equation then becomes:

$$(\mathcal{N}_i^C r_a)_n - (\mathcal{N}_i^C r_a)_{n+1} = \sum_{m=1}^{r} \nu_{i,m} R_m \epsilon_k \mathcal{V}_n \tag{2.61}$$

The last equation to be discretized is the energy transfer equation. The energy transfer rate equation consists of a convective and a conductive contribution. We shall assume that the catalyst matrix and the liquid filling the pores have the same temperature profile. The total conductive energy flux may then be written as:

$$q = -\left((1-\epsilon^C)\lambda^C + \lambda^L \frac{\epsilon^C}{\tau}\right) \bigtriangledown T \tag{2.62}$$

The catalyst porosity ϵ^C and tortuosity τ are added here to take into account the tortuous paths followed by the gas in the catalyst. The discretized equation is then given by:

$$q = -\left((1-\epsilon)\lambda^C + \lambda^L \frac{\epsilon^C}{\tau}\right)\left(\frac{T_{n+1} - T_{n-1}}{\mathcal{L}_n + \mathcal{L}_{n-1}}\right) \tag{2.63}$$

Combining the convective and conductive contributions and multiplying by the interfacial area then gives:

$$a^C (r_a)_n \left((1-\epsilon)\lambda^C + \lambda^L \frac{\epsilon^C}{\tau}\right)\left(\frac{T_{n+1} - T_{n-1}}{\mathcal{L}_n + \mathcal{L}_{n-1}}\right) + \sum_{i=1}^{c} \mathcal{N}_i^C \mathcal{H}_i = 0 \tag{2.64}$$

This completes the model definition for the Dusty Fluid Model.

2.4 Flow on Distillation Trays

It has long been recognized that liquid staging results in improved performance of a distillation tray. Because a liquid is never perfectly mixed on a distillation tray, concentration profiles along the liquid flow path will arise in the liquid phase under the influence of mass transfer. If there is no horizontal vapor mixing, this will cause concentration profiles in the vapor flow leaving the stage. Consequently, the overall tray efficiency will be higher than the Murphree Point efficiency (see Lockett, 1986). Lewis (1936) derived an expression for the maximum achievable tray efficiency, as a function of the point efficiency, assuming there is no liquid backmixing. In reality, the tray efficiency will fall short of the maximum achievable efficiency due to various nonidealities in the flow pattern. These may be caused by liquid backmixing, horizontal vapor mixing, non-uniform liquid flow across the tray, non-uniform vapor flow through the tray, and entrainment and weeping. This work is focused on the first point, although the outlined methodology allows for studying of all of these issues.

Liquid backmixing occurs mainly due to two mechanisms: Turbulence in the liquid continuous region, and motion of liquid droplets in the vapor continuous region (Bennett and Grimm, 1991). A first study on liquid backmixing on distillation trays was presented by Kirschbaum (1937), who compares flow on a distillation tray to

flow through a cascade of perfectly mixed pools of liquid. Gautreaux and O'Connell (1955) used the liquid mixing pool concept to derive an expression relating the point efficiency to the plate efficiency. Wijn (1996) used a cell model to study the influence of downcomer layout patterns on the tray efficiency. Alejski (1991) presented and equilibrium stage model, in which the liquid phase is split up in a number of equilibrium cells along the liquid flow path to account for backmixing in a reactive distillation column. Point efficiencies were used to take into account mass transfer in the equilibrium cells.

In all of the above studies a liquid mixing pool concept is used to determine the effect of staging in the liquid flow direction. Quantification of backmixing usually is done by means of eddy diffusion models. (e.g. Bennett and Gimm, 1991; Raper *et al.*, 1984; Barker and Self, 1962; Sohlo and Kinnunen, 1977). These models assume that the axial spreading of a tracer in the liquid flow (z) direction on a distillation tray can be described by:

$$\frac{1}{Pe}\frac{\partial^2 x}{\partial z^2} - \frac{\partial x}{\partial z} = 0 \tag{2.65}$$

in which x is the mole fraction of the tracer and z is the axial coordinate. The Peclet number Pe is given by:

$$Pe = \frac{u^L \cdot l}{D_e} \tag{2.66}$$

D_e is the eddy diffusion coefficient, l is the flow path length and u^L is the superficial

liquid velocity on a stage. Important limitations of the eddy diffusivity model are that it only applies to isotropic liquid flow, and, therefore, that it cannot be used for description of circulation patterns at, for instance, the column wall or the outlet weir. A summary of estimation methods for the axial dispersion coefficient is given by Lockett (1986) and Bennett and Grimm (1991). Most of these methods are curve fits to experimental data, in which a functional dependence is assumed with respect to parameters such as the vapor and liquid flows and the liquid holdup. The method of Bennett and Grimm (1991) is based on a drop trajectory model.

The Peclet number for the axially dispersed flow model can be related to a number of well mixed liquid pools in the liquid flow direction, N,by the following equation:

$$\frac{1}{N} = \frac{2}{Pe} - \frac{2}{Pe^2}\left(1 - exp(-Pe)\right) \tag{2.67}$$

In this paper a nonequilibrium mixing pool concept will be used to describe the mass transfer/reaction/flow problem. The two phase mixture on a tray is split up in a number of contacting cells, for each of which mass and energy balances can be written, along with mass transfer rate equations. A schematic representation (side view) of a general stage j is given in Fig. 2.4. Stage numbering in a column is from top to bottom. Fig. 2.4 also serves as an introduction to the notation used in this paper. L_j^S and V_j^S represent the liquid and vapor molar flow rates from stage j respectively.

The mole fractions of component i in the liquid and vapor streams are denoted by $x_{i,j}$ and $y_{i,j}$, and H_j^{LS} and H_j^{VS} represent the enthalpies of the liquid and vapor streams leaving stage j. T_j^{LS} and T_j^{VS} are the temperatures of the streams leaving stage j. $f_{i,j+1}^{VS}$ is the vapor feed rate of component i to stage $j+1$, and $f_{i,j}^{LS}$ is the liquid feed rate of component i to stage j. Q_j^{VS} and Q_j^{LS} are external heat duties that may be specified to either phase of stage j. The cell numbering is also illustrated in Fig. 2.4. n^V is the number of cells in a vapor flow path, and n^L is the number of cells in a liquid flow path. Cell numbering is from left to right and from bottom to top.

2.4.1 Stage Equations - Tray columns

The overall mass balances for each stage, for the liquid and vapor phase, are given by:

$$(1 + r_j^L) \cdot L_j^S - \sum_{k=1}^{n^V} L_{(n^L,k)}^C - F_j^{LS} = 0 \tag{2.68}$$

$$(1 + r_j^V) \cdot V_j^S - \sum_{k=1}^{n^L} V_{(k,n^V)}^C - F_{j+1}^{VS} = 0 \tag{2.69}$$

Here r_j^V and r_j^L are the vapor and liquid sidestream ratios. These are nonzero only if a sidestream is specified to stage j. $V_{(k,n^V)}^C$ is the vapor flow coming from the $k-th$ cell in the top row of cells in the nonequilibrium stage, and $L_{(n^L,k)}^C$ is the liquid flowrate from the $k-th$ cell in the last column of cells in the nonequilibrium stage

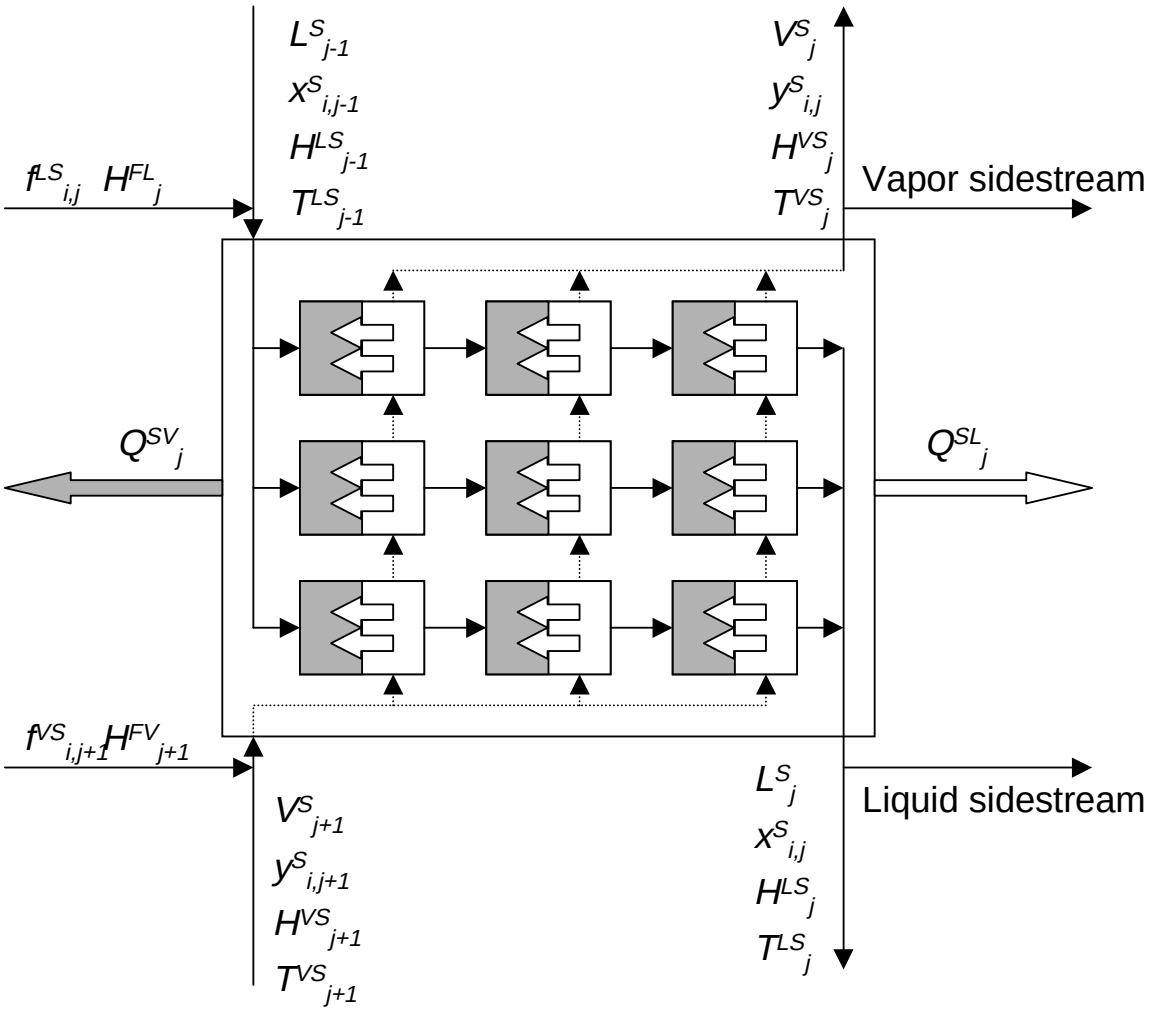

Figure 2.4: Schematic representation of nonequilibrium stage for a distillation tray

(see Fig. 2.4). F_j^L and F_{j+1}^V are the overall liquid and vapor feed rates to stage j and $j+1$ respectively. The vapor feed to stage $j+1$ is added to stage j, as it is assumed that the vapor fraction of a feed goes up instantly and does not interfere with the tray below.

The stage component balance equations for the liquid and vapor phase are given by.

$$(1+r_j^L)\cdot x_{i,j}^S \cdot L_j^S - \sum_{k=1}^{n^V} x_{i,(n^L,k)}^C \cdot L_{(n^L,k)}^C - f_{i,j}^{LS} = 0 \tag{2.70}$$

$$(1+r_j^V)\cdot y_{i,j}^S \cdot V_j^S - \sum_{k=1}^{n^L} y_{i,(k,n^V)}^C \cdot V_{(k,n^V)}^C - f_{i,j+1}^{VS} = 0 \tag{2.71}$$

$x_{i,(n^L,k)}^C$ and $y_{i,(k,n^V)}^C$ are the liquid and vapor phase mole fractions leaving cell k. $f_{i,j+1}^{VS}$is the vapor feed rate of component i to stage $j+1$ and $f_{i,j}^{LS}$ is the liquid feed rate of component i to stage j. The stage energy balances are given by:

$$(1+r_j^L)\cdot H_j^{LS} \cdot L_j^S - \sum_{k=1}^{n^V} H_{(n^L,k)}^{LC} \cdot L_{(n^L,k)}^C - F_j^{LS} H_j^{FL} + Q_j^{LS} = 0 \tag{2.72}$$

$$(1+r_j^V)\cdot H_j^{VS} \cdot V_j^S - \sum_{k=1}^{n^L} H_{(k,n^V)}^{VC} \cdot V_{(k,n^V)}^C - F_{j+1}^{VS} H_{j+1}^{FV} + Q_j^{VS} = 0 \tag{2.73}$$

$H_{(n^L,k)}^{LC}$ and $H_{(k,n^V)}^{VC}$ are the enthalpies of the streams leaving the appropriate cells on the stage. H_{j+1}^{FV} is the vapor phase enthalpy of the feed to stage $j+1$ and H_j^{FL} is the enthalpy of the liquid feed to stage j. The stage equations are completed by the stage hydraulic equation.

$$p_j - p_{j-1} - (\Delta p_{j-1}) = 0 \tag{2.74}$$

Where p_j and p_{j-1} are the stage pressures on stages j and $j-1$ respectively. Δp_{j-1} is the pressure drop per tray from stage $j-1$ to stage j. The pressures in all cells on a stage are assumed to be equal to the stage pressure. The pressure drop over the stage is considered to be a function of the stage flows, the fluid properties and the equipment layout parameters.

A few remarks need to be made here with respect to the feed streams and heat duties. In the presented model, one has the option to specify the feeds to either the cells or the stage under consideration. In a real column, feeds are supplied to a column between two stages, in such a way, that the liquid part of the feed is preferably equally distributed over the tray. The vapor fraction of the feed goes up instantly and does normally not interfere with the tray below. Thus, in most cases, the vapor feed stream should be added to the stage flow leaving the feed stage. This means that the vapor feeds will normally be treated in Eq. (2.69), Eq. (2.71) and Eq. (2.73), rather than in cell equations Eq. (2.2), Eq. (2.7) and Eq. (2.9). Since the liquid is normally distributed over the stage, the liquid will enter the cells directly, and the feed flows should be added to the cell equations Eq. (2.1), Eq. (2.6) and Eq. (2.9), rather than Eq. (2.68), Eq. (2.70) and Eq. (2.72). However, all this depends on the configuration used.

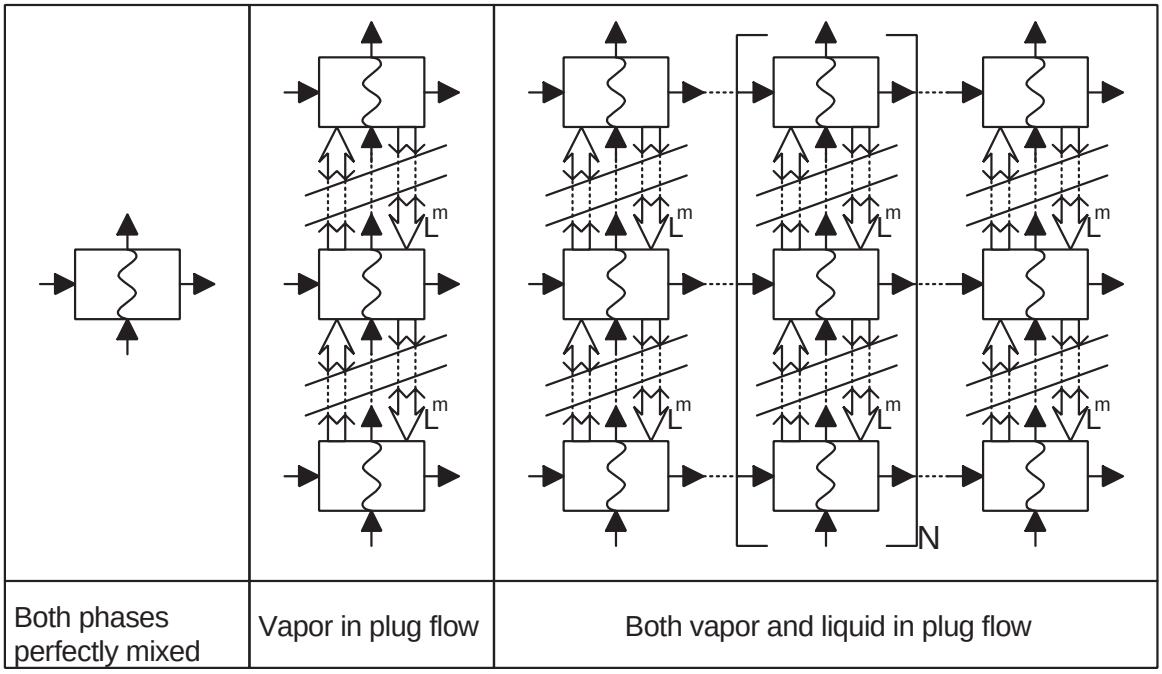

Figure 2.5: Cell description of various flow models

2.4.2 Flow Models

Although it is possible, in principle, to describe almost any kind of flow pattern using exotic cell layout and connection patterns, this work is focussed on the influence of vapor and liquid backmixing on distillation trays. The limiting cases that will be considered are illustrated in Fig. 2.5.

The simplest, shown on the left of the figure, has both vapor and liquid phases perfectly mixed. In this case the cell description is superfluous, since the stage and

cell flows will be the same. This case is, however, not representative of the true flow patterns on a tray. There is general agreement on the assumption that vapor rises in plug flow through the layer of liquid on a stage. In addition it is often assumed that the liquid is well mixed in the vertical direction, due to the vapor jets and bubbles. The liquid phase may be assumed to be completely well mixed for trays with short flow paths. However, significant staging is to be expected for longer flow path lengths.

The first of these cases in which the vapor rises in plug flow through an ideally mixed pool of liquid is illustrated in the middle of Fig. 2.5. Vertical mixing is established by additional liquid mixing flows, denoted by L^M and represented by the broad arrows. The flow rates of all the mixing streams are assumed to be equal. In the third case, shown on the right of Fig. 2.5, staging in the liquid flow direction is taken into account by specifying multiple columns of cells. The number of cells needed to model a realistic flow pattern may be derived from literature correlations for axial dispersion coefficients (see: Lockett, 1986) and Eq. (2.67). The cell component and enthalpy balances will have to be adjusted to account for the mixing flows.

Because the liquid mixing streams for all cells are assumed to be equal, the overall liquid phase mass balance for a cell will not change. The modified liquid phase

component balance for an arbitrary cell is given by:

$$L^C_{(k,m)} \cdot x^C_{i,(k,m)} - L^C_{(k-1,m)} \cdot x^C_{i,(k-1,m)} - f^{LC}_{i,(k,m)} - \mathcal{N}^L_{i,(k,m)} \mathcal{N}^S_{i,(k,m)}$$
$$+ \sum_{l=1}^{r} \nu_{i,l} R_{l,(k,m)} \epsilon_{(k,m)} L^M \cdot (2x^C_{i,(k,m)} - x^C_{i,(k,m-1)} - x^C_{i,(k,m+1)}) = 0 \qquad (2.75)$$

Here $x^C_{i,(k,m+1)}$ and $x^C_{i,(k,m-1)}$ are the liquid phase compositions in the cells above and below the cell under consideration. L^M is the liquid mixing flowrate. This equation differs slightly for the top and bottom cells in a column. The cells in the top row of a stage have liquid exchange only with the cells below. The bottom cells only mix with the cells directly above.

The liquid phase energy balance for a cell with mixing flows is given by:

$$L^C_{(k,m)} \cdot H^{LC}_{(k,m)} - L^C_{(k-1,m)} \cdot H^{LC}_{(k-1,m)} - F^{LC}_{(k,m)} H^{FL}_{(k,m)} + Q^{LC}_{(m,k)}$$
$$- \mathcal{E}^L_{(k,m)} - \mathcal{E}^S_{(k,m)} + L^M \cdot (2H^{LC}_{(k,m)} - H^{LC}_{(k,m-1)} - H^{CL}_{(k,m+1)}) = 0 \qquad (2.76)$$

The liquid mixing flow has to be large enough to ensure ideal liquid mixing in the vertical direction.

Kooijman (1995) derives and uses an analytical approximation for the mass transfer rates for this model, but he assumes the vapor interface concentration and the matrix of vapor phase mass transfer coefficients to be constant over the froth height. This assumption is legitimate only if the resistance to mass transfer is assumed to be

confined entirely to the vapor phase and the liquid phase is well mixed. For the liquid flow model Kooijman corrects the vapor interface concentration because it is not justifiable to assume a constant vapor interface concentration everywhere on the tray. The changes in interface mole fractions are related to the average liquid mole fraction differences over the mass transfer film on the tray and at the outlet. The correction factor was chosen by matching numerical calculations to experimental data. These assumptions are not made in the cell model, since mass transfer coefficients and interface concentrations are calculated for each cell independently.

2.5 Maldistribution in Packed Columns

From the work of Hoek *et al.* (1986), Stikkelman (1989) and Stoter (1993), we can conclude that there is an understanding of flow maldistribution in packing, and that there are models that appear adequate for describing the development of these large scale maldistributions. In addition, there is general agreement, and sufficient evidence, to support the statement that maldistribution has a detrimental effect on column performance. However, what fails is a direct method of determining the influence of these maldistributions, particularly for multicomponent systems. The method of Zuiderweg *et al.* (1993) requires two calculation steps, and has a number of draw-

backs. Firstly, it does not take into account the effect of local flow on the interfacial area. This is, however, one of the main reasons for bad behavior. Secondly, it does not take into account the differences in residence times for various maldistribution flows along the column. Furthermore, the method requires one to use the HETP concept, which in itself can be very confusing when used in multicomponent systems (Wesselingh, 1997).

Nawrocki *et al.* (1991) present a model for determining the influence of maldistribution in structured packings. Their approach uses empirical correlations for the interfacial area and mass transfer coefficients modified by taking into account flow mixing and splitting on the cross over length scale. As Zuiderweg *et al.* (1993) point out, such models can lead to very tedious calculations for commercial size columns, as there are thousands of cross-overs in a column cross section. On this scale radial mixing compensates largely for maldistribution and this eliminates the need for modeling on the cross-over scale.

Podrebarac *et al.* (1998) present a nonequilibrium model for a bale type packed column, in which they make a distinction between liquid inside and liquid outside the bale. The authors assume that a fraction f will flow through the packing, while the remainder $1 - f$ will flow outside of the packing. Only the liquid outside of the catalyst is assumed to be in contact with the vapor. Thus there are two mass transfer

steps; between the liquid inside the bale and the liquid outside the bale, and between the liquid outside the bale and the vapor. At the bottom of each bale, liquid streams are mixed and split up in the next bale. Although this method does not allow for evaluation of the effect of large scale maldistributions, it offers an interesting approach to investigate the influence of wall flow in a packed column.

In this work we present a direct approach for evaluating the influence of flow maldistribution on the distillation process. Here, we use the zone-stage flow model as presented by Zuiderweg *et al.* (1993). However, instead of just using it to determine the flow patterns, we will assume each cell to be a nonequilibrium vapor/liquid contacting cell. Flow maldistributions are evaluated by means of the linking pattern, and the effects of this maldistribution on mass transfer is directly evaluated inside the nonequilibrium cells. This way one can directly calculate the influence of large scale flow maldistributions on the distillation process, without having to revert to HETPs.

The model by Zuiderweg *et al.* (1993) has two independent calculation steps. The first step calculates the liquid maldistribution based on a natural flow model as outlined by Stikkelman (1989). In the second step, the influence of this maldistribution on the HETP (Height Equivalent of a Theoretical Plate), and thereby on the packing efficiency, is determined.

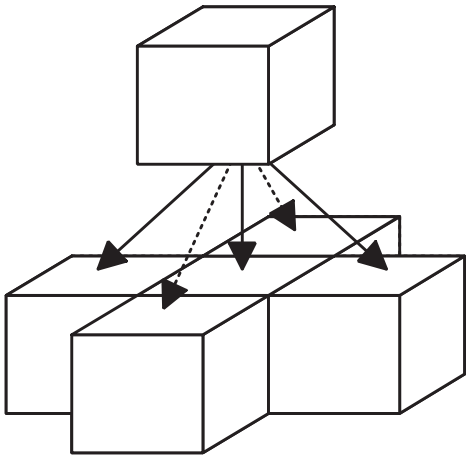

Figure 2.6: Flow splitting pattern in zone stage model

The effect of the maldistribution on the flow pattern is determined by means of a cell model, in which it is assumed that a fraction $\mathcal{K}^L$ of the liquid leaving the cell will flow down to the cell below. The remaining fraction of liquid $(1-\mathcal{K}^L)$ will flow to the adjacent cells below, whereby the flows are split up according to the ratio of the cell surface areas between the cells. The resulting flow pattern is shown in Fig. 2.6. This is referred to as the natural flow model. The underlying idea of this flow model is that a liquid flowing down a section of packing will spread according to a diffusional type equation. For a radial cell model we have:

$$\frac{\partial u}{\partial z} = D_r \left(\frac{1}{r} \frac{\partial u}{\partial r} + \frac{\partial^2 u}{\partial r^2} \right) \tag{2.77}$$

This is a standard convection diffusion equation, in which D_r is a radial spreading

coefficient that depends on the type and size of the packing, and u is the superficial liquid velocity in the packing. In order to establish a link between this equation and the natural flow model we will now discretise the above expression. We will use a forward difference expression in z-direction and an implicit central difference expression in r-direction The resulting expression is:

$$\frac{u_{n+1,m} - u_{n,m}}{h_z} = D_r \cdot \left(\frac{1}{2mh_r} \cdot \frac{u_{n,m+1} - u_{n,m-1}}{h_r} + \frac{u_{n,m+1} - 2u_{n,m} + u_{n,m-1}}{h_r^2} \right) \quad (2.78)$$

Here h_z is the cell height, and h_r is the cell width. Solving for $u_{n+1,m}$ results in:

$$\begin{aligned} u_{n+1,m} &= \frac{1}{2}\frac{(2m-1)\cdot D_r \cdot h_z}{m \cdot h_r^2} \cdot u_{n,m-1} + \frac{h_r^2 - 2D_r \cdot h_z}{h_r^2} \cdot u_{n,m} \\ &+ \frac{1}{2}\frac{(2m+1)\cdot D_r \cdot h_z}{m \cdot h_r^2} \cdot u_{n,m+1} \end{aligned} \quad (2.79)$$

This is an expression for the flow to cell $(n, m+1)$ coming from the three cells above. For a zone stage model using radial cells, we can write the following equation:

$$L_{j+1,k} = (1 - \mathcal{K}^L) \cdot (r_a^L)_{k-1} \cdot L_{j,k-1} + \mathcal{K}^L \cdot L_{j,k} + (1 - \mathcal{K}^L) \cdot (r_a^L)_{k+1} \cdot L_{j,k+1} \quad (2.80)$$

Here $L_{j,k}$ is the flow leaving cell k on stage j, and r_a^L is the 'area ratio' of the cell under consideration. For a cylindrical geometry, the area ratios are given by

$$(r_a^L)_{k-1} = \frac{a_{k-1}^o}{a_{k-1}^o + a_{k-1}^i} = \frac{k-1}{2 \cdot k - 3} \quad (2.81)$$

and

$$(r_a^L)_{k+1} = \frac{a_{k+1}^i}{a_{k+1}^o + a_{k+1}^i} = \frac{k}{2 \cdot k + 1} \quad (2.82)$$

Here a^o is the outside cylindrical area of the cell under consideration, and a^i is the inside cylindrical area. One can see that apart for some constants, these equations have the same structure. We will now make the simplifying assumption that:

$$\mathcal{K}^L = 1 - \frac{2 \cdot D_r \cdot h_z}{h_r^2} \tag{2.83}$$

With this we assume the amount of flow to go straight down to be equal in both models. Only the ratio of the splitting flows will be slightly different. Zuiderweg *et al.*, (1993) state that the zone/stage model is compatible with the diffusion model only if $\mathcal{K}^L = 2/3$, but based on the above derivation it may be concluded that this is not necessarily true. For a given cell size and radial spreading coefficient one can use Eq. (2.83) to calculate a value for $\mathcal{K}^L$.

For an equidistant square grid one can deduce that:

$$\mathcal{K}^L = 1 - \frac{4 \cdot D_r \cdot h_z}{h_r^2} \tag{2.84}$$

Hoek *et al.* (1986) measured the spreading coefficient for various types of packing and found that the spreading coefficient is strongly dependent on the type of packing and the packing size. Billingham *et al.* (1997) suggest values for the radial spreading coefficients for various types of packing:

1st generation random packings	$D_r = 0.12\ d_p$
2nd generation random packings	$D_r = 0.06\ d_p$
Structured packing	$D_r = 0.0035$

where d_p is the packing size in m.

It should be noted here that, although we have made derivations just for the natural flow model, other flow models may be studied as well with our nonequilibrium Zone Stage model. This may be done by adopting another flow splitting policy.

With respect to the cell sizes and splittting factors, we have to keep in mind that in practice they will be different for columns of different aspect ratios. For small diameter columns, the development of maldistributions along the height of the packing will be different as compared to columns with a larger diameter. In addition, for small diameter columns, the influence of the wall is much more important than for large diameter columns. All of these types of maldistribution may be studied with the presented technique, if the appropriate flow pattern is superimposed on the cell structure.

2.5.1 Characterization of Maldistribution

One of the parameters most commonly used for quantifying the maldistribution is the coefficient of variation for the velocity profile C_v (Billingham *et al.*, 1997).

$$C_v = \sqrt{\frac{1}{A_t} \int \left(\frac{u - \bar{u}}{\bar{u}} \right)^2 dA} \tag{2.85}$$

Where A_t is the total cross sectional area of the column, and the mean velocity $\bar{u}$ is calculated by:

$$\bar{u} = \frac{1}{A_t} \int u dA \tag{2.86}$$

Perry *et al.* (1990) state that a C_v of less than 0.1 for distributors is adequate, provided that the deviations are randomly dispersed. Furthermore, it is assumed that the detrimental effects of small scale maldistributions is compensated for by radial mixing. Therefore, there is no need to take these into account in the evaluation of C_v.

In the most common approach for calculation of C_v, the cross sectional area of a column is split up into a number of cells. The cell size is then chosen in such a way that variations in the velocity profiles within the cell are compensated for by radial mixing. The value of C_v may then be determined by:

$$C_v = \sqrt{\frac{1}{A_t} \sum_{i=1}^{N} A_i \left(\frac{u_i - \bar{u}}{\bar{u}} \right)^2} \tag{2.87}$$

Where N is the total number of cells and $\bar{u}$ is the average velocity over the entire cross sectional area which may be determined by:

$$\bar{u} = \frac{1}{A_t} \sum_{i=1}^{N} A_i \cdot u_i \tag{2.88}$$

This coefficient of maldistribution does not, however, take into account possible clustering of large scale maldistributions. An alternative 'coefficient of maldistribution' was devised by Billingham *et al.* (1997). This new coefficient C_m is evaluated in very much the same way as C_v except that the local mean velocity, rather than the overall mean velocity is used. The coefficient of variation for a cell configuration is given by:

$$C_m = \sqrt{\frac{1}{A_t} \sum_{i=1}^{N} A_i \left(\frac{u_i - \bar{u}_i}{\bar{u}_i} \right)^2} \tag{2.89}$$

Here $\bar{u}_i$ is the local mean velocity which is calculated from:

$$\bar{u}_i = \frac{\sum \delta_{ij}(A_i u_i + A_j u_j)}{\sum \delta ij (A_i + A_j)} \tag{2.90}$$

Where $\delta_{ij} = 1$ if i and j are neighbors, and $\delta_{ij} = 0$ if i and j are not located next to each other. One should note here that when flow variations are about uniformly distributed over the cross sectional area, the values of C_v and C_m do not differ very much. However, if the maldistributions are clustered, the value of C_m will be much lower than the value of C_v. For simplification of the interpretation, a Maldistribution Index, MI is defined by (Billingham *et al.*, 1997):

$$MI = \frac{C_v}{C_m} \tag{2.91}$$

This maldistribution index is a measure of the clustering of maldistributions. If MI is close to unity, maldistributions will be distributed evenly over the cross sectional area. A larger value of MI indicates clustering of the large scale maldistributions.

The above methods help to characterize the initial flow maldistributions, but they do not provide much insight into the depth to which the maldistribution persists. This was pointed out by Edwards *et al.* (1998) who developed a method for the prediction of the maldistribution depth of penetration l_m. This is defined as the depth into the packing over which the coefficient of variation exceeds a design limit. The method is based on solving a simplified flow model, and is strongly correlated to the maldistribution index of Billingham *et al.* (1997). These indices do give some indication on the degree of maldistribution of the phases in a packed column. However, they do not say anything about the effect of these maldistributions on the packing efficiency and, hence, on the distillation process.

2.5.2 Stage Equations - Packed columns

The stage equations for a packed column are not much different from the stage equations for a tray column. For each 'slice' or 'stage' we can write a set of mass and energy conservation equations that organizes the calculation of the interstage flows.

For each stage we have:

$$(1 + r_j^L) \cdot L_j^S - \sum_{k=1}^{n^Z} L_k^C = 0 \tag{2.92}$$

In which L_j^S represents the stage liquid flow leaving stage j, and L_k^C represents the liquid flows coming from the cells on stage j. n^Z is the number of cells on a stage and r_j^L is the ratio of the liquid side stream flow rate to the stage liquid flow rate. This value is nonzero if stage j has a liquid side-drawoff, otherwise it is zero. Similarly, we have an expression for the stage vapor flow.

$$(1 + r_j^V) \cdot V_j^S - \sum_{k=1}^{n^Z} V_k^C = 0 \tag{2.93}$$

Here, V_j^S is the stage vapor flow leaving stage j and V_k^C is the vapor flow coming from cell k on stage j. In addition we have the stage component balance equations for the liquid and vapor phase respectively. r_j^V is the vapor side drawoff ratio, which is nonzero if stage j has a vapor side drawoff.

$$(1 + r_j^L) \cdot x_{i,j}^S \cdot L_j^S - \sum_{k=1}^{n^Z} x_{i,k}^C \cdot L_k^C = 0 \tag{2.94}$$

$$(1 + r_j^V) \cdot y_{i,j}^S \cdot V_j^S - \sum_{k=1}^{n^Z} y_{i,k}^C \cdot V_k^C = 0 \tag{2.95}$$

In the above equations, $x_{i,j}^S$ and $y_{i,j}^S$ are the liquid and vapor mole fractions of component i leaving stage j. $x_{i,k}^C$ and $y_{i,k}^C$ are the liquid and vapor phase mole fractions of component i leaving cell k. In addition, we have the enthalpy balance equations

for each phase.

$$(1 + r_j^L) \cdot H_j^{SL} \cdot L_j^S - \sum_{k=1}^{n^Z} H_k^{CL} \cdot L_k^C = 0 \tag{2.96}$$

$$(1 + r_j^V) \cdot H_j^{SV} \cdot V_j^S - \sum_{k=1}^{n^Z} H_k^{CV} \cdot V_k^C = 0 \tag{2.97}$$

H_j^{SL} and H_j^{SV} are the liquid and vapor enthalpies of the streams leaving the stage. H_k^{CL} and H_k^{CV} are the enthalpies of the streams leaving cell k on the stage. To complete the stage equations we have the stage hydraulic equation.

$$p_j - p_{j-1} - (\Delta p_{j-1}) = 0 \tag{2.98}$$

Where p_j and p_{j-1} are the stage pressures on stages j and $j-1$ respectively. Δp_{j-1} is the pressure drop per slice from stage $j-1$ to stage j. The pressure drop over the stage is considered to be a function of the stage flows, the fluid physical properties (such as densities and surface tension) and the packing type. This completes the definition of the equations required for the stage flows, compositions, temperatures and pressures.

Feedstreams do not appear in the stage equations.

2.5.3 Radial Flow Model

In the classical zone-stage model as presented by Zuiderweg *et al.* (1993), it is assumed that a stage is split up in a number of annular zones. This is illustrated in Fig. 2.7. A fraction $\mathcal{K}^L$ out of the liquid stream in every zone flows downward, while the remaining fraction flows sideways to the adjacent zones. The flow coming in from the adjacent cells has to be weighted by the ratio of the 'inside' and 'outside' interfacial areas of the cell. If the liquid comes from the 'inner' annular space, we need to multiply the flow by the relative fraction of the 'outside area' of the inner annular space. This is given by

$$r_k^{ao} = \frac{a_k}{a_k + a_{k-1}} = \frac{r_k}{r_k + r_{k-1}} = \frac{k}{2k-1} \tag{2.99}$$

Similarly, if the liquid comes from the cell 'outside' the cell under consideration, we have to multiply by the 'inside area fraction' of the cell.

$$r_k^{ai} = \frac{a_{k-1}}{a_k + a_{k-1}} = \frac{r_{k-1}}{r_k + r_{k-1}} = \frac{k-1}{2k-1} \tag{2.100}$$

This linking patterns also requires some modifications in the cell mass and energy balances. For example In Eq. (2.1), Eq. (2.6) and Eq. (2.8) for the general cell, only the liquid flow from an arbitrary cell 'above' is specified. However, in the radial cell model there is flow from three cells above, and the following substitutions need to be

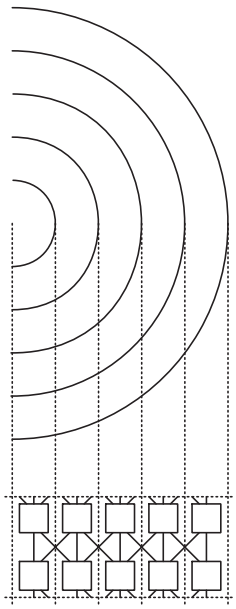

Figure 2.7: Radial mixing model for maldistribution

made. For the mass balance:

$$L_{k-1} \equiv \mathcal{K}^L L_{k,j-1} + (1 - \mathcal{K}^L) \cdot \left(L_{k-1,j-1} \cdot r^{ao}_{k-1} + L_{k+1,j-1} \cdot r^{ai}_{k+1} \right) \tag{2.101}$$

For the component balance:

$$L_{k-1} \cdot x_{i,k-1} \equiv \mathcal{K}^L L_{k,j-1} \cdot x_{i,k,j-1} + (1 - \mathcal{K}^L)$$

$$\cdot \quad \left(L_{k-1,j-1} \cdot x_{i,k-1,j-1} \cdot r^{ao}_{k-1} + L_{k+1,j-1} \cdot x_{i,k+1,j-1} \cdot r^{ai}_{k+1} \right) \tag{2.102}$$

And for the energy balance:

$$L_{k-1} \cdot H^L_{k-1} \equiv \mathcal{K}^L L_{k,j-1} \cdot H^L_{k,j-1} + (1 - \mathcal{K}^L)$$

$$\cdot \quad \left(L_{k-1,j-1} \cdot H^L_{k-1,j-1} \cdot r^{ao}_{k-1} + L_{k+1,j-1} \cdot H^L k+1, j-1 \cdot r^{ai}_{k+1} \right) \tag{2.103}$$

Similar considerations apply for the vapor flows.

Furthermore, it is assumed in the ideal case that any feed, the liquid reflux, and the reboiled vapor flow will be distributed equally over the cross sectional area of the column. Thus, only a fraction, r_k^A which is the ratio of the cross sectional annular area to the total column cross sectional area, will be supplied to cell k on stage j. The area ratio r_k^A is given by:

$$r_k^A = \frac{\pi r_k^2 - \pi r_{k-1}^2}{\pi R^2} = \frac{k^2 - (k-1)^2}{(n^Z)^2} = \frac{2k-1}{(n^Z)^2} \tag{2.104}$$

r_k and r_{k-1} are the outside and inside radius of the annular cell under consideration. R is the column radius. The cell feed rates in Eq. (2.1), Eq. (2.6) and Eq. (2.8) may be determined from the stage feed rates and the area ratio:

$$F_k^L = r_k^A \cdot F_j^L \tag{2.105}$$

and

$$F_k^V = r_k^A \cdot F_j^V \tag{2.106}$$

The liquid streams entering the cells on the first stage, and the vapor streams entering the cells on the last stage are determined by similar relations:

$$L_k^C = r_k^A \cdot L_1^S \tag{2.107}$$

and

$$V_k^C = r_k^A \cdot V_{ns}^S \tag{2.108}$$

Maldistribution patterns in any of the streams supplied to the packing may be modeled by adjusting the r_k^A factors.

2.5.4 Square Grid Model

It may be clear that the radial model as outlined above may be used only for studying maldistributions that, by themselves are radial. For studying other maldistribution patterns we will use a square grid, in which we will have a flow distribution as depicted in Fig. 2.6. The liquid from each square cell flows to 5 different cells on the next layer. Once again, we assume that a fraction $\mathcal{K}^L$ flows straight down to the cell directly below and a fraction $1-\mathcal{K}^L$ is split up in four streams. Of this latter fraction another fraction, $\mathcal{K}_x^L$, is distributed equally over the two cells 'east' and 'west' of the cell under consideration. The other fraction $\mathcal{K}_y^L = 1 - \mathcal{K}_x^L$ is distributed equally over the cells 'north' and 'south' of the cell under consideration. For random packings, $\mathcal{K}_x$ will be 0.5, resulting in equal quantities going to all cells. For structured packings, there will be a preferred flow direction in either north-south or east-west direction, resulting in different values of $\mathcal{K}_x^L$ and $\mathcal{K}_y^L$. In a normal column with structured packing, the preferred flow direction of the packing will switch every so often. This can be taken into account by switching the values of $\mathcal{K}_x^L$ and $\mathcal{K}_y^L$ on the appropriate stages.

2.5.5 Redistribution

In practice, liquid will be redistributed over the cross sectional area of the column every 2 - 4 m of packing, depending on packing type, flow conditions etc. This is to insure that possible maldistributions arising due to a bad initial distribution of the reflux, or packing anisotropy cannot propagate through the entire column. In our model we may redistribute the liquid at specified stages. Redistribution itself can also be a source of maldistribution, which may be modeled by specifying a maldistribution pattern for the redistributor.

2.5.6 Hydrodynamics

When using a zone stage description of a distillation column, one should keep in mind that local differences in concentrations and flow densities etc. will lead to local differences in various hydrodynamic parameters as well. Most notably the vapor/liquid interfacial areas and holdups, and to a lesser extent the mass transfer coefficients. For calculation of the mass transfer rates, local differences of the last two factors may safely be neglected. It has often been stated that the detrimental effect of maldistribution in packed columns is largely due to the loss of interfacial area due to liquid and vapor channelling. For correct prediction of column behavior it is, therefore,

important to evaluate the vapor/liquid interfacial area for each cell individually. In the proposed model, the interfacial areas are evaluated for each cell using local cell flow rates and averaged physical properties.

The approach outlined above will allow us to model maldistribution only to a certain extent. The most common correlations for interfacial areas, holdups etc. were not derived at, and were not meant to be applied to the hydrodynamic conditions that will arise locally in cases of severe maldistribution. The model is, therefore, applicable only to cases of moderate maldistribution, in which we do not have complete flooding or drying of the packing.

In addition, the fact that flow profiles are generated based on an imposed flow splitting policy, means that we cannot account for changes in vapor flow profiles due to maldistributed liquid flows and vice versa.

2.6 Reboiler and Condenser

The reboiler and condenser will be modeled as equilibrium stages. For each equilibrium stage the total mass balance is given by:

$$L_j^S - L_{j-1}^S + V_j^S - V_{j+1}^S - F_j + \sum_{l=1}^{r} \left(\sum_{i=1}^{c} \nu_{i,l} \right) R_{l,j} \cdot \epsilon_j = 0 \tag{2.109}$$

The individual component balances are given by:

$$L_j^S \cdot x_{i,j}^S - L_{j-1}^S \cdot x_{i,j-1}^S + V_j^S \cdot y_{i,j}^S - V_{j+1}^S \cdot y_{i,j+1}^S - f_{i,j} + \sum_{m=1}^{r} \nu_{i,m} \cdot R_{m,j} \cdot \epsilon_j = 0 \quad (2.110)$$

The overall energy balance of an equilibrium stage is given by:

$$L_j^S \cdot H_j^{LS} - L_{j-1}^S \cdot H_{j-1}^{LS} + V_j^S \cdot H_j^{VS} - V_{j+1}^S \cdot H_{j+1}^{VS} - H^F \cdot F_j + Q_j = 0 \quad (2.111)$$

In addition, phase equilibrium is assumed between the two bulk phases:

$$y_{i,j}^S - K_{i,j} x_{i,j}^S = 0 \quad (2.112)$$

The mole fractions of both phases should sum up to 1. These summation equations may be combined to give:

$$\sum_{i=1}^{c} x_{i,j}^S - \sum_{i=1}^{c} y_{i,j}^S = 0 \quad (2.113)$$

The pressure in the reboiler may be calculated from:

$$p_j - p_{j-1} - (\Delta p_{j-1}) = 0 \quad (2.114)$$

The pressure of the condenser has to be specified:

$$p_1 - p_{spec} = 0 \quad (2.115)$$

2.7 Model System

2.7.1 Variables

We will first determine the variables for which we have to solve the model equations. Subsequently we will list the equations to be solved. The variables for each nonequilibrium stage are listed in Table 2.1. The variables related to the dusty fluid model are listed in Table 2.2. The number of variables per equilibrium stage is listed in Table 2.3.

The total number of stage variables is $(2 \cdot c + 5)$. The total number of cell variables per cell $(6 \cdot c + 5 + n_1 \cdot (2 \cdot c + 1) + n_2 \cdot (c + 1))$. For the simplest system with an homogeneous reaction, just using one cell per stage and just one discretisation point in both mass transfer films there are $(11 \cdot c + 12)$ variables per stage.

The use of the Dusty Fluid equations, using n_3 discretisation points in the liquid film around the catalyst, and using n_4 discretisation points inside the catalyst, leads to an additional $c + n_3 \cdot (c + 1) + n_4 \cdot (2 \cdot c + 2)$ variables.

The reboiler and condenser (if present) are modeled as equilibrium stages. The variables on the equilibrium stages are summarized in Table 2.3. For each equilibrium stage there are $(2 \cdot c + 5)$ variables per stage.

Flows from each stage	Flowrates	L_j^S and V_j^S	2
	Compositions	$x_{i,j}^S$ and $y_{i,j}^S$	$2 \cdot c$
	Temperatures	T_j^{SL} and T_j^{SV}	2
	Stage pressure	p_j	1
Each cell	Cell flowrates	L_k^C and V_k^C	2
	Compositions	$x_{i,k}^C$ and $y_{i,k}^C$	$2 \cdot c$
	Temperatures	T_k^{CL} and T_k^{CV}	2
	Mass transfer rates	$N_{i,k}^C$	c
Liquid transfer film	Composition	$x_{i,k}^C$	$c \cdot n_1$
n_1 *discretisation points*	Mass transfer rates	$N_{i,k}$	$c \cdot n_1$
	Temperatures	T_k^C	n_1
Vapor transfer film	Composition	$y_{i,k}^C$	$c \cdot n_2$
n_2 *discretisation points*	Temperature	T_k^C	n_2
Interface	Composition	$x_{i,k}^{IC}$ and $y_{i,k}^{IC}$	$2 \cdot c$
	Mass transfer rates	$N_{i,k}$	c
	Temperature	T_k^C	n_2

Table 2.1: Variables for a nonequilibrium stage

Bulk of each cell	Catalyst mass transfer rates	$\mathcal{N}_{i,k}^{S}$	c
for the liquid transfer film	Composition	$x_{i,k}$	$c \cdot n_3$
n_3 *discretisatoin points*	Temperatures	T_k	n_3
Inside the catalyst	Composition	$x_{i,k}$	$c \cdot n_4$
n_4 *discretisation points*	Temperatures	T_k	n_4
	Catalyst mass transfer rates	$\mathcal{N}_{i,k}^{C}$	$c \cdot n_4$
	Catalyst pressure	p	n_4

Table 2.2: Variables related to the dusty fluid model

Stage flows	L_j^S and V_j^S	2
Compositions	$x_{i,j}^S$ and $y_{i,j}^S$	2c
Temperatures	T_j^S	1
Stage pressure	p_j	1
Heat duty	Q_j	1

Table 2.3: Variables for an equilibrium stage

2.7.2 Equations

The equations to be solved for each nonequilibrium cell are listed in Table 2.4. The equations for the Dusty Fluid model description of heterogeneous reactions are listed in Table 2.5.

For each stage we now have $(2 \cdot c + 5)$ equations, and for each cell we have $(6 \cdot c + 5 + n_1 \cdot (2 \cdot c + 1) + n_2 \cdot (c + 1))$ equations, and for the catalyst and transfer film around it, we have $(c + n_3 \cdot (c + 1) + n_4 \cdot (2 \cdot c + 2))$ equations. The equations for the reboiler and condenser are listed in Table 2.6. For each equilibrium stage we now have $2c + 4$ equations.

2.7.3 Degrees of Freedom Analysis

The resulting total number of variables and equations for an entire column of n_s stages, n_c cells per stage, using n_1 discretisation points in the liquid film, and n_2 discretisation points in the vapor film, n_3 discretisation points in the liquid film around the catalyst, and n_4 discretisation points inside the catalyst, for a c component system then becomes: $n_s \cdot (2 \cdot c + 5 + n_c \cdot (7 \cdot c + 5 + n_1 \cdot (2 \cdot c + 1) + n_2 \cdot (c + 1) + n_3 \cdot (c + 1) + n_4 \cdot (2 \cdot c + 2))$. Thus, there are no degrees of freedom for the nonequilibrium stages.

For each stage		
Mass conservation equations	Eq. (2.92) and Eq. (2.93)	2
Component conservation equations	Eq. (2.94) and Eq. (2.95)	$2 \cdot c$
Energy conservation equations	Eq. (2.96) and Eq. (2.97)	2
hydraulic equation	Eq. (2.98)	1
For each cell		
Mass conservation equations	Eq. (2.1) and Eq. (2.2)	2
Component conservation equations	Eq. (2.6) and Eq. (2.7)	$2 \cdot c$
Energy conservation equations	Eq. (2.8) and Eq. (2.9)	2
For the liquid and vapor transfer films		
Mass transfer correlations	Eq. (2.10) and Eq. (2.11)	$(c-1) \cdot (n_1 + n_2 + 2)$
Summation equations	Eq. (2.12) and Eq. (2.13)	$n_1 + n_2$
Species conservation equations	Eq. (2.14)	$c \cdot (n_1 + 1)$
Energy transfer equations	Eq. (2.17) and Eq. (2.18)	$n_1 + n_2$
For the interface		
Interface equilibrium equations	Eq. (2.19)	c
Interface summation equations	Eq. (2.21) and Eq. (2.22)	2
'Bootstrap' equation	Eq. (2.24)	1

Table 2.4: Equations for a nonequilibrium stage

For the liquid film n_3 discretisation points		
Mass transfer correlations	Eq. (2.25)	$(c-1)\cdot n_3$
Summation equation	Eq. (2.26)	n_3
Energy transfer equation	Eq. (2.27)	n_3
For the catalyst n_4 discretisation points		
Dusty Fluid Equations	Eq. (2.44)	$c\cdot(n_4-1)$
Summation equation	Eq. (2.26)	n_4-1
Reaction equation	Eq. (2.49)	$n_4\cdot(c-1)$
'Bootstrap' equation	Eq. (2.48)	n_4
Energy transfer equation	Eq. (2.50)	n_4-1
Boundary conditions	Eq. (2.52) and Eq. (2.53)	$2\cdot c+2$

Table 2.5: Equations related to the dusty fluid model

Total mass conservation equation	Eq. (2.109)	1
Total component conservation equation	Eq. (2.110)	c
Total energy conservation equation	Eq. (2.111)	1
Equilibrium equations	Eq. (2.112)	c
Summation equation	Eq. (2.113)	1
pressure equation	Eq. (2.114) or Eq. (2.115)	1

Table 2.6: Equations for an equilibrium stage

For the condenser and the reboiler we have $2 \cdot c + 5$ variables and $2 \cdot c + 4$ equations, resulting in one degree of freedom for each stage. These are implemented by replacing the energy balance by a specification on for instance the reflux ratio, the bottom product flowrate etc.

2.7.4 Additional Specifications

The additional specifications required for a complete column simulation with the new nonequilibrium model are detailed below.

- **Configuration**

The configuration of the column needs to be fixed. This requires specification of the number of trays, reboiler type (if any), condenser type (if any), and the number of feeds and their locations the number and location of any sidestreams and the external heat duties (if any).

- **Pressure model and condenser pressure**

  The condenser pressure has to be specified. In addition it is common practice to give an independent specification for the pressure of the top stage, as, depending on the design, the top stage pressure may be very different from the condenser pressure. Furthermore, a pressure drop model for the nonequilibrium stages is required. Possible options are:

  - Zero pressure drop. All stages in the column operate at the specified top stage pressure.
  - Fixed pressure drop. The stage pressure drop is specified. The stage pressure is evaluated using Eq. (2.74).
  - Fixed Bottom pressure. With the top and bottom pressures fixed, the pressures on all other stages are evaluated by means of interpolation.
  - Estimated pressure drop. A value for the pressure drop is estimated from a semi empirical correlation. For bubble cap trays, the correlation due to

Bolles (1963) is used, for sieve trays the correlation due to Bennett *et al.* (1983) is used. The stage pressure is evaluated using Eq. (2.74).

- **Feeds**

  Specification of the flow rate, composition and thermodynamic state of each feed are required. The latter can be determined after specification of any two of the following three parameters: Temperature, pressure and vapor fraction.

- **Thermodynamic models and Physical properties**

  Specification of a thermodynamic model is required for the calculation of, among other things, vapor-liquid equilibrium ratios, reaction rates, enthalpies and chemical potential gradients. In addition, a nonequilibrium model requires information about physical properties such as surface tension, density and heat capacity, for evaluation of parameters such as the mass transfer coefficients, pressure drops and interfacial areas. A more complete listing of the available property models can be found in Taylor *et al.*, (1994).

- **Design**

  Some of the quantities appearing in the equations given above depend on the internals design and configuration (pressure drop, vapor-liquid interfacial area, reaction volume, mass and heat transfer coefficients). This inevitable link between

design and model equations is discussed extensively by Taylor et al. (1994) and they point out that the nonequilibrium model can only be used for an existing column. To alleviate this problem, they proposed an integration of a design procedure together with the model equations. During the calculations, a design is evaluated based on calculated liquid and vapor flows and physical properties. The same approach is adopted in our model. For more details about the design mode, see Taylor et al. (1994) and Kooijman (1995). At the very least one is required to specify the internals type, although specification of detailed designs remains a possibility.

- **Mass and heat transfer model**

  The binary pair mass transfer coefficients are calculated from empirical correlations (Taylor and Krishna, 1993). In the calculations presented in this work, the AIChE (1958) correlation was used. For calculation of the vapor phase heat transfer coefficients, the Chilton-Colburn analogy between mass and heat transfer is used. For the calculation of the liquid heat transfer coefficients, the penetration theory is used.

- **Discretisation Points**

In addition, the number of discretisation points in the vapor and liquid transfer films needs to be fixed. In choosing the number of discretisation steps we would like to combine accuracy and calculation speed. In nonreactive systems, where concentration gradients are typically not very large, one or two discretisation points in both the vapor and liquid transfer films are usually sufficient. In these cases, the model by Kooijman and the model presented here give the same results. For systems with reactions, or for systems with strong thermal effects in mass transfer, more points should be specified. In the presented calculations we have used 5 points in both the vapor and the liquid film.

- **Homogeneous Reaction**

  A reaction rate expression along with kinetic parameter data are required for evaluation of the reaction rates. For calculation of the reaction volume in pseudo-homogeneous systems, the total catalyst mass present on a stage, and the catalyst activity have to be specified. For a homogeneous system, the reaction can take place in the liquid bulk and in the liquid transfer film. The reaction volume of the liquid bulk is taken to be the total liquid inventory on a tray. This is obtained by multiplying the clear liquid height by the active tray area. The clear liquid height is calculated from the semi empirical correlation due to Bennet *et al.* (1983). The film volume is the product of the interfacial

area and the liquid film thickness, which is obtained from:

$$\delta^L = \frac{\bar{\kappa}}{\bar{\bar{D}}} \tag{2.116}$$

In which $\bar{\kappa}$ and $\bar{\bar{D}}$ are averaged values for the binary pair mass transfer and diffusion coefficients.

- **Catalyst properties**

  In the dusty fluid model there are several parameters that need to be known in order that a simulation can be carried out. The following catalyst data needs to be known beforehand:

  - Specific catalyst area, a^C
  - Catalyst porosity, ϵ^C
  - Catalyst tortuosity, τ^C
  - Catalyst mean pore size, d_p
  - Catalyst thermal conductivity, λ^C

  The porosity and tortuosity are required for evaluation of the catalyst diffusion coefficients. The mean pore size is required for evaluation of the catalyst permeability. The catalyst thermal conductivity is required for calculation of the conductive contribution of the catalyst matrix to heat transfer inside the

catalyst particles. In addition, the number of discretisation steps inside and around the catalyst needs to be fixed. In this work, two discretisation points were used for the liquid transfer film around the catalyst, and 20 points were used inside the catalyst.

Inside the catalyst, nonideal component behavior will be influenced by the catalyst itself. For a consistent description one should incorporate the effect of the catalyst into evaluation of the chemical potential gradients. No suitable model for this is available. For evaluation of the chemical potential gradients a conventional activity coefficient model will be used.

Estimation of the mass transfer coefficients and of the physical properties for the vapor/liquid transport process is discussed at length by Taylor and Krishna (1993). For mass transfer from the liquid bulk to the catalyst phase the correlations due to Van Krevelen and Krekels (1948) were used. These are:

$$\frac{\kappa_{i,j}^{LS}}{\mathcal{D}_{i,j}^{L} a^{C}} = 1.8 \cdot \left(\frac{\rho^{L} u^{L}}{\eta^{L} a^{C}}\right)^{1/2} \cdot \left(\frac{\eta^{L}}{\rho^{L} \mathcal{D}_{i,j}^{L}}\right)^{1/3} \tag{2.117}$$

Under the condition that:

$$0.013 < \frac{\rho^{L} u^{L}}{\eta^{L} a^{C}} < 12.6 \tag{2.118}$$

The binary pair Maxwell-Stefan diffusion coefficients ($Đ^{e}_{i,j}$) are related to the free diffusion binary pair Maxwell Stefan diffusion coefficients by:

$$Đ^{e}_{i,j} = \frac{\epsilon}{\tau} Đ_{i,j} \tag{2.119}$$

Where ϵ is the catalyst porosity and τ is the catalyst tortuosity. The catalyst porosity and tortuosity are added here to take into account the tortuous paths followed by the fluid in the catalyst. Consider the case of very large pores, where the effects of the walls will be negligible. This assumption is valid for the macroporous catalysts used by Sundmacher *et al.* (1994a), as it will be in most cases. In this case, one could argue that we are basically dealing with a simple free diffusion problem. The diffusion coefficients would be the normal liquid phase Maxwell Stefan diffusion coefficients, corrected by the catalyst tortuosity and porosity as in Eq. (2.119). Berg and Harris (1993) and Sundmacher and Hoffmann(1992) have used this approach but these authors have ignored the last term on the right hand side of equation (28). There is no available theory for estimation of D^{e}_{i} for liquid diffusion inside porous particles. In the calculations presented later in this thesis we consider two limiting cases: (a) one in which D^{e}_{i} is large, in which case the last term can be ignored (corresponding to Berg-Harris and Sundmacher approaches), and (b) one in which D^{e}_{i} is a factor five times smaller than the smallest of the $Đ_{i,j}$ values. D^{e}_{i} is assumed to be the

same for all components.

Diffusion coefficients normally are concentration dependent. Thus, they should be dependent on the concentration and the physical properties of the dust species. Any such dependence is, however, neglected here due to the absence of any reliable estimation method.

- **Tray columns**

  The following degrees of freedom result from the cell description of tray columns:

  - Number of cells in a liquid flow branch
  - Number of cells in a vapor flow branch
  - Mixing flow rate.

  The number of cells in both flow paths depends on the flow model under consideration. The appropriate number of cells depends on the configuration and operating conditions used. In a column simulation, one would typically first do column calculations without assuming staging in the liquid flow direction. From these calculations one can obtain information about the hydrodynamic conditions on the stages. These can be used to evaluate an axial dispersion coefficient, employing a semi-empirical correlation. These axial dispersion coefficients can be used to estimate the number of cells required for description of

flow behavior on a distillation tray. The vapor stream is normally assumed to be in plug flow and may be modeled by using at least 5 cells in the vapor flow direction.

The vertical liquid mixing flow rate should be such that the bulk liquid concentrations of all cells in a vapor foot path are equal. This is usually satisfied if the mixing flow rate is taken to be 10 times the stage flow rate.

- **Packed Columns**

  The following degrees of freedom result from the cell description of tray columns:

  - Cell layout pattern
  - Cell sizes
  - Liquid Splitting factor
  - Vapor Splitting factor
  - Maldistribution pattern
  - Redistribution stages

  First the cell layout pattern has to be fixed. Subsequently the cell sizes may be calculated, and based on the packing type and the radial spreading coefficient, splitting factors for both vapor and liquid phases may be evaluated using

Eq. (2.83) or Eq. (2.84).

The most likely sources for maldistribution of vapor and liquid are found at inlets. Most notably the reflux and reboiler inlet and, to a lesser extent the feed inlet. In the zone stage model as presented we assume, in the ideal case, that reflux, reboil and feed streams are distributed equally over the cross sectional area of the packing. Maldistributions may be introduced by redirecting the flow according to specified maldistribution patterns. This may be done by assigning weighing factors to the values of r_k^A in Eq. (2.105) to Eq. (2.108).

The redistribution stages and appropriate distribution patterns for these redistribution stages have to be defined.

2.8 Solution Methods

2.8.1 Newton's Method

Krishnamurthy and Taylor (1985) and Kooijman and Taylor (1995) employed a simultaneous correction strategy using Newton's method for solving the model equations. We shall do the same. If we denote our system of equations by

$$\bar{F}(\bar{x}^*) = 0 \tag{2.120}$$

Then the solution to our problem is given by $\bar{x}^*$. If we have a current estimate x^k, for which this equation is not satisfied, then the correction factors for the next estimate may be obtained by solving the following linearized system

$$[J^k] \cdot (\bar{x}^{k+1} - \bar{x}^k) = -\bar{F}(\bar{x}^k) \tag{2.121}$$

Here $[J^k]$ is the jacobian matrix with elements:

$$J_{i,j} = \frac{\partial F_i(\bar{x})}{\partial x_j} \tag{2.122}$$

By successive calculations of new estimates, we will try to meet any one of the following two criteria

$$\left|\left|\bar{F}(\bar{x}^k)\right|\right| \leq \epsilon \tag{2.123}$$

or

$$\left|\left|\frac{\bar{x}^{k+1} - \bar{x}^k}{\bar{F}(\bar{x}^k)}\right|\right| \leq \epsilon \tag{2.124}$$

The first criterion follows straightforward from Eq. (2.120). The second assumes convergence if the difference between two successive estimates is smaller than the specified tolerance. Convergence is assumed if either one of the above criteria is satisfied.

2.8.2 Continuation Method

Introduction of the reaction in the distillation column model greatly increases the nonlinear interactions and model complexity. A good initial guess is, therefore, very

important in order to insure a high probability of convergence. For normal distillation, the initial guess is based on a stage by stage flash of the feed. However, in reactive distillation, one is normally dealing with a system in which the primary distillation product is not supplied in the feed, but is formed by the reaction. This makes specification of a good initial guess much more difficult.

Because we do not want to depend too much on the quality of the initial guess, the model was equipped with a differential arc length continuation method. This method may be used to obtain a solution to the problem by means of a purely mathematical homotopy. It may also be used to track steady state behavior of the problem as a function of an arbitrary independent model parameter. In the following section we will first focus on the mathematical homotopy, and subsequently discuss the steady state tracking routine.

In a mathematical sense, homotopy continuation methods form a class of methods for solving difficult systems of nonlinear algebraic equations. In addition they can be used for tracking solutions to nonlinear algebraic equations depending on a parameter. The idea behind homotopy methods is that of path following where a path is tracked from a solution to a simple problem to the solution of the difficult problem. The path

is implicitly defined by the homotopy equation:

$$\bar{H}(\bar{x}, t) = 0 \tag{2.125}$$

This homotopy function is a continuous blending of two functions $\bar{F}(\bar{x})$ and $\bar{G}(\bar{x})$, by means of a homotopy parameter t. In the following, $\bar{F}(\bar{x})$ represents the difficult problem, $\bar{G}(\bar{x})$ the easy problem. The class of equations we will be looking at is that of linear convex homotopies given by:

$$\bar{H}(\bar{x}, t) = t \cdot \bar{F}(\bar{x}) + (1 - t) \cdot \bar{G}(\bar{x}) = 0 \tag{2.126}$$

This equation reduces to $\bar{G}(\bar{x}) = 0$ for $t = 0$ and to $\bar{F}(\bar{x}) = 0$ for $t = 1$. If $\bar{F}(\bar{x})$ and $\bar{G}(\bar{x})$ are n-dimensional problems, then $\bar{H}(\bar{x}, t)$ describes a curve in $n+1$ dimensional space going through $\bar{G}(\bar{x}) = 0$ and $\bar{F}(\bar{x}) = 0$ (Wayburn and Seader, 1987).

The choice of $\bar{G}(\bar{x})$ can be quite arbitrary, as long as the problem has the same dimension as the original problem. In our model, we use the Newton homotopy method, for which $\bar{G}(\bar{x})$ is given by:

$$\bar{G}(\bar{x}) = \bar{F}(\bar{x}) - \bar{F}(\bar{x_0}) \tag{2.127}$$

Leading to the homotopy equation:

$$\bar{H}(\bar{x}, t) = \bar{F}(\bar{x}) - (1 - t) \cdot \bar{F}(\bar{x_0}) \tag{2.128}$$

Here $\bar{x_0}$ is an arbitrary starting guess for $\bar{F}(\bar{x})$. This method does not require us to solve an easy problem first, because it is already known. Another important feature is that by specifying different starting guesses, we can generate different paths that can lead to different solutions. This way multiple solutions to $\bar{F}(\bar{x}) = 0$ (if they exist) can be found with relative ease.

The mathematical foundations of the homotopy method are given by the implicit function theorem and the path theorem given by:

> IMPLICIT FUNCTION THEOREM Let $H : \mathbb{R}^{n+1} \to \mathbb{R}^n$ be continuously differentiable, $(\tilde{x}, \tilde{t}) \in H^{-1}$ and H'_x be invertible. Then in a neighborhood of $(\tilde{x}, \tilde{t})$ all points (x, t) that satisfy $H(x, t) = 0$ are on a single continuously differentiable path through $(\tilde{x}, \tilde{t})$.

in which

$$H^{-1} = \{(x, t)|H(x, t) = 0\} \tag{2.129}$$

and H'_x represents the Jacobian

> PATH THEOREM Let $H : \mathbb{R}^{n+1} \to \mathbb{R}^n$ be continuously differentiable and suppose that for every $y \in H^{-1}$, the Jacobian is of full rank, then H^{-1} consists only of continuously differentiable paths.

From the implicit function theorem it follows that $\bar{H}(\bar{x}, t)$ represents a path in $n+1$ dimensional space. If we want to find a solution to $\bar{F}(\bar{x})$ we only have to follow that path from $t = 0$ and $\bar{G}(\bar{x}) = 0$ to $t = 1$ and $\bar{F}(\bar{x}) = 0$. In other words, we have to evaluate how the various variables change along the curve, and correct each accordingly as we walk along the curve. Evaluating how the variables change along the curve can be done by differentiating the homotopy equation with respect with the arclength:

$$\frac{\partial \bar{H}(\bar{x}, t)}{\partial s} = \left[\frac{\partial \bar{F}(\bar{x})}{\partial \bar{x}}\right] \cdot \left(\frac{\partial x}{\partial s}\right) + \bar{F}(\bar{x_0}) \left(\frac{\partial t}{\partial s}\right) = 0 \tag{2.130}$$

In addition we have one extra equation. The changes of the variables are restricted by the change in arc length, which is given by the multidimensional Pythagorean theorem:

$$(dx_1)^2 + (dx_2)^2 + \ldots + (dt)^2 = (ds)^2 \tag{2.131}$$

Which can be rewritten to:

$$\left(\frac{dx_1}{ds}\right)^2 + \left(\frac{dx_2}{ds}\right)^2 + \ldots + \left(\frac{dt}{ds}\right)^2 = 1 \tag{2.132}$$

$\bar{F}(\bar{x_0})$ is an n-dimensional vector and may be added to the Jacobian matrix which

results in the following:

$$\frac{\partial \bar{H}(\bar{x},t)}{\partial s} = \begin{bmatrix} \frac{\partial F_1}{\partial x_1} & \cdots & \frac{\partial F_1}{\partial x_n} & F_1(x_0) \\ \vdots & & \vdots & \vdots \\ \frac{\partial F_n}{\partial x_1} & \cdots & \frac{\partial F_n}{\partial x_n} & F_n(x_n) \end{bmatrix} \cdot \begin{pmatrix} \frac{\partial x_1}{\partial s} \\ \vdots \\ \frac{\partial x_n}{\partial s} \\ \frac{\partial t}{\partial s} \end{pmatrix} = 0 \tag{2.133}$$

This is where the importance of the path theorem becomes clear: In order to be able to solve the above system of equations, the matrix should be of full rank. Then we can choose a partial Jacobian and solve the system. Resulting in the following system:

$$\begin{bmatrix} \frac{\partial F_1}{\partial x_1} & \cdots & \frac{\partial F_1}{\partial x_{i-1}} & \frac{\partial F_1}{\partial x_{i+1}} & \cdots & \frac{\partial F_1}{\partial x_n} & F_1(x_0) \\ \vdots & & \vdots & \vdots & & \vdots & \vdots \\ \frac{\partial F_n}{\partial x_1} & \cdots & \frac{\partial F_n}{\partial x_{i-1}} & \frac{\partial F_n}{\partial x_{i+1}} & \cdots & \frac{\partial F_n}{\partial x_n} & F_n(x_n) \end{bmatrix} \cdot \begin{pmatrix} \frac{\partial x_1}{\partial s} \\ \vdots \\ \frac{\partial x_{i-1}}{\partial s} \\ \frac{\partial x_{i+1}}{\partial s} \\ \vdots \\ \frac{\partial x_n}{\partial s} \\ \frac{\partial t}{\partial s} \end{pmatrix} = - \begin{bmatrix} \frac{\partial F_1}{\partial x_i} \\ \vdots \\ \frac{\partial F_n}{\partial x_i} \end{bmatrix} \cdot \left(\frac{\partial x_i}{\partial s} \right) \tag{2.134}$$

x_i is called the independent variable. This system may be solved using any sparse

matrix solver to give:

$$\begin{bmatrix} 1 & & 0 \\ & \ddots & \\ 0 & & 1 \end{bmatrix} \cdot \begin{pmatrix} \frac{\partial x_1}{\partial s} \\ \vdots \\ \frac{\partial x_{i-1}}{\partial s} \\ \frac{\partial x_{i+1}}{\partial s} \\ \vdots \\ \frac{\partial x_n}{\partial s} \\ \frac{\partial t}{\partial s} \end{pmatrix} = - \begin{bmatrix} \beta_1 \\ \vdots \\ \beta_{i-1} \\ \beta_{i+1} \\ \vdots \\ \beta_n \\ \beta_{n+1} \end{bmatrix} \cdot \frac{\partial x_i}{\partial s} \tag{2.135}$$

This is actually an expression for the changes of all variables along the curve in terms of the change in x_i. The total change in x_i along the curve can now be evaluated using Eq. (2.132). This then leads to

$$\left(\frac{\partial x_i}{\partial s}\right) = \sqrt{\frac{1}{1 + \sum_{k=1}^{n+1} \beta_k^2}} \tag{2.136}$$

Substitution of Eq. (2.136) into Eq. (2.135) then leads to a system of ODE's that is not stiff and may be integrated numerically. This integration gives an estimate of the 'next' point on the curve. The exact location of this point may be determined in a subsequent calculation in which the value of the independent variable is fixed at the newly estimated value. The resulting system of n equations and n variables may be solved with a standard Newton-Raphson technique, using the estimated values as initual guess.

Selection of the independent variable should be such that the resulting Jacobian is of full rank. If the reduced Jacobian is not of full rank, but the augmented Jacobian is, this means that the value of the independent parameter does not change along the curve, indicating a turning point. In practice we will choose the variable that changes most in the previous step.

If the augmented Jacobian is not of full rank, we are at a singular point on the curve, which may indicate the presence of a bifurcation in the homotopy path.

2.8.3 Steady State Tracking

The above development is done for a purely mathematical homotopy given by Eq. (2.128). In fact, the theory of curve tracking is the same for any system of n equations and $n+1$ variables (Kubicek, 1976). Thus, any of the systems we are dealing with may be turned into such a system by treating one of the specifications as a variable. The homotopy equation is then given by:

$$\bar{F}(\bar{x}, y) = 0 \tag{2.137}$$

In which y is an arbitrary specification, for example on the reflux ratio or the bottom product flow rate, which is now treated as a variable. Differentiating this equation with respect to the arc length results in an equation system which is analoguous to

Eq. (2.133):

$$\frac{\partial \bar{H}(\bar{x},t)}{\partial s} = \begin{bmatrix} \frac{\partial F_1}{\partial x_1} & \cdots & \frac{\partial F_1}{\partial x_n} & \frac{\partial F_1}{\partial y} \\ \vdots & & \vdots & \vdots \\ \frac{\partial F_n}{\partial x_1} & \cdots & \frac{\partial F_n}{\partial x_n} & \frac{\partial F_n}{\partial y} \end{bmatrix} \cdot \begin{pmatrix} \frac{\partial x_1}{\partial s} \\ \vdots \\ \frac{\partial x_n}{\partial s} \\ \frac{\partial y}{\partial s} \end{pmatrix} = 0 \tag{2.138}$$

Thus, once a solution at $y = y_0$ is obtained, the homotopy method can be used to track the steady state solution between y_0 and y_1, under the condition that the system has physically realistic solutions in the interval under consideration.

Chapter 3

Reactive Distillation in Tray Columns

In this chapter we will apply the nonequilibrium cell model to Reactive Distillation in tray columns. It is shown that efficiencies are influenced by the chemical reaction, making their a priori prediction difficult. In addition, the influence of staging in both vapor and liquid flow directions is studied by means of various cell configurations. The issue of multiple steady states is discussed, along with its implications for hardware design.

3.1 Introduction

In this chapter various issues related to modeling of reactive distillation will be discussed with the help of three examples. The first example involves the metathesis reaction of 2-pentene to butene and hexene. This example will be used to illustrate the influence of flow patterns on distillation trays on the Reactive Distillation process. In addition, the model system is used to show the influence of chemical reactions on tray efficiencies, underlining the need for nonequilibrium models.

In a second example we will use the nonequilibrium cell model for simulation of a column for separation of water and acetic anhydride. In this column an unwanted reaction takes place between water and acetic anhydride to form acetic acid. The results of the calculations will be compared to some experimental data presented by Marek (1956).

The last example treats the possible application of reactive distillation for production of ethylene glycol. The issue of multiple steady states in distillation columns will be addressed, along with design issues.

3.2 Example 1: Metathesis Reaction

The first example under consideration is a reactive system that is similar to one considered by Okasinski and Doherty (1998). The following reaction takes place:

$$2A \rightarrow B + C \tag{3.1}$$

A typical reaction system fitting this scheme is the metathesis reaction of 2-pentene to 3-hexene and 2-butene. Reaction kinetic data were taken from Hughes (1970). An overall reaction rate expression is given by (Okasinski and Doherty, 1998):

$$R_i = \nu_i \cdot (k_f \cdot x_{c5}^2 - k_b \cdot x_{c4} \cdot x_{c6}) \tag{3.2}$$

with the following rate constants:

$$k_f = 78.2 \cdot e^{\left(-\frac{27.6 \cdot 10^3}{\mathcal{R} \cdot T}\right)} [s^{-1}] \tag{3.3}$$

and,

$$k_b = 312.8 \cdot e^{\left(-\frac{27.6 \cdot 10^3}{\mathcal{R} \cdot T}\right)} [s^{-1}] \tag{3.4}$$

The following configuration is used: A 25 stage column with a liquid feed of pure 2-pentene to stage 13 (counting from the top). The feed rate is fixed at 10 mol/s. The condenser and column top pressure are fixed at 101.3 kPa, while the stage pressure drop is calculated with the correlation due to Bennett *et al.* (1983). The top product

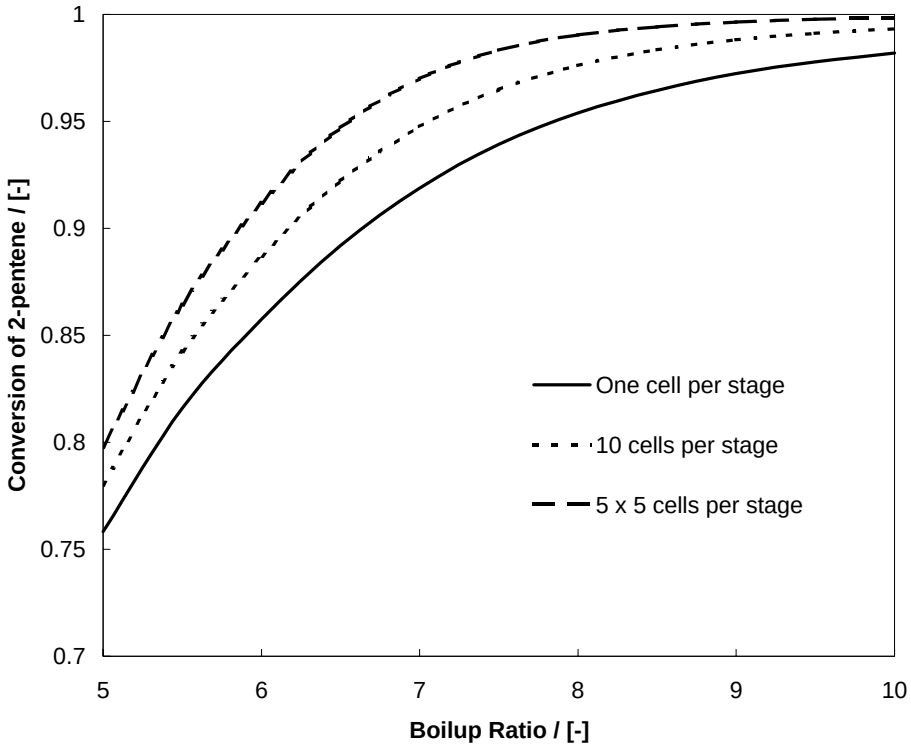

Figure 3.1: Conversion as a function of boilup ratio for various flow models

flow rate was fixed to half the feed rate. The boilup ratio was varied in a parametric study, as was the number of cells. For calculation of thermodynamic properties the Peng-Robinson equation is used. Reaction rates are calculated using the kinetic expressions as given by Eq. (3.2) to Eq. (3.4). Mass transfer coefficients are evaluated using the AIChE (1958) method.

3.2.1 Calculations

Calculations were done for the above column, in which the boilup ratio was varied from 5 to 10. The cell configurations used were: (1) A single cell per stage (corresponding to both phases perfectly mixed), (2) a single column of cells (approximating vapor plug flow through a well mixed pool of liquid) and (3) Multiple columns of cells (approximating vapor rising in plug flow through the liquid in plug flow across the tray).

All calculations were done in design mode, using single pass sieve trays with conventional downcomers. The calculated column diameters range between 1 m for a boil-up ratio of 5 and 1.3 m for a reflux ratio of 10. The presented results do not, therefore, apply to a single column. The calculated flow path lengths range between 0.78 m and 0.91 m. Fig. 3.1 shows the conversion of butene as a function of the reflux ratio for the three flow models. The differences between the models are quite substantial, especially since reactive distillation is a high purity business. The best performance is obtained with cell configuration 3. Increasing the reflux ratio should be avoided at all costs since it will require a larger column and additional reboiler and condenser duties. This means that for this process a column with one longer flowpass is to be desired over a column with more flowpasses.

3.2.2 Cells or Not

It would be useful to know, if this very detailed way of describing the reaction and mass transfer processes is really required. The calculations become substantially more time consuming on adding more and more cells. Thus, we need to determine the exact influence of the cell description on the overall production rate, particularly for the liquid flow models. Two different effects need to be separated here. First, the effect of staging in the liquid flow direction on mass transfer, and second, the effect of staging on the local concentrations along the liquid flow path, and, through that, on the production rates. If the influence of the latter is not significant, a much smaller model may give usable results.

Such a smaller model may be obtained by extending the model of Taylor *et al.* (1994) to take into account chemical reactions. Assuming the reaction takes place only in the bulk liquid, only the overall mass and component balances for the liquid phase have to be modified. This implicitly assumes there is no direct interaction between mass transfer and reaction.

Shown in Fig. 3.2 is the conversion of 2-pentene as a function of the reflux ratio, assuming vapor and liquid plug flow, for both models. The differences are small and will, in the high conversion region, fall within the range of accuracy for both models.

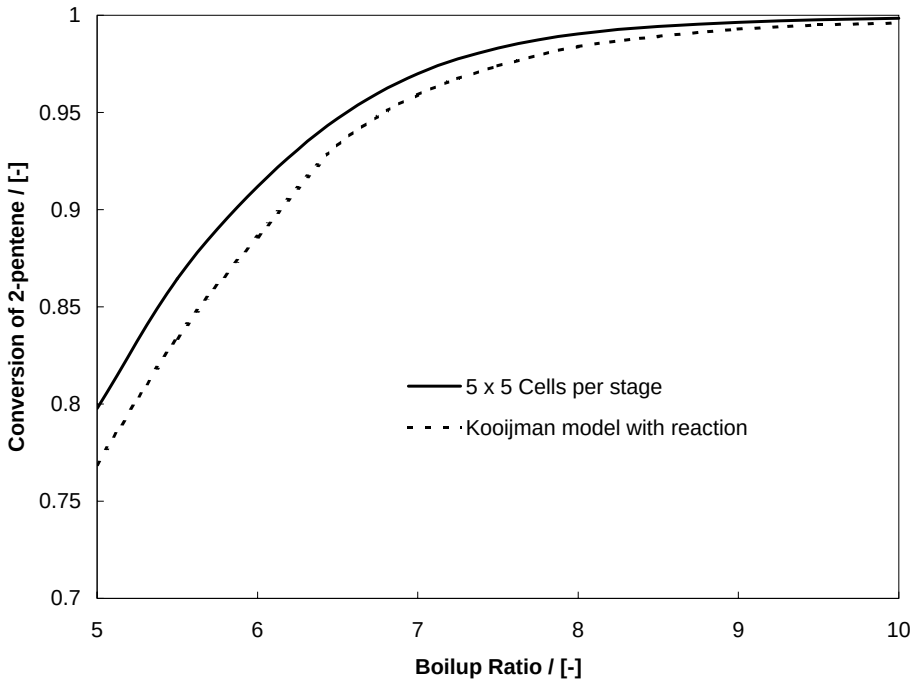

Figure 3.2: Comparison of Cell model to modified Kooijman (1995) model extended with bulk liquid reaction

Although the simplified model has some fundamental weaknesses, it may in some cases offer a fast alternative to the cell model. Some caution is in order however: The simplified model should not be used for systems in which very fast reactions occur, such as acid gas stripping. In such cases mass transfer is very strongly influenced by the reaction.

3.2.3 Nonequilibrium Model vs. Equilibrium Model

Based on the previous observations one might argue that it is possible to save even more calculation time by reverting to an equilibrium stage approach. There are, however, some fundamental objections to this approach. The most important one is the fact that there is no correct way of linking a theoretical equilibrium stage to a real tray. This is normally done by means of an efficiency factor, and the most commonly used is the Murphree vapor phase efficiency defined by:

$$E^{MV} = \frac{y_{i,j} - y_{i,j+1}}{y^*_{i,j} - y_{i,j+1}} \tag{3.5}$$

In which $y_{i,j+1}$ is the composition of the vapor below the tray, $y_{i,j}$ is the composition of the vapor above the tray, and $y^*_{i,j}$ is the concentration of vapor that would be in equilibrium with the liquid bulk on the tray. This may be replaced by $K_i \cdot x_{i,j}$ to give:

$$E^{MV} = \frac{y_{i,j} - y_{i,j+1}}{K_i \cdot x_{i,j} - y_{i,j+1}} \tag{3.6}$$

K_i is the vapor liquid equilibrium constant, and $x_{i,j}$ is the bulk liquid mole fraction of component i on stage j. The liquid phase mole fraction will not only change due to mass transfer, but also due to the reaction. Figure 3.3 shows the actual efficiency profiles, back-calculated from column concentration profiles obtained with the nonequilibrium model. Although it is a well known fact that in multicomponent

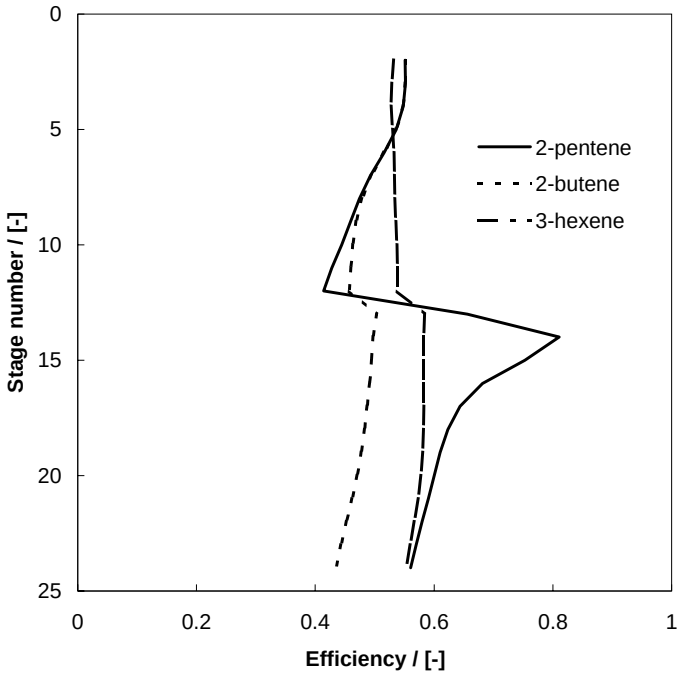

Figure 3.3: Efficiency profiles for reactive system, calculated from Nonequilibrium model results

systems these efficiencies tend to 'misbehave', there are a several observations to be made about the profiles in Figure 3.3.

The efficiencies of pentene just above the feed are much higher than just below the feed. This is due to the fact that above the feed pentene is a relatively 'heavy' component, and below the feed, it is relatively light. Furthermore, it is a reactant. Below the feed, where pentene is relatively light, the vapor phase concentration on

the tray above will be larger than the vapor phase concentration of the tray below. This means that the numerator of Eq. (3.5) will be larger than zero. The same will usually be the case for the denominator. However, because pentene is a reactant, it will be consumed, lowering its mole fraction. This means that the denominator will be smaller than for a system without a reaction, resulting in higher calculated efficiencies. Similar considerations can be given for the rectifying section. The result of all this is that if component i is a reactant and is relatively light, the measured efficiency will be higher than normal. However, if component i is a reactant but now relatively heavy, the measured efficiency will be lower than normal. This is indeed what is observed in Fig. 3.3

The same 'behavior' is found for products: For a relatively light product, lower efficiencies are to be expected, and for a heavy product we expect to see a higher efficiency. Clearly, the efficiencies are reaction dependent, which makes them difficult to predict. Using an efficiency model for a reactive distillation columns is, therefore, not recommended.

3.3 Example 2: Acetic Anhydride Reactive Distillation

The first work in the field of integrating a liquid flow model in a numerical model for a reactive distillation column was by Alejski (1991), who modeled the system water, acetic anhydride and acetic acid. The modeled column was part of a plant for the production of acetic anhydride described by Marek (1956). The objective of the column is to separate water and acetic anhydride to avoid hydrolysis of the anhydride to acetic acid.

Alejski uses a model in which the liquid phase on a tray is split up in a number of equilibrium cells along the liquid flow path. To take into account mass transfer effects, locally evaluated point efficiencies are used in the phase equilibrium calculation of each cell. The number of cells was evaluated from expressions for the eddy diffusivity. Alejski found that the conversion of anhydride as calculated assuming a perfectly mixed liquid phase was higher than when assuming that the liquid flows in plug flow across the tray. The numerical model was tested against experimental data for a bubble cap column of 0.6 m diameter, containing 30 bubble cap trays, with a total height of 10 m (Marek, 1956).

3.3.1 Reaction

The reaction equation is:

$$(CH_3CO)_2O + H_2O \rightarrow 2CH_3COOH \tag{3.7}$$

The reaction is assumed to be irreversible and the reaction rate equation is given by:

$$r = k_f \cdot c_{(CH_3CO)_2O} \cdot c_{H_2O} \tag{3.8}$$

The reaction rate constant is given by Marek (1956):

$$ln(k_f) = 11.742 - \frac{6887.7}{T} \tag{3.9}$$

3.3.2 Configuration

The column has 30 trays, with a total condenser and a partial reboiler (total 32 stages), with a feed to stage 16. The column diameter was set to 0.6 m during the calculations. The condenser pressure is 53.0 kPa. The reboiler pressure is 54.2 kPa The column is operated at a reflux ratio of 5.18 and a bottom product flow rate of 0.43 mol/s. Feed specifications are given in Table 3.1. Since the exact sizes and layout of the bubble caps was not given, the tray design routine was used to determine a possible layout pattern. One should keep in mind here that the internals design used

Pressure	53.0 kPa
Temperature	290 K
Flow rate	0.92 mol/s
Component mole fractions	
Acetic Aanhydride	0.161
Water	0.484
Acetic Acid	0.355

Table 3.1: Feed properties for acetic anhydride column

by Marek (1956) may be different from the internals evaluated with the design mode. The most important parameter in this respect is the weir height. This factor plays an important role in determining the liquid inventory on a tray, and thus, in determining the reaction volume. This means that the liquid volume may very well be under or overestimated and may have to be adjusted to fit experimental data.

3.3.3 Thermodynamic Data

A limited quantity of vapor-liquid equilibrium data is provided by Marek (1956). These data were obtained only in a very small region of the ternary triangle, that is, nevertheless, representative of the compositions observed in the actual column. We

Component i	Component j	$a_{i,j}$ $[J/mol]$	$a_{j,i}$ $[J/mol]$
Acetic Anhydride	Water	2214.3	5024.6
Acetic Anhydride	Acetic Acid	-407.2	3323.7
Water	Acetic Acid	4714.4	-4062.78

Table 3.2: Wilson parameters Acetic Anhydride - Water - Acetic Acid system

have correlated these data with the Wilson equation, for which the relative differences between the experimental and calculated V/L-equilibrium compositions were minimized. The parameters used in this work are given in Table 3.2.

3.3.4 Calculations

Calculations were done for the above system with our nonequilibrium model. With the specifications given above, the trays operate at a flooding fraction of about 0.18. This operating point falls outside the range of applicability of all published hydrodynamic correlations. This means that the predictions for parameters such as the interfacial areas, clear liquid heights and mass transfer coefficients will not be reliable, and may have to be adjusted to fit the experimental data.

Initial calculations suggest that an acceptable fit of experimental data was obtained by

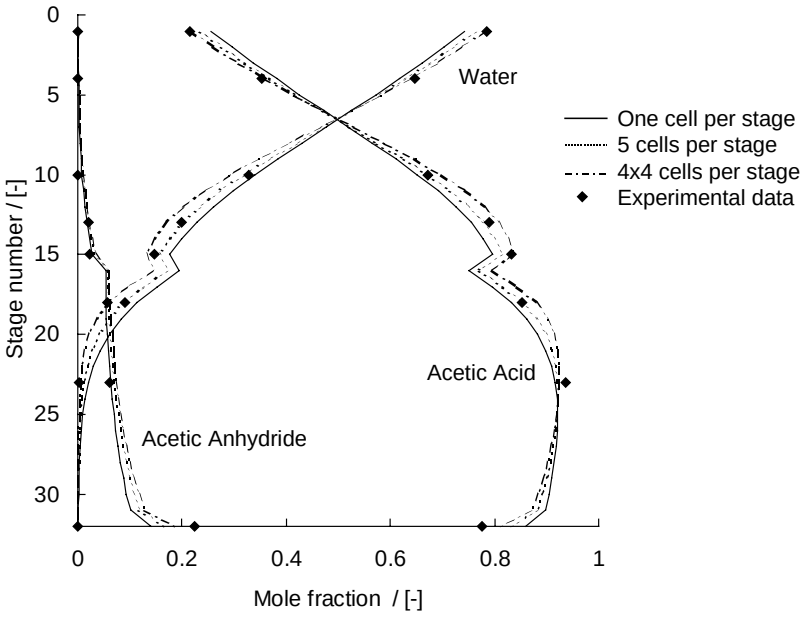

Figure 3.4: Column Concentration profiles for Acetic Anhydride - Water - Acetic acid system

1 Cell	0.58
5 Cells (vapor plug flow)	0.51
4 x 4 Cells (vapor and liquid plug flow)	0.45

Table 3.3: Conversion of acetic anhydride for the various flow models

multiplying the estimated clear liquid height by 0.4 and the estimated mass transfer coefficients by 0.5. This also suggests that the actual weir height is lower than the weir height used in the calculations. Subsequent calculations were done for the three different flow models described above. Concentration profiles are presented in Fig. 3.4. The shift in the concentration profiles due to increased staging in the vapor and liquid flow paths follows the trends as observed by Alejski (1991).

Table 3.3 shows that there is a drop in conversion with increased staging in liquid and vapor flow directions. This should be no surprise from a mass transfer perspective. In the system under consideration, water is the lightest and acetic anhydride is the heaviest component. The mass transfer rates for each species are shown in Fig. 3.5. In the top section, where the mixture consists mostly of water and acetic acid, we see that increased staging leads to a higher rate of transfer of water from the liquid to the vapor phase (negative direction). At the same time there is increased transfer of acetic acid from the vapor to the liquid phase (positive direction). Similar behavior

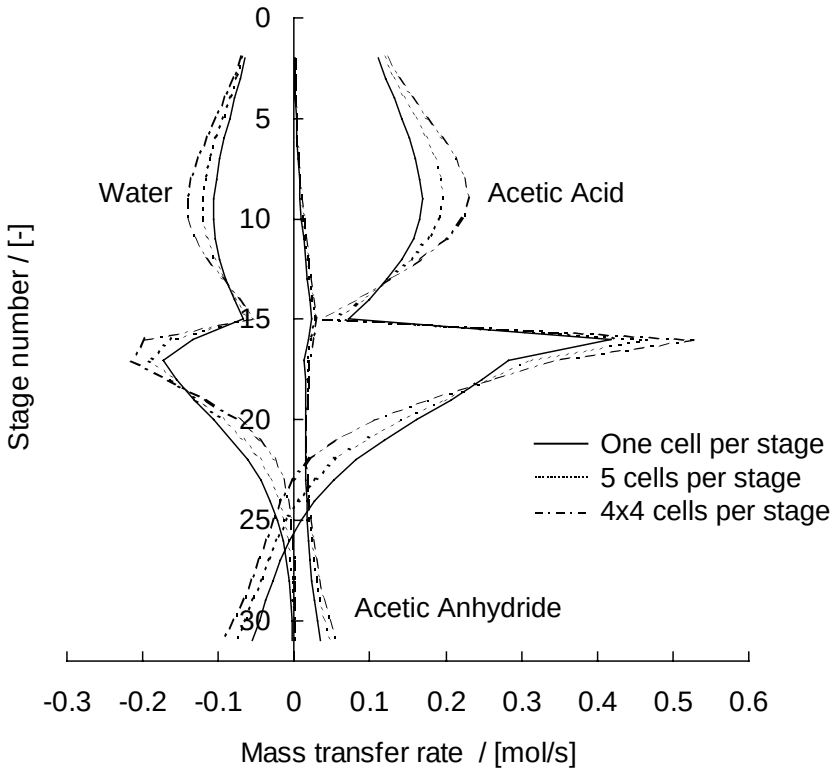

Figure 3.5: Mass transfer rates for Acetic Anhydride - Water - Acetic acid system

is seen at the feed stage.

Below the feed stage, however, the trends are reversed. Here, staging seems to reduce the mass transfer rate of water. The reason for this is offered by the concentration profiles. Due to the improved performance of the top section, there is not much water left below the feed stage. Thus, the mass transfer rates drop due to staging. On the trays in the bottom section of the column, acetic acid moves from the liquid into the

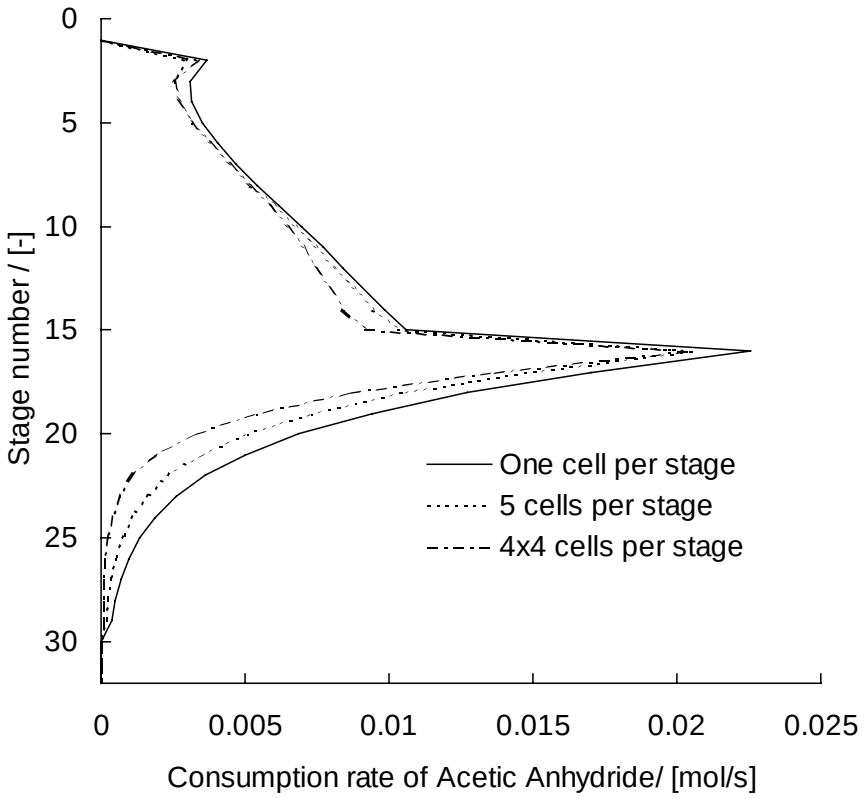

Figure 3.6: Consumption rate of Acetic Anhydride

vapor phase, while acetic anhydride moves from the vapor into the liquid phase. Here, increased staging leads to higher mass transfer rates and improved performance.

As a result, the concentrations of water and acetic anhydride will be lowered in the center of the column, thereby reducing the reaction rate and the consumption of acetic anhydride. The consumption rate of acetic anhydride is shown in Fig. 3.6. The

expected effects are clearly visible. Particularly below the feed stage, the consumption rate has dropped considerably, due to the lower concentration of water.

3.3.5 Film Reaction

Calculations were done to test the influence of the reaction in the liquid mass transfer film. This was done by switching off the reaction in the transfer film and rerunning the reactions. No significant differences in the results were found. This is due to the fact that for the system under consideration the Hatta number is very low (< 0.2). In these cases the influence of the film reaction is negligible. One should keep in mind however, that the system under consideration is reasonably well behaved. It is equistoichiometric, it has a low reaction enthalpy and all concentration gradients are relatively flat. For systems with very fast reactions, and more pronounced thermal effects, such as acid gas stripping, this is usually not the case, and the film reaction needs to be taken into account.

3.4 Example 3: Ethylene Glycol

The third example system is the production of ethylene glycol (EG) from ethylene oxide and water. Ethylene glycol is formed in an irreversible reaction from ethylene oxide and water:

$$EtO + H_2O \rightarrow EG \tag{3.10}$$

In addition, we have an unwanted consecutive reaction in which ethylene glycol reacts with ethylene oxide to di-ethylene-glycol (DEG)

$$EtO + EG \rightarrow DEG \tag{3.11}$$

The reaction rate constant of the second reaction is, under reaction conditions, about three times as large as the rate constant of the first reaction. Therefore, in a conventional reactor with equimolar feed, a considerable amount of DEG is produced. Furthermore, the reactions are both highly exothermic, requiring good temperature control. The classical strategy to tackle this selectivity problem is to use a high surplus of water in the reactor and operate the reactor at low conversion. In this manner the concentration of both ethylene oxide and ethylene glycol are kept relatively low, suppressing the rate of the unwanted second reaction. This, however, requires an extra separation unit to separate the product from the reactor exit stream and to recycle the unused reactants.

A good alternative for this conventional process is offered by reactive distillation. Here product formation, product separation and reactant recycle can be integrated into one piece of process equipment. The main advantage of using reactive distillation in this case is that it combines the preferred reaction conditions with direct heat integration. By choosing the right operation conditions one can ensure that the column is largely filled with water. The ethylene oxide that is supplied to the column reacts almost instantly to EG and because of the high surplus of water, the concentrations of ethylene oxide and ethylene glycol will be very low. This results in a low production rate of DEG. Furthermore, the distillation process provides direct temperature control, since the liquid phases will always be at boiling point. Hot spot formation, and therefore, the danger of runaway reactions is non-existent in reactive distillation.

Ciric and Gu (1994) proposed a 10-stage column for production of ethylene glycol. Water is supplied to the top of the column, while the ethylene oxide feed is distributed over the top section of the column. The reaction is assumed to take place only on the top five stages of the column. The column is operated at infinite reflux ratio, while in the bottom a boilup ratio of approximately 23 is maintained. Ciric and Miao (1994) used a homotopy continuation method to prove the existence of multiple steady states in the proposed setup. In both these studies an equilibrium stage approach was used.

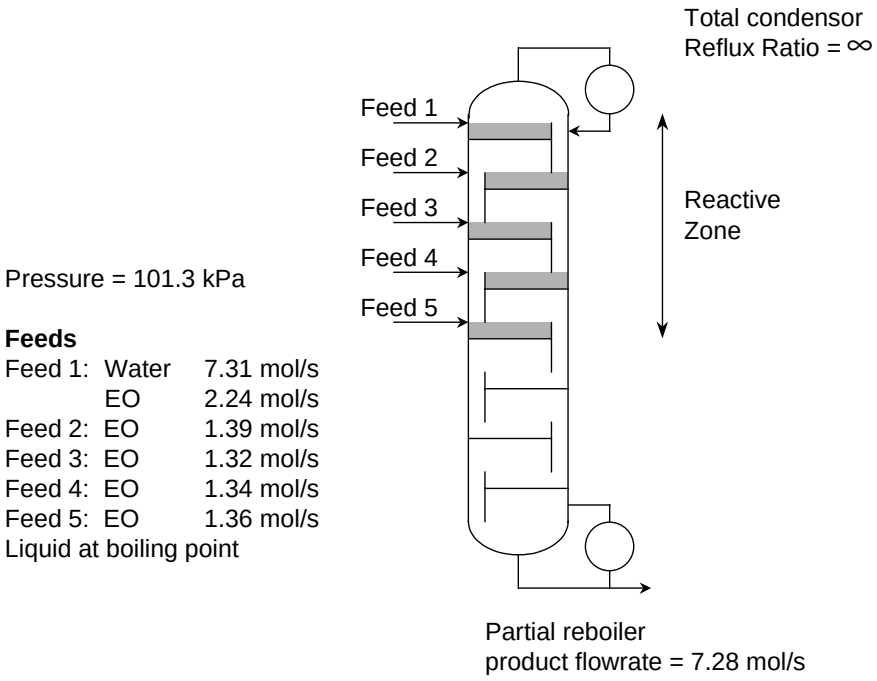

Figure 3.7: Configuration of reactive distillation column for hydration of ethylene oxide to ethylene glycol

In our case we have used a similar set-up to that of Ciric and Miao (1994), details of which are given in Fig. 3.7. In our calculations the nonequilibrium cell model was used for description of the stages 2 - 9. The reaction kinetics and thermodynamic data are the same as those reported in the papers by Ciric *et al.*. The condenser (stage 1) and the reboiler (stage 10) are modeled as equilibrium stages. Reactions are assumed to take place only on stages 2 to 6. Several calculations were carried out by

varying the number of cells in the vapor and liquid flow directions. The calculation results for the nonequilibrium cell model will be denoted by NEQ (n^L, n^V) where the numbers n^L and n^V refer to the number of mixing cells in the liquid and vapor phases, respectively. To compare our results with those of Ciric and Miao (1994), we also performed calculations in which phase equilibrium was 'forced' on all the stages by using extremely high values of the interphase transfer coefficients of heat and mass (obtained by multiplying the estimated values of the transfer coefficients by a factor of 10^5). The results from these calculations are denoted by EQ.

One should note here that the use of a conventional equilibrium model requires the specification of a reaction volume for evaluation of the production rates. For homogeneous reactions, the reaction volume is equal to the total liquid inventory on a tray and, therefore, depends on the tray layout used, the interstage vapor and liquid flows and the physical properties of the mixture on the stage. As a result of this the reaction volumes will, in some cases, be vastly different from tray to tray.

Correct prediction of the reaction volume would, therefore, require the evaluation of a tray design for each tray based on the vapor and liquid internals flows and physical properties. However, here one is faced with a chicken-and-egg problem: The reaction volume will depend on the internals flows and physical properties, but these, in turn, depend on the reaction volume. This may be circumvented by using a design

methodology, as outlined by Kooijman (1995) along with the equilibrium model. One should, however, keep in mind that equilibrium stages do not represent trays in a real column and that there is no sound way to link equilibrium stages to real trays, as illustrated in the first example. The design that is obtained will, therefore, just be indicative of a possible layout.

The calculation of the liquid volumes in the nonequilibrium model is based on the tray layouts generated by the design mode.

3.4.1 Multiple Steady States

Both EQ and NEQ(1,1) model calculation results yielded three steady state solutions: High conversion steady state, SS-1, low conversion steady state SS-3 and intermediate conversion steady state, SS-2. The temperature profiles for these models are shown in Fig. 3.8. The EQ model calculations match those obtained by Ciric and Miao (1994). For the low conversion steady state, SS-3, there is hardly any difference in the temperature profiles of the NEQ(1,1) and EQ model. This is to be expected because there is hardly any reaction taking place in the column. For the other states, SS-1 and SS-2, there is a considerable difference in the temperatures in the bottom section, emphasizing the strong influence of interphase mass transfer. The reason

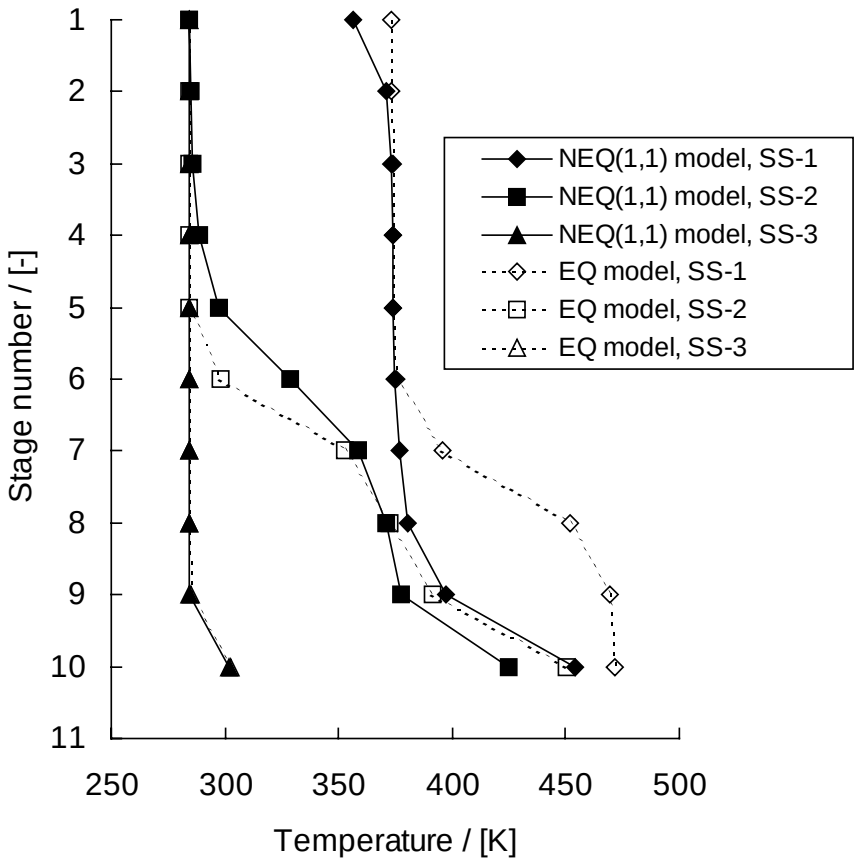

Figure 3.8: Column temperature profiles for the three steady-state solutions using the EQ and the NEQ(1,1) models

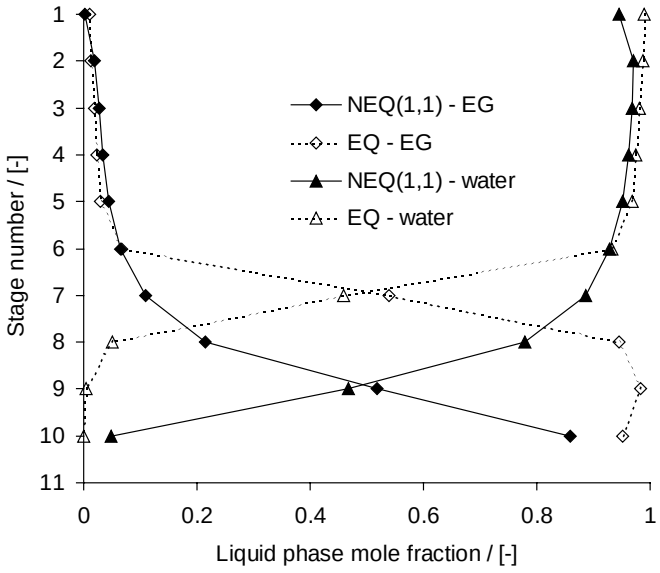

Figure 3.9: Column composition profiles for the high conversion steady state SS-1 using the EQ and the NEQ(1,1) models

for this strong influence becomes clear when we compare the composition profiles for SS-1 using the EQ and NEQ(1,1) models. See Fig. 3.9.

There is a significant difference in the composition profiles in the bottom section. Due to the influence of interphase mass transfer it is more difficult to strip water from the liquid phase in the bottom section. The lower EG liquid compositions obtained in the bottom section with the NEQ(1,1) model leads to significantly lower temperatures.

Fig. 3.10 presents a comparison of the vapor and liquid molar flows in the column for

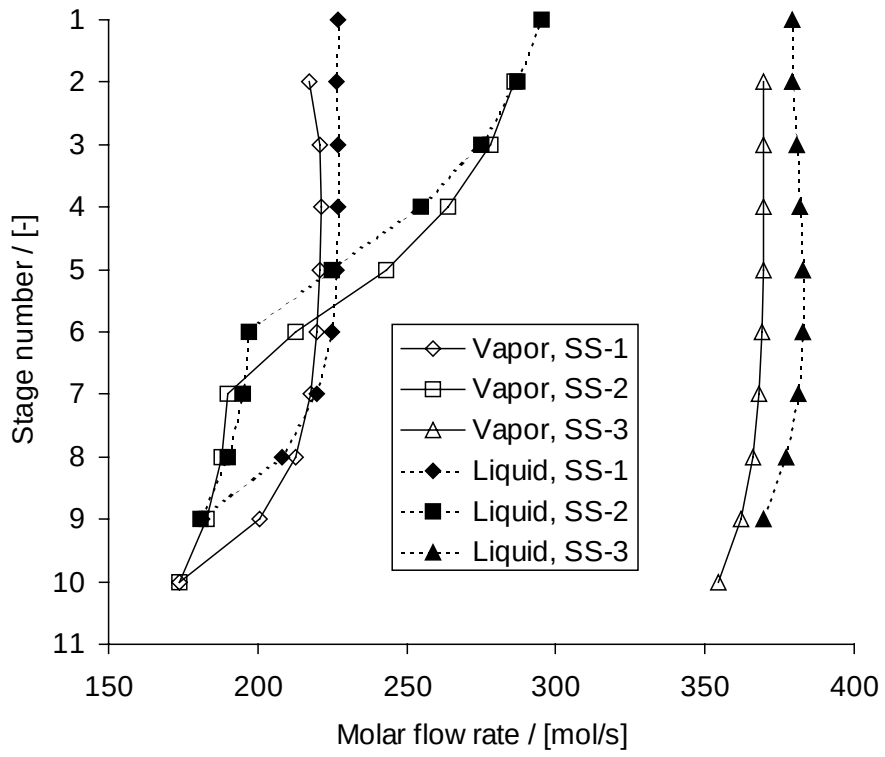

Figure 3.10: Column molar flow profiles of the liquid and vapor phases for the three steady-state solutions using the NEQ(1,1) model.

the three steady state solutions obtained with the NEQ(1,1) model. It is interesting to note that the low conversion steady state SS-3 has the highest vapor-liquid traffic inside the column. A further point to note is that in SS-1 and SS-2 there is a considerable difference in the molar flows in the top (reactive) and the bottom (stripping) sections. The differences in the molar flows in the top and bottom sections are due to the considerable differences in the molar heats of vaporisation of the four species present in the mixture. Relative to that of water, the heats of vaporization are EO = 0.7, EG = 1.3 and DEG = 1.5. For SS-1, for example, the concentration of EO in the bottom section is practically zero and the mixture contains EG, DEG and water, all of which have a high heat of vaporization. It should also be clear that the commonly used assumption of equimolar overflow in conventional distillation is not valid for the reactive distillation study under consideration. The necessity of using a proper energy balance at the interface (Taylor and Krishna, 1993) as used in this study is underlined.

Using the sieve tray sizing routine as outlined by Kooijman (1995) we can calculate the column diameters assuming 75% of the flooding limit for each stage; The column diameter calculations are shown in Fig. 3.11. We note that for SS-3 the column diameter is 2.4 m for all stages, whereas the high-conversion steady state solution demands 1.5 m column diameter in the reactive section and 1.8 m in the stripping

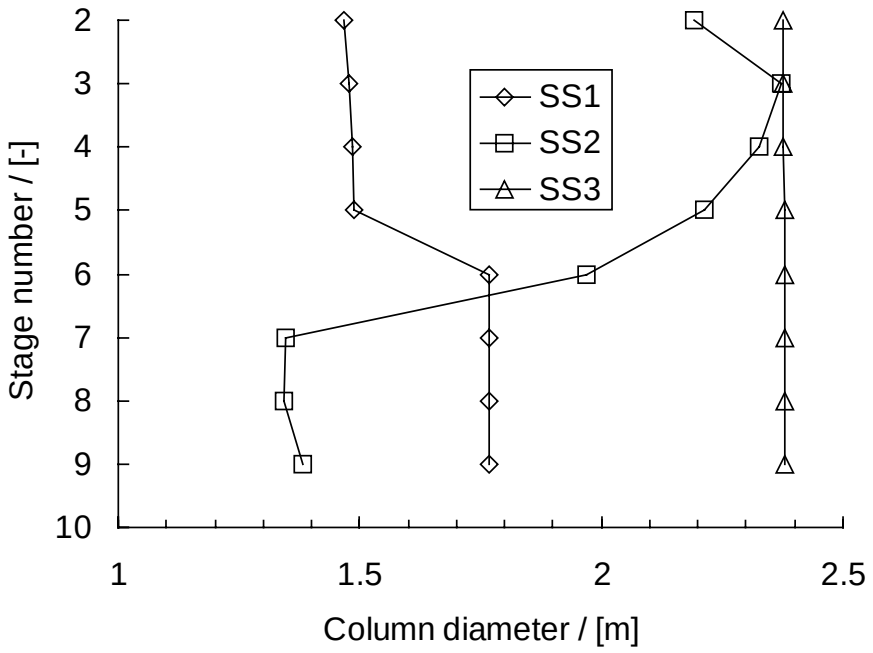

Figure 3.11: Column diameters calculated for each stage assuming 75% flooding factors for the three steady-state solutions using the NEQ(1,1) model.

(non-reactive) section. The important conclusion to be drawn from the results of Fig. 3.10 and Fig. 3.11 is that if a column of an average diameter of say 1.6 m is built for the production of EG, it would be impossible to realize the states SS-2 and SS-3 because the column would be inoperable due to flooding of some (in case SS-2) or all (in the SS-3 case) of the trays (see also Baur *et al.*, 1999). On the other hand, overdimensioning the column will guarantee that only the low conversion steady state can be realized.

Put another way, for a chosen column hardware design, only one steady-state solution may be achievable in the column. In the literature on reactive distillation, considerable attention has been paid to the phenomena of multiple steady states (Eldarsi and Douglas, 1998; Jacobs and Krishna, 1993; Nijhuis *et al.*, 1993; Hauan *et al.*, 1995). However, in all these models, no attention has been paid to the column design aspects and the influence of vapor-liquid traffic thereon. The case study above has emphasized the importance of column design on the realizability, or otherwise, of multiple steady states.

3.4.2 Influence of Mass Transfer and Mixing

Applying chemical reaction engineering principles we should expect that the selectivity to EG should improve with improved mass transfer, and with increased staging in the vapor and liquid phases. To demonstrate this aspect we compare the selectivities for SS-1 obtained with NEQ(1:1), NEQ(1:4), NEQ(4:4) and EQ models (see Fig. 3.12). The best selectivity is obtained with the EQ model. Increasing the number of non-equilibrium cells in the vapor phase improves mass transfer performance and therefore conversion of EO. Increasing the number of well mixed stages in the liquid phase has a beneficial effect both on interphase mass transfer and on the reaction selectivity. From a hardware design viewpoint it is preferable to choose a tray design with a long liquid flowpath, which will ensure sufficient staging in the liquid phase. It appears that the usual design rules for conventional distillation cannot be carried over to reactive distillation columns, because, for a column of 1.6 m diameter the conventional design philosophy (Lockett, 1986) would be to use 2 flow passes for the liquid flow. One flowpass will give better staging, and, therefore, better selectivity.

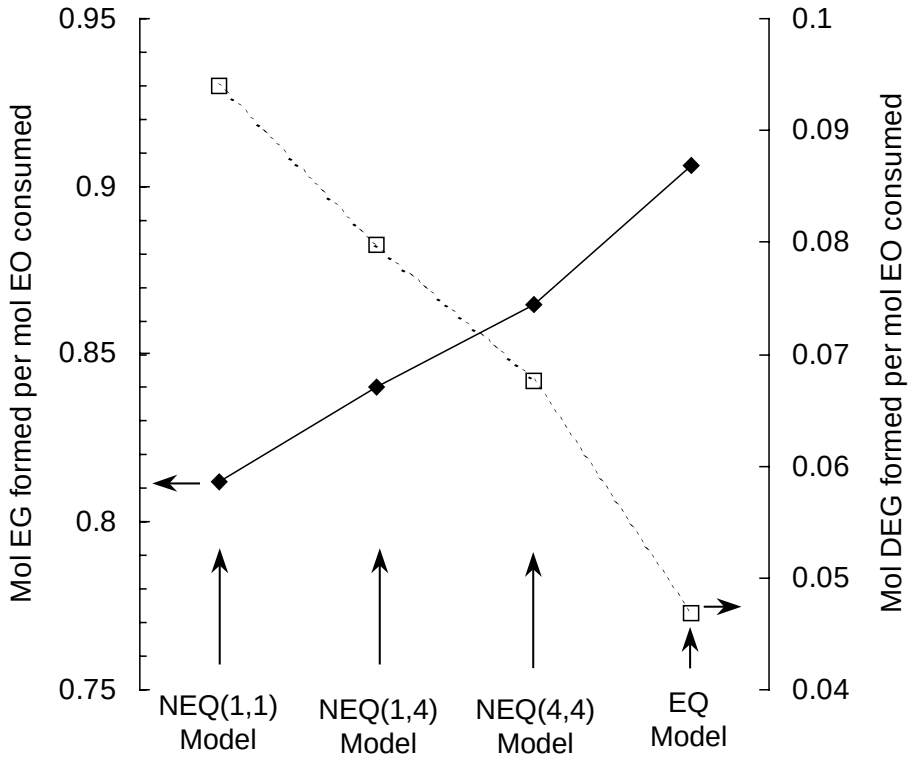

Figure 3.12: Selectivity towards production of EG and DEG for the high conversion steady state using NEQ(1,1), NEQ(1,4), NEQ(4,4) and EQ models.

3.5 Conclusions

In this chapter we have presented some examples for reactive distillation in tray columns. Is was shown that efficiencies in the reactive distillation process could, under certain conditions, be affected by the reaction. The use of efficiencies and equilibrium models should, therefore, be avoided.

In all case studies, a significant influence of staging was found. In both the acetic anhydride process and the ethylene glycol process, staging has a beneficial influence on conversion and selectivity. Usual design methodologies and scale-up philosophies for normal distillation may, therefore, have to be reviewed before being applied to reactive distillation.

Using a case study of the hydration of ethylene oxide to ethylene glycol, we have shown that interphase mass and energy transfer resistances have a significant effect on the formation of the by-product di-ethylene glycol. Staging in the vapor and liquid phases also influences reaction selectivity to EG. While multiple steady states are possible using both NEQ and EQ models, it is possible that not all steady states would be realizable in practice due to flooding phenomena. In addition, overdimensioning may, in some cases, lead to undesirable situations. This underlines the importance of simultaneous considering hardware design along with process aspects.

Chapter 4

Reactive Distillation in Packed Columns

In this chapter we will illustrate the application of the nonequilibrium cell model to Reactive Distillation in packed columns. The influence of the mass transfer resistance at the vapor/liquid interface is studied by comparing the results from an equilibrium model to the results from the nonequilibrium cell model. The influence of mass transfer resistances inside and around a heterogeneous catalyst are studied by means of the Dusty Fluid Model.

4.1 Introduction

In this chapter, the use of the nonequilibrium model for reactive distillation in packed columns is illustrated by means of two examples. The first example describes a process for the production of methyl-*tert*-butyl-ether (MTBE). This process has been the subject of several studies (Jacobs and Krishna, 1993; Nijhuis *et al.*, 1993; Hauan *et al.*, 1995), all of which employ an equilibrium model in the description of the column. In this chapter we will show that multiple steady states may also be found with a nonequilibrium model, however the 'realizable window' for these steady states is much smaller due to the presence of the mass transfer resistances.

The Dusty Fluid Model is used to analyse the influence of additional mass transfer resistances in the heterogeneous catalyst phase. For the MTBE process it will be seen that the multiple steady state region disappears completely when these additional resistances are taken into account.

In a second example, a process for production of *tert*-amyl-methyl-ether (TAME) is studied. The model system is quite similar to that of MTBE. For the TAME process multiple steady states for this process have been found experimentally. (Mohl *et al.*, 1999). However from model simulations it is observed that the multiple steady state region is relatively insensitive to additional mass transfer resistances.

4.2 Example 1: MTBE process

We analyze the MTBE process described by Jacobs and Krishna (1993) using an equilibrium stage (EQ) approach. This column contains a total of 17 equilibrium stages: condenser, 2 rectifying stages, 8 reactive stages (containing 8000 kg of catalyst) 5 stripping stages and a reboiler; see Fig. 4.1. In our NEQ model, the non-reactive rectifying and stripping sections are configured as sieve trays. The reactive section is made up of Raschig ring shaped catalyst packing as used by Sundmacher and Hoffmann (1994). In order to fix the column specifications for the NEQ calculations, such as the column diameter and the catalyst packed section height, we first ran our model in design mode. The internals design procedure is that of Kooijman (1995). The design specifications are given in Tab. 4.1 and Tab. 4.2.

The UNIQUAC model was used for description of liquid phase nonideality, while the Soave-Redlich-Kwong equation of state was used for the vapor phase. The extended Antoine equation was used for calculation of the vapor pressure. Thermodynamic and kinetic data were taken from Rehfinger and Hoffmann (1990a, 1990b).

From earlier work of Jacobs and Krishna (1993) and Nijhuis *et al.* (1993) we know that multiple steady states are to be expected for the chosen column configuration shown in Fig. 4.1. The shape and location of the multiple steady state region were determined

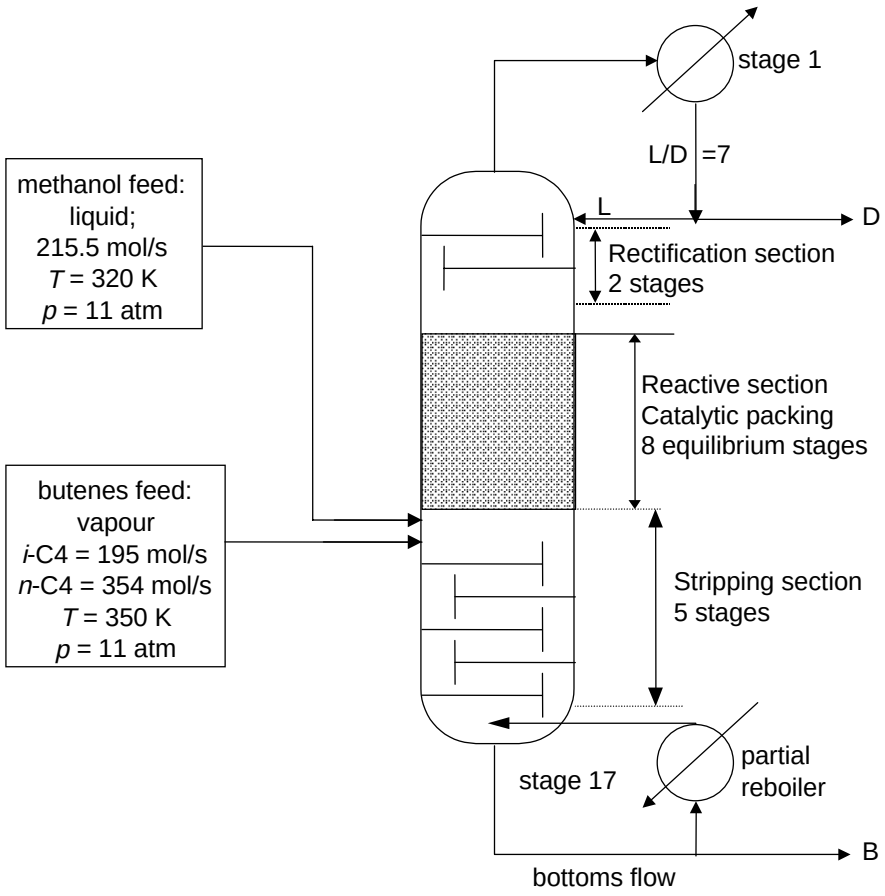

Figure 4.1: Configuration of 17 stage reactive distillation column for production of MTBE

	Rectifying section	Stripping section
Type	Sieve Tray	Sieve Tray
Column diameter (m)	5.595	5.019
Total tray area (m^2)	24.58	19.78
Number of passes (-)	5	5
Tray spacing (m)	0.61	0.61
Flow path length (m)	0.92	0.82
Active area (m^2)	19.21	15.32
Total hole area (m^2)	2.12	1.52
Downcomer area (m^2)	2.68	2.23
Hole diameter (m)	0.0047625	0.0047625
Weir length (m)	22.95	20.62
Weir height (m)	0.0508	0.0508
Weir type (m)	Segmental	Segmental
Downcomer clearance (m)	0.0381	0.0381
Deck thickness (m)	0.00254	0.00254

Table 4.1: Tray specifications MTBE column

	Reactive section
Type	Raschig ring random packing
Column diameter (m)	6
Total column area (m^2)	28.27
Packing height (m)	0.7
Specific packing surface (m^{-1})	600
Packing size (in)	0.25
Void fraction (-)	0.72
Nominal size (m)	0.00635
Critical surface tension ($N \cdot m^{-1}$)	0.061
Packing factor (-)	5249.34
Packing density ($kg \cdot m^{-3}$)	410
Internal porosity (-)	0.45
Exchange capacity ($eq(H^+) \cdot g^{-1}$)	4.54

Table 4.2: Reactive packed section specifications MTBE column

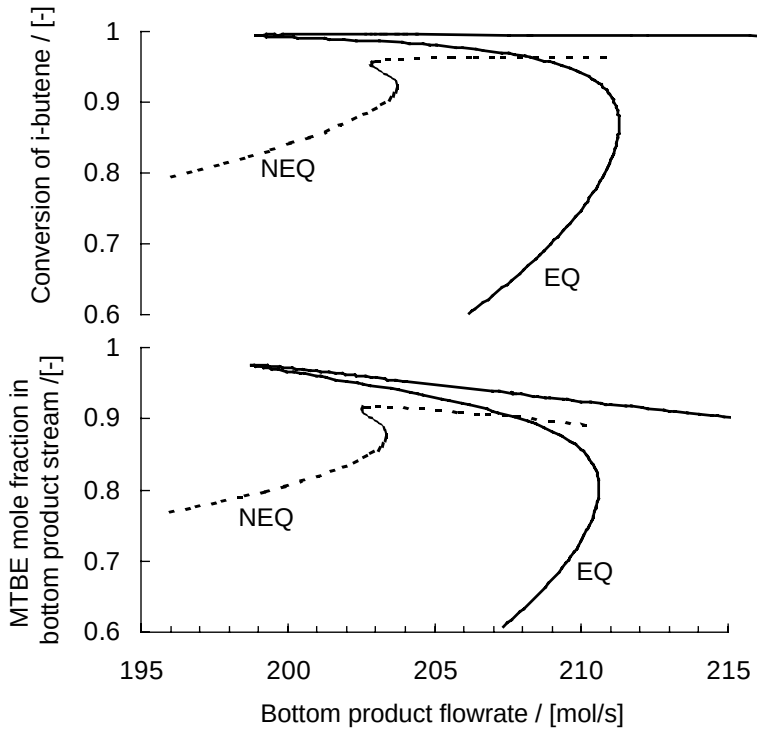

Figure 4.2: Comparison of EQ and NEQ models for MTBE synthesis

with the continuation method outlined in Section 2.8.3. The bottom product flowrate was taken as the continuation parameter. In the EQ model implementation we have assumed a tray efficiency of 60% for the non-reactive stages. In the NEQ model a sufficient number of slices is required for accurate calculations; our study shows that at least 90 slices are required for the 0.7 m high packed section for acceptable accuracy. For the packed section the mass transfer coefficients were calculated using

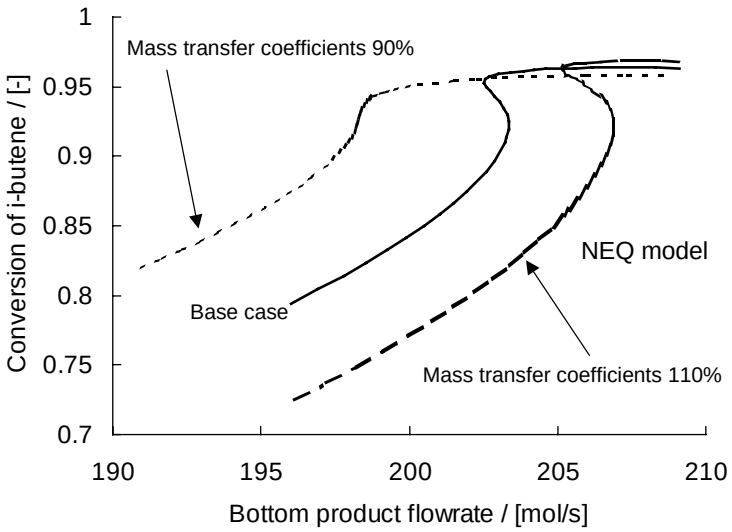

Figure 4.3: Sensitivity of the NEQ model to mass transfer coefficients

the correlations by Onda *et al.* (1968). The AIChE method (1958) was used for the sieve tray mass transfer calculations.

Fig. 4.2 shows that multiple steady states exist for both the EQ and NEQ models and the differences between these models are significant. It is interesting to note that the low conversion branch of the NEQ model lies above that of the EQ model. In the low conversion branch of the curve, the reaction proceeds in the reverse direction; incorporation of a mass transfer resistance (as in the NEQ model) hinders this and improves conversion and the bottom product purity.

To reinforce the above observations we carried out a sensitivity analysis for the NEQ model in which the mass transfer coefficient was taken to be 90% and 110% of the base case Fig. 4.3 shows that the 90% conversion case leads to *higher* conversions in the low conversion branch, whereas the 110% case leads to *lower* conversions. This counter-intuitive effect is because in the low conversion branch the reaction is proceeding in the wrong direction and decreasing the interphase transfer facility helps by mitigating a bad situation. The results of Fig. 4.3 emphasize the need for accurate estimation of mass transfer coefficients and the importance of ensuring operating conditions to stay in the high conversion branch; in the latter case the sensitivity to the estimation of the mass transfer coefficients is minimal. These results also indicate potential areas for application of novel type structured catalytic packings that allow for close control of facility for reaction and facility for mass transport.

The effect of decreasing catalyst activity, due to catalyst aging or deactivation, on the overall process performance are shown in Fig. 4.4. With decreasing catalyst activity, the conversion does not change substantially in the high conversion branch. This is because the reaction in the case under consideration is fast enough to come close to chemical equilibrium. In the low conversion branch, decreasing catalyst activity improves the conversion, another counter intuitive effect.

Calculations were done in which the flowrate of 'inert' n-butene was chosen to be

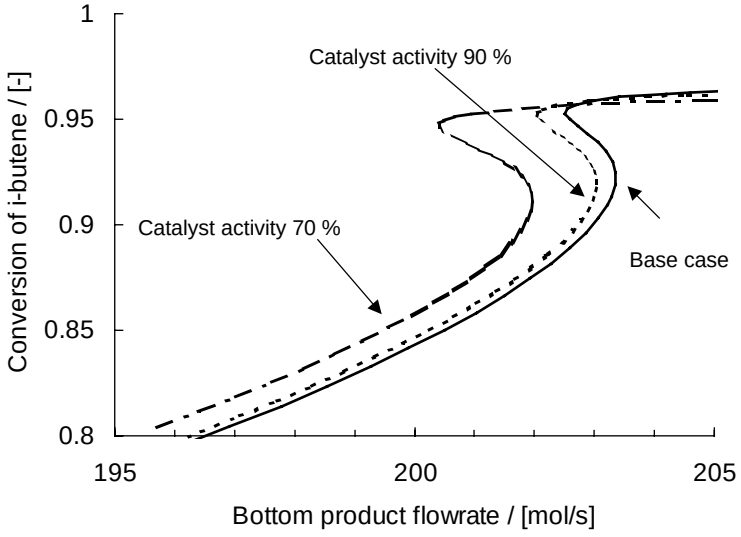

Figure 4.4: Sensitivity of the NEQ model to the catalyst activity

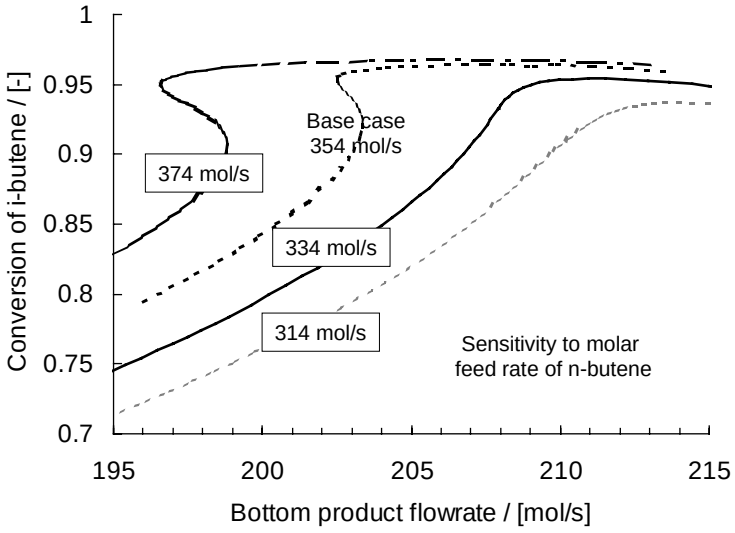

Figure 4.5: Sensitivity of the NEQ model to n-butene feed flowrate

354 (base case), 314, 334 and 374 mol/s and results are presented in Fig. 4.5. It is interesting to note that a certain minimum amount of n-butene is required for good operation of the given column. Normal butene serves as a 'coolant' of the reactive zone, thereby keeping the temperature of the reactive zone at a level where the equilibrium constant is favorable for the production of MTBE; reducing the feed of n-butene results in loss of conversion. We also note that the phenomena of multiple steady states tends to disappear for low values of n-butene feed to the column. This role of 'inerts' has not been stressed earlier in the literature on reactive distillation for MTBE.

The necessity of using the full Maxwell-Stefan description for mass transfer, rather than an effective diffusivity approach is illustrated by Baur *et al.* (1999). They found considerable differences in the location and size of the multiple steady state region for the two diffusivity models.

4.2.1 The Dusty Fluid Model

In this section we will repeat the calculations for the MTBE column using the Dusty Fluid Model. The catalyst shape was assumed to be planar. This may be a reasonable approximation for Raschig rings, if they are not too thick. Other catalyst data are

given in Tab. 4.2.

It has already been stated that there is no theory available for estimation of the Knudsen diffusion coefficients D_i^e for liquid diffusion inside porous particles. In the calculations presented here we will, therefore, consider two limiting cases: (a) one in which D_i^e is large, in which case the last term can be ignored and, (b) one in which D_i^e is a factor five times smaller than the smallest of the $Đ_{i,j}$ values. D_i^e is assumed to be the same for all components.

Fig. 4.6 shows the steady state conversion of *iso*-butene as a function of the bottom product flow rate for the pseudo-homogenous model and for the dusty fluid model. Two observations can be made immediately: First, the multiple steady state region has completely disappeared for the dusty fluid model, and second, the Knudsen diffusion term has a substantial influence on the results of the Dusty Fluid Model simulations.

The first observation can be explained by the fact that in the lower branch of the multiple steady state region in part of the reactive section the reverse reaction (reaction of MTBE to Methanol and iso-butene) takes place. Introduction of a mass transfer resistance to account for transport inside the catalyst reduces the influence of this backward reaction. The introduction of extra mass transfer resistances also leads to

the observed drop in the maximum achievable conversion. Furthermore, Knudsen Case B includes an additional resistance term due to Knudsen diffusion. Thus, the model predicts an even lower maximum conversion than for Knudsen Case A. One conclusion that can be drawn from these findings is that equilibrium models tend to exaggerate the phenomenon of multiple steady states, and that addition of mass transfer resistances results in a much smaller realisable 'window' for the multiple steady states.

Fig. 4.7 Shows the mass transfer rates in the catalyst on stage 15 obtained with the dusty fluid model for both Knudsen cases at a bottom product flowrate of 200 mol/s. The situation shown in Fig. 4.7 is representative for all stages. In Knudsen Case B, mass transfer inside the catalyst only takes place in a small section close to the catalyst outside surface (catalyst wall). For Knudsen Case A, mass transfer takes place throughout the entire catalyst particle. Since changes in the mass transfer rate correspond to the rate of reaction (see Eq. (2.49)) it follows that in Knudsen Case B, only part of the catalyst is used for chemical conversion.

The values of the catalyst thickness, catalyst porosity and other parameters were all varied over the ranges given in Tab. 4.3. For Knudsen case A we found no significantly different results for any of these parameter variations. For Knudsen case B, the influence of the catalyst thickness is substantial. Shown in Fig. 4.8 is the steady

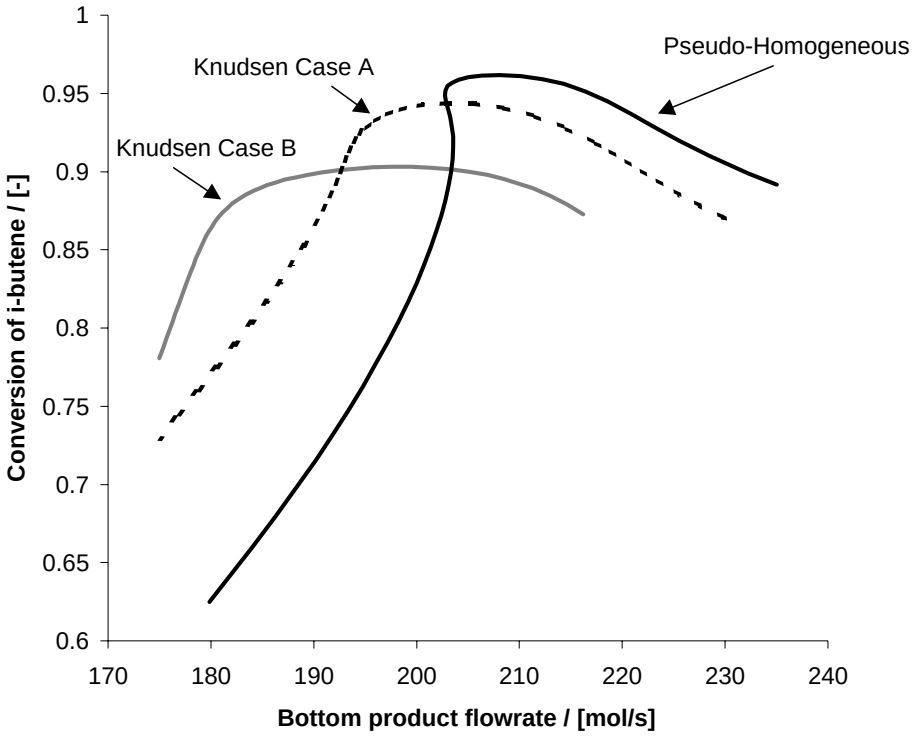

Figure 4.6: Steady state conversion of i-butene in MTBE column as a function of the bottom product flow rate. Comparison of Pseudo homogeneous and dusty fluid models.

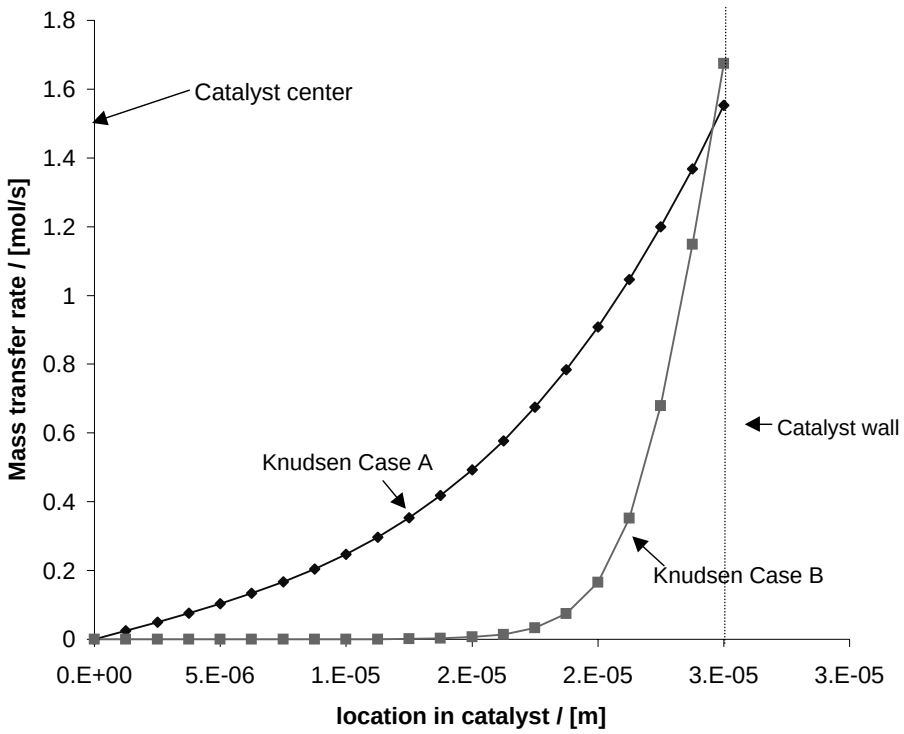

Figure 4.7: Mass transfer rates inside a catalyst particles

Catalyst parameter	Base value	Range considered
Thickness, (m)	$0.5 \cdot 10^{-3}$	$0.25 \cdot 10^{-3}$ - $1.0 \cdot 10^{-3}$
Porosity, $(-)$	0.6	0.5 - 0.7
Tortuosity, $(-)$	1.5	1 - 2
Thermal Conductivity $(J \cdot K^{-1} \cdot m^{-1} \cdot s^{-1})$	λ^L	$0.01 \cdot \lambda^L - 100 \cdot \lambda^L$

Table 4.3: Base values and tested ranges for model parameters.

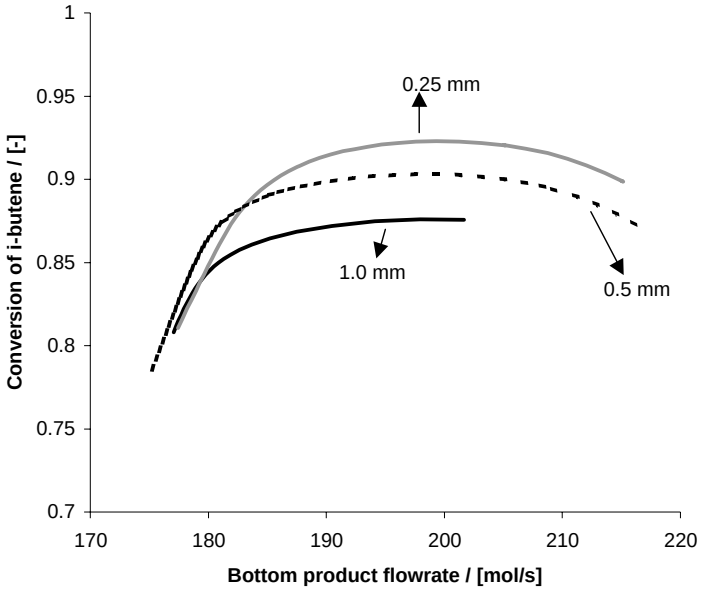

Figure 4.8: Conversion of i-butene as a function of the bottom product flowrate for various catalyst thicknesses

state conversion of i-butene as a function of the bottom product flowrate for various catalyst thicknesses. The maximum achievable conversion is significantly lower for the thicker catalyst. This is due to the fact that for Knudsen case B, the column operates in a diffusion limited regime.

Additional calculations were done in which the mass transfer resistances to and inside the catalyst were neglected. This can be done by multiplying the outside catalyst area by a very large number. These calculations confirm our expectation that with

removal of these additional mass transfer resistances the full Nonequilibrium Dusty Fluid model gave results that were the same as obtained with the pseudo-homogeneous model.

4.3 TAME Case Study

For our second case study we will consider the reactive distillation process for *tert*-amyl-methyl-ether (TAME). The reaction under consideration is the acid catalyzed formation of TAME from 2-methyl-1-butene, 2-methyl-2-butene and methanol using a heterogeneous catalyst.

4.3.1 Reaction System

Extensive discussions on the kinetics of the above reaction is given by Oost and Hoffmann, (1995) and Rihko and Krause (1995). The reaction system is depicted schematically in Fig. 4.9. TAME is formed out of the two pentene isomers, for which we can write the following reaction equations

$$R_1 = k_1 \cdot \left(\frac{a_{2M1B}}{a_{MeOH}} - \frac{1}{K_1} \cdot \frac{a_{TAME}}{a_{MeOH^2}} \right) \tag{4.1}$$

$$R_2 = k_2 \cdot \left(\frac{a_{2M2B}}{a_{MeOH}} - \frac{1}{K_2} \cdot \frac{a_{TAME}}{a_{MeOH^2}} \right) \tag{4.2}$$

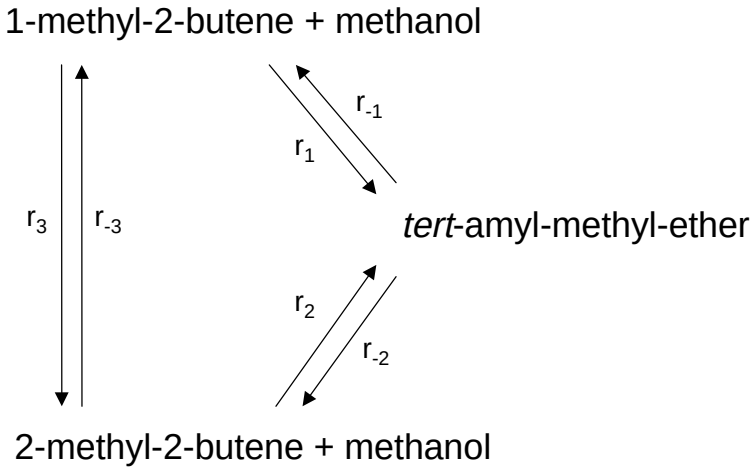

Figure 4.9: Schematic representation of reaction system.

In addition there is a rapid isomerisation reaction between the two pentene isomers:

$$R_3 = k_3 \cdot \left(a_{2M1B} - \frac{1}{K_3} \cdot a_{2M2B} \right) \tag{4.3}$$

The equilibrium constants for the above reactions are given by Rihko *et al.* (1994):

$$K_1 = 1.057 \cdot 10^{-4} \cdot exp \left\{ \frac{4273.5}{T} \right\} \tag{4.4}$$

$$K_2 = 1.629 \cdot 10^{-4} \cdot exp \left\{ \frac{3374.4}{T} \right\} \tag{4.5}$$

$$K_3 = \frac{K_1}{K_2} = 0.648 \cdot exp \left\{ \frac{899.1}{T} \right\} \tag{4.6}$$

Due to the rapid isomerisation reaction, it is very hard to determine the individual rate constants of the first two reactions separately. Therefore, lumped reaction kinetics

have to be used. The overall reaction rate of TAME is given by summation and rearrangement of Eq. (4.1) and Eq. (4.2):

$$R_{1+2} = (k_1 + k_2 \cdot K_3) \left(\frac{a_{2M1B}}{a_{MeOH}} - \frac{1}{K_1} \cdot \frac{a_{TAME}}{a_{MeOH}^2} \right) \tag{4.7}$$

Thiel *et al.* (1997) give the following expression for the forward reaction rate constant:

$$k_1 + k_2 \cdot K_3 = (1 + K_3) \cdot 2.576 \cdot exp \left\{ 32.3 - \frac{10764}{T} \right\} \tag{4.8}$$

For the isomerisation reaction we have:

$$k_3 = 1078 \cdot exp \left\{ 32.6 - \frac{10861}{T} \right\} \tag{4.9}$$

4.3.2 Calculations

Bravo *et al.* (1993) suggested the presence of multiple steady states in their pilot plant column for this process. Conclusive experimental evidence of multiple steady states in this process was described by Mohl *et al.* (1999). In the following section we will take the configuration presented by Mohl *et al.* as a testcase for our model. We model a packed column with an inner diameter of 0.076 m, consisting of two sections. The top section is 0.5 m high and packed with catalytic Raschig rings. The bottom section is 0.5 m high and packed with inert (glass) Raschig rings. A feed is supplied between the two sections. For more details about the column, see Mohl *et al.* (1999).

Component i	Component j	$a_{i,j}$ $[J/mol]$	$a_{j,i}$ $[J/mol]$
methanol	2-methyl-1-butene	9772.3	1376.5
methanol	2-methyl-2-butene	10147	968.81
methanol	methyl-*tert*-pentyl-ether	4826.3	-177
methanol	n-pentane	11749	1946.7
2-methyl-1-butene	2-methyl-2-butene	487.8	-477.94
2-methyl-1-butene	methyl-*tert*-pentyl-ether	-611.75	951.33
2-methyl-1-butene	n-pentane	326.74	-194.18
2-methyl-2-butene	methyl-*tert*-pentyl-ether	-386.04	712.33
2-methyl-2-butene	n-pentane	362.28	-265.49
methyl-*tert*-pentyl-ether	n-pentane	1143.9	-447.84

Table 4.4: Wilson parameters for TAME system

The column pressure was 0.25 MPa, the reflux ratio 15. The feed consisted of methanol, the two pentenes, and inert n-pentane. The feed rate was $4.17 \cdot 10^{-3}$ mol/s, with: $x_{MeOH}/x_{C5=} = 0.8$ and $x_{C5=}/(x_{C5=} + x_{n-C5}) = 0.3$ using the information given by Mohl *et al.*, (1999). Sundmacher *et al.* (1999) suggest that the Wilson equation should be used for describing nonideal liquid phase behavior. Parameters for this model are given in Table 4.4.

Simulations were done with three different models: An equilibrium stage model with 12 stages and a stage efficiency of 0.8, a nonequilibrium model in which the reaction is assumed to be pseudo-homogeneous, and a nonequilibrium model incorporating the dusty fluid model described here. For the nonequilibrium model, the packed section is divided into a number of slices, each considered to be a nonequilibrium cell. Calculations with the pseudo homogeneous model and 40 slices gave results that coincided with those obtained using only 10 slices. 10 slices were used in all subsequent calculations. It was further assumed that the column was packed with 1.3 kg of packing and that the catalyst activity was set to 1.2 eq/kg (Mohl *et al.*, 1999).

We have assumed the same catalyst geometry and properties as for the MTBE problem. In addition, we have done calculations to determine the influence of the various geometrical parameters. In no case was there a significant influence of these parameters.

Three steady states were found for the base case column configuration. For obtaining the multiple steady states, a continuation method was used in which the reboiler duty was the independent parameter. Figure 7 shows the temperature profiles obtained for the high and the low production steady state, for the equilibrium model, for the nonequilibrium model with a pseudo homogeneous reaction and for the nonequilibrium model with a dusty fluid description of the catalyst. All three models are largely

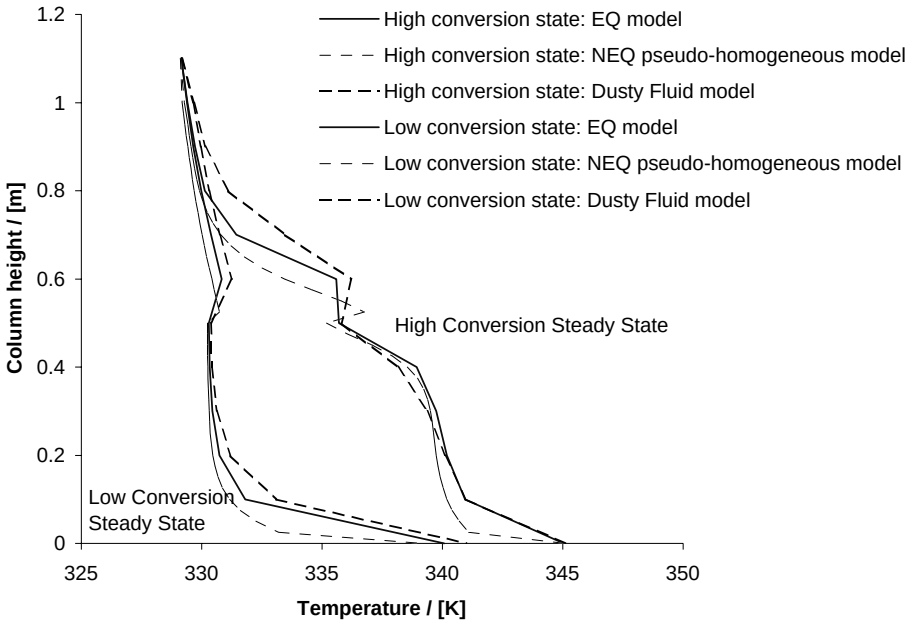

Figure 4.10: Temperature profiles for high and low conversion steady states in TAME column for Equilibrium (Eq), Nonequilibrium (NQ) and Dusty Fluid (DF) models.

in agreement with the calculated temperature profiles presented by Mohl *et al* (1999) and the differences between the models are minor. The same observation has been made by Sundmacher (1999). For this process, the overall conversion is not affected significantly by the mass transfer resistance inside the porous catalyst.

4.4 Discussion

In the two case studies presented above we have found apparently contradictory findings. For the MTBE process, the differences between the equilibrium, pseudo homogeneous nonequilibrium and dusty fluid nonequilibrium models are substantial. For the TAME process, all models give more or less similar results.

A reason for the difference must lie in the fact that in the MTBE process is relatively sensitive to mass transfer resistances, whereas the TAME process is not. There may be two reasons for this. First, for the TAME system, the entire catalytic section is used for production of TAME both in the high and the low production steady states. In no case did we find consumption of TAME. Second, the TAME reaction rate is much lower than that for the MTBE system. The forward reaction rate constant for TAME is about an order of magnitude lower than for MTBE throughout the entire reactive section. The production rate of TAME will, therefore, be much less sensitive to changes in the mass transfer resistance.

For the MTBE process there are substantial differences between equilibrium and nonequilibrium models (Higler *et al.*, 1999b). In the equilibrium approach the reactive section is described by only 7 stages, whereas 90 slices were used in the in the nonequilibrium model calculations. The approximation of the real concentration

and temperature profiles is, in the equilibrium stage model, much coarser than in the nonequilibrium model. The coarse prediction could give rise to significant deviations for systems with large temperature and concentration gradients in combination with highly nonlinear interactions between the reaction rates and the temperature profiles.

In addition, caution should be exercised in the application of efficiency factors for multiple steady state calculations. Mohl *et al.* (1999) describe calculations done with an equilibrium model, in which the value of the efficiency factor was fixed. However, one should keep in mind that the hydrodynamic conditions in the various steady states may be quite different from each other, and so may the efficiencies. Fig. 4.11 shows the Murphree efficiency profiles for methanol and n-pentane in the TAME column that were back-calculated from the results of the Nonequilibrium Dusty Fluid model. As can be seen, the differences between the efficiencies in the high and low conversion steady states are quite considerable. Similar results are found for other components. The effect of the efficiencies on the overall conversion in the TAME process is not very large, since the overall production rate is relatively insensitive to mass transfer resistances. However, this will not always be the case.

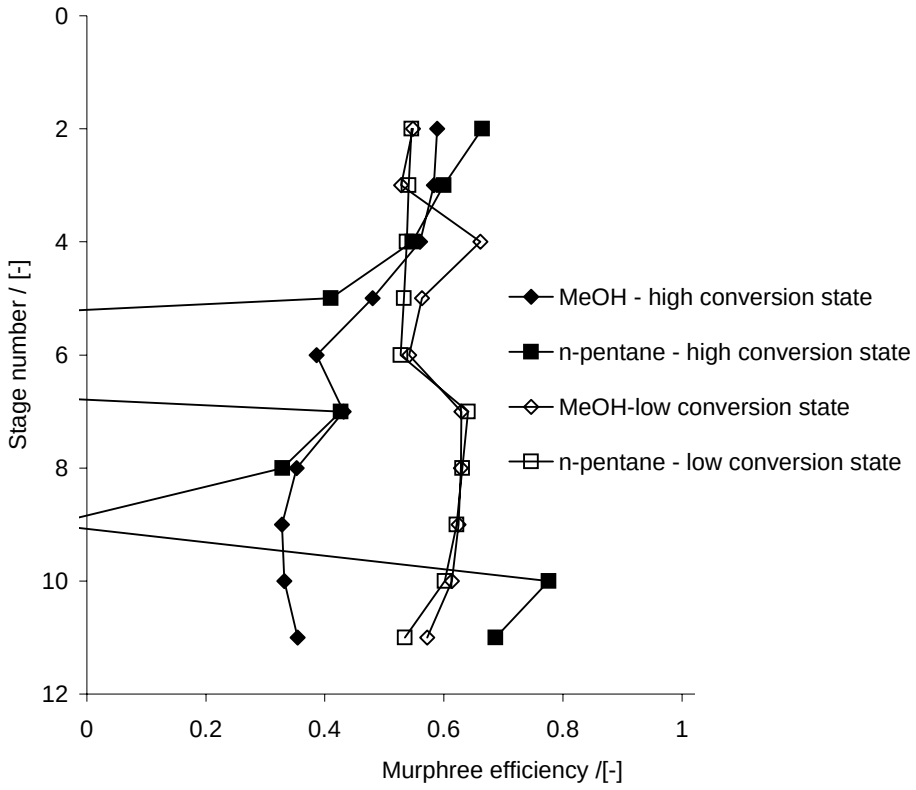

Figure 4.11: Murphree efficiency profiles for Methanol and n-Pentane at high and low conversion steady states.

4.5 Conclusions

A NEQ model is indispensible for design, because there is no simple procedure for estimation of HETP for the reactive packed section; such HETP values are required for the use in EQ model based design. We have demonstrated that the phenomenon of multiple steady states is also found for the NEQ model. However, the 'realizable

window' is much smaller if interphase mass and heat transfer resistances are taken into account, and disappears entirely once catalyst mass transfer is taken into account

There were hardly any differences between a pseudo homogenous nonequilibrium model and a dusty fluid nonequilibrium model for the production of TAME. In the TAME process the overall production rate does not depend on mass transfer resistances (at least, in the range of parameter values studied here). The converse is true for the MTBE process. The rate of consumption of MTBE is very much influenced by additional mass transfer resistances. This indicates that knowledge from one system cannot always be carried over to a similar system.

For the Dusty Fluid Model, there are several model parameters for which good estimation methods are absent. There is a need for methods to estimate diffusion coefficients inside the catalyst. Diffusion coefficients can be concentration dependent, and will, therefore, depend on the concentration and type of the catalyst. Secondly, there are no methods for evaluating nonideal thermodynamic behavior inside a catalyst. Finally, there is a need for correlations for the estimation of mass and heat transfer coefficients from the liquid bulk to the catalyst. This is particularly important for the newest generations of structured catalytic packing.

Chapter 5

Maldistribution in Packed Columns

In this chapter we will illustrate the use of the nonequilibrium zone stage model. We will study the influence of maldistribution on the packing efficiency for a random and for structured packing using a binary system. In addition we will study the influence of maldistribution on two ternary systems. In a final example, the influence of maldistribution in reactive distillation is illustrated. Column behavior due to maldistribution may be explained partly based on the loss of interfacial area. However, we have also found that the performance of the column is influenced by the interaction between maldistribution and the reaction.

5.1 Introduction

In this chapter, we will present various examples to illustrate the use of the nonequilibrium zone-stage model. In the first part of this chapter we will focus on the effect of maldistribution on conventional distillation processes without reaction. We will first consider a binary system of propane and butane. In these systems, the Height Equivalent of a Theoretical Plate (HETP) normally provides an adequate link between the equilibrium stage and the height of a section of packing required to establish the equilibrium stage separation. The influence of maldistribution normally is neglected, or taken into account by means of a correction to the HETP. The nonequilibrium zone stage model offers a direct way to provide insight in the influence of maldistributed internal flows on the packing efficiency for random and structured packings.

Subsequently, we will study the influence of maldistribution on two non-reactive ternary mixtures (Methanol - *iso*-Propanol - Water) and *iso*-Propanol - Benzene - *n*-Propanol. Both systems have a distillation boundary, and multicomponent mass transfer interactions play an important role. It will be shown how maldistribution may significantly influence column behavior.

In the second part of the chapter, the NEQ model will be used to study the influence of maldistribution in reactive distillation by means of the MTBE process. In reactive

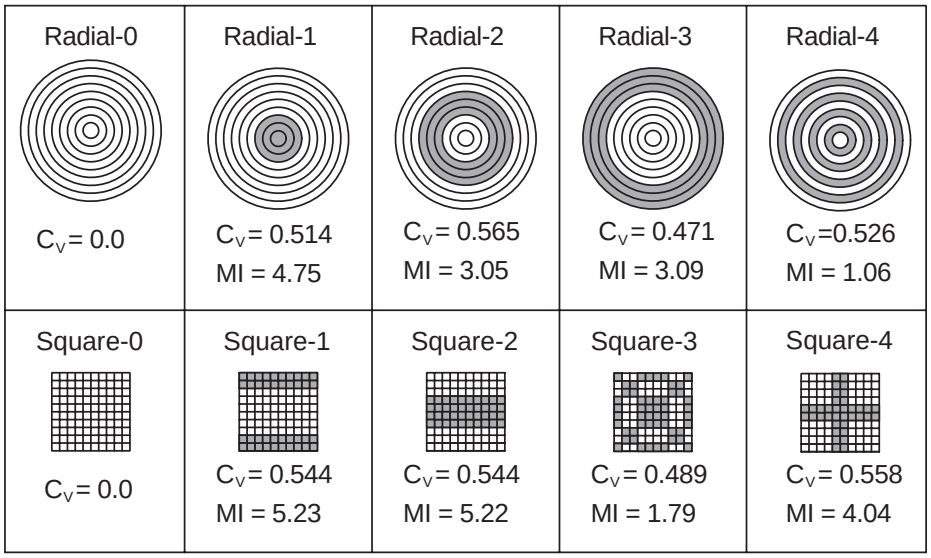

Figure 5.1: Maldistribution patterns

distillation, maldistribution will not only influence the process due to the loss of interfacial area, but also due to changes in the residence time and the residence time distribution.

5.2 Maldistribution Patterns

In the following examples for distillation without reaction we will use various maldistribution patterns for the reflux streams supplied to the packing, represented in Figure 5.1. It is assumed that the superficial velocity of liquid supplied to the grey

zones is three times the superficial velocity supplied to the white zones.

The values of C_v and MI are given in Figure 5.1 as well. Models Radial-0 and Square-0 are the base cases, assuming no maldistribution. It should be noted that all of the square grid cases are axisymmetric and will be modeled by using just part of the column. However, it is quite simple to tackle non-axisymmetric initial distributions with the model as described.

5.3 Random Packing

In this section the effect of maldistribution on random packing is discussed. For simplicity a binary system is used. This is because the HETP concept really only has a physical meaning for binary systems, and the component HETPs are, by definition, equal. For more than two components, the individual component HETPs usually are not equal, and can behave oddly (see, for example, Wesselingh, 1997).

Our case study is based on a column with a packed height of 6 m, which is split up into 60 slices, each of 0.1 m. The column has a total condenser and a partial reboiler. The column is packed with 2 inch Raschig rings. A liquid feed is supplied between stages 31 and 32 at a pressure of 506.6 kPa and a flowrate of 100 $mol \cdot s^{-1}$. The feed is a 50/50 mixture of propane and n-butane The Peng - Robinson equation of state is

used for calculation of the thermodynamic properties. The mass transfer coefficients and the interfacial area are calculated with the method of Onda *et al.* (1968). The column is operated at a reflux ratio of 2.5 and a bottom product flow rate of 50 mol/s.

From initial calculations in design mode, using just a single zone per stage, we find that the column diameter is about 1.1 m. In the remainder of the calculations, the column diameter was fixed at 1.1 m. It follows from Eq. (2.84) that, using a 10 by 10 cell layout in the square grid model, a liquid splitting factor of about 0.66 has to be used. Since we consider our maldistribution patterns to be axisymmetric, a 5 by 5 configuration, with appropriate boundary conditions, will suffice. For the radial model, we use 9 annular zones, resulting in the same splitting factor as for the square model. In addition we will assume that the column internal flows will be perfectly redistributed every 2 m of packing. This corresponds to stages 20 and 40.

For interpretation of the effect of maldistribution on the efficiency of the packing we will use the differential packing HETP, defined by:

$$HETP_i = z_l / E_i^{MV} \tag{5.1}$$

Where z_l is the height of the slice of packing under consideration (in this example z_l = 0.1 m), and E_i^{MV} is the Murphree vapor phase efficiency of component i, calculated

from the results of a nonequilibrium simulation by:

$$E_i^{MV} = \frac{\bar{y}_{i,j} - \bar{y}_{i,j+1}}{\bar{y}^*_{i,j} - \bar{y}_{i,j+1}} \tag{5.2}$$

In which $\bar{y}_{i,j}$ is the average composition of the vapor leaving the slice of packing under consideration, $\bar{y}^*_{i,j}$ is the average concentration of vapor that would be in equilibrium with the liquid phase on the stage under consideration and is obtained from a bubble point calculation of the liquid phase. $\bar{y}_{i,j+1}$ is the average composition of the vapor exiting from the slice below. If the individual component efficiency equals 1, then the stage can be considered an equilibrium stage and the z_l corresponds to the HETP. The HETP for the radial and axisymmetric cases are shown in Figure 5.2 and Figure 5.3 for the 30 stages above the feed. Several observations can be made from these figures: The cases without maldistribution (Radial-0 and Square-0) are reasonably well behaved. The differences between the Square-0 and Radial-0 models are due to the differences in the column flow profiles, that arise in the natural flow model. The natural flow model does not predict a flat velocity profile over the cross section of the column. In the radial model, it is true that for the inner cells the velocity profile is flat, however the velocity in the outer ring is lower. Similarly, in the square grid model, the velocities in the corner cells will be different from the velocities in the cells adjacent to the column wall, which in turn will have velocities different from cells that are fully surrounded by other cells. These 'naturally' occurring different

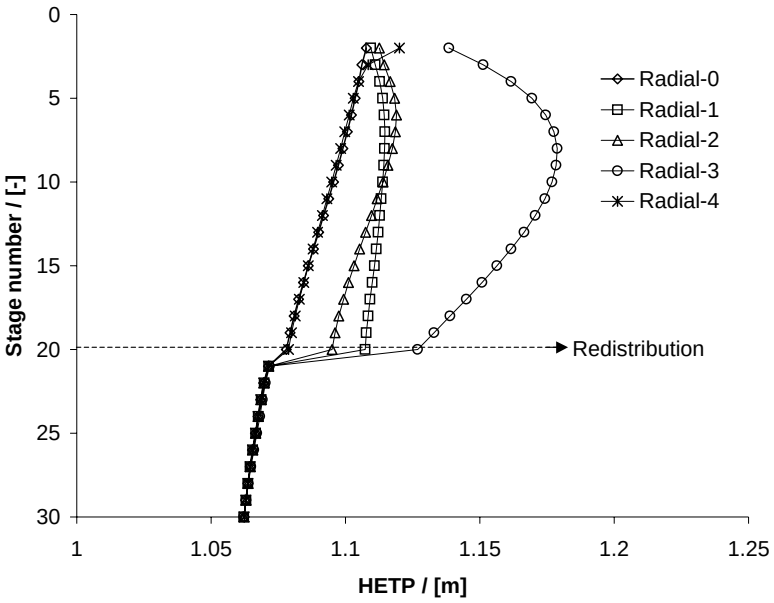

Figure 5.2: Differential HETPs for radial maldistribution cases

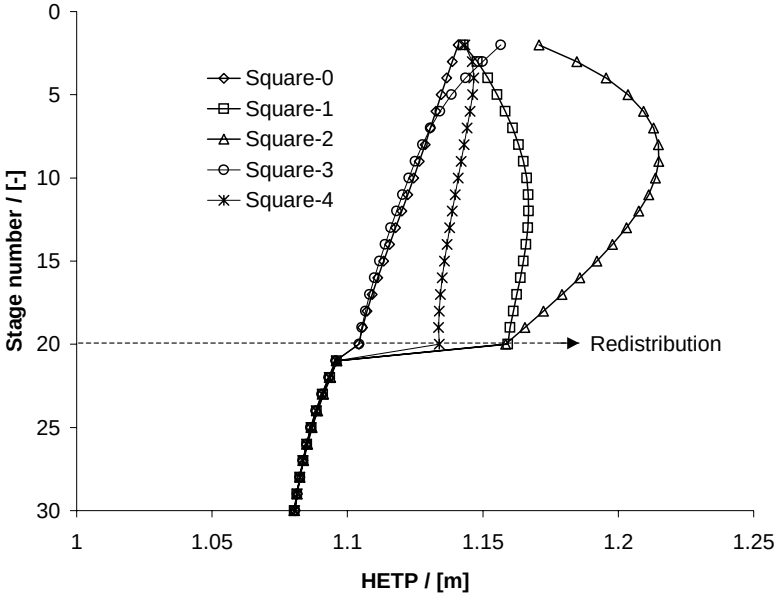

Figure 5.3: Differential HETPs for square grid maldistribution cases

flow profiles give rise to the differences observed between the nonmaldistributed cases Radial-0 and Square-0. It should be noted that normally one would expect higher velocities along the wall and lower velocities closer to the center of the column. This may easily be modeled by adopting an different flow splitting model. The same holds for wall effects in small diameter columns. By adjusting the cell sizes and splitting factors in an appropriate way, one can theoretically impose any kind of flow profile to match flows in a real column.

In addition, there seems to be is some kind of correlation between the deviation of the HETP from the ideal case to the value of the maldistribution index MI. For a low value of MI, cases Radial-4 and Square-3, the behavior is very close to cases Radial-0 and Square-0. For the higher values of MI, the deviations are larger. However, it is also clear that the predictive value of C_v and MI is suspect. This is illustrated by cases Square-1 and Square-2. Although these cases have almost the same values for C_v and MI, the HETP patterns are very different. This is probably due to wall effects that play a much more important role in case Square-1.

The effect of ideally redistributing the flow on stage 20 is clearly visible for both the square grid and the radial cases. As a result of the redistribution, the flow profiles on the stages below stage 20 will be the same for all cases and so will the mass transfer characteristics (HETPs). Above the redistribution the average HETPs are, clearly,

height dependent.

The overall effect of maldistribution is more complicated than can be summarized by a C_v and an MI. These parameters do give adequate information about the degree of maldistribution of the flow, however they do not indicate how the maldistribution influences the column efficiency. It is usually true that maldistribution leads to reduced column efficiency. However, poorer maldistribution characteristics do not necessarily lead to degraded column performance.

5.4 Structured Packing

The development of maldistribution in sheet type structured packing requires some more attention. In sheet type packings, the direction of the channels formed by the sheets dictates a specific spreading direction. Sheets are packed together in a packing element, and a stack of these elements forms the column packing. The elements are placed such that the orientation of the flow direction in the adjacent elements changes by 90^0. This means that after several layers of packing a good redistribution of both phases in all directions should occur.

In modeling the effect of maldistributions on the performance of structured packings, the change in orientation needs to be accounted for. This is particularly interesting

for maldistribution cases in which the initial maldistribution has the same orientation as the first layer of packing. This can be illustrated by looking at cases Square-1 and Square-2 in Fig. 5.1. It is assumed that the first packing element has its sheets oriented along the maldistribution. In this case there will be hardly any exchange between the highly irrigated zone and the lower irrigated zones in the first packing element. This also means that, due to the higher loading, the interfacial area will be lower in the highly irrigated section, reducing the mass transfer efficiency of this section.

To test the above, calculations were done for the same binary system outlined above, with a structured packing replacing the dumped packing. A general sheet type packing is used, with a specific surface area of 300 m^2/m^3, a channel base width of 0.0259 m and a corrugation angle of 45^o. A packed height of 6 m is used, which is split up into slices of 0.1 m each. The feed specification from the original example was maintained, as was the bottom product flow rate. The reflux ratio was set to 1, to obtain a column diameter in the top section of about 0.8 m. This may be adequately described by a 10 by 10 cell layout pattern as represented in Fig. 5.1. Mass transfer coefficients and interfacial areas were calculated with the method of Bravo *et al.* (1992).

Calculations will be done for case Square-2, in which we consider three different

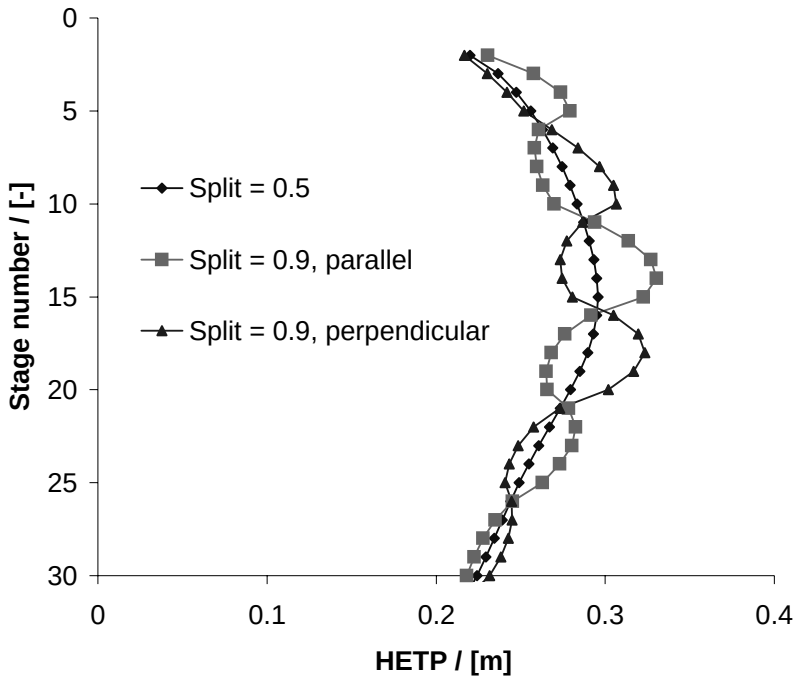

Figure 5.4: Differential HETPs for structured packing

situations. First, we assume that splitting in the x and y directions is equal. Second, we consider a case in which 90 % of the flow splits along the packing, assuming the initial maldistribution has the same orientation as the packing, and third, we will look at a similar situation in which the orientation of the initial maldistribution is perpendicular to the orientation of the packing sheets. We further assume that after each 5 stages (0.5 m) the packing orientation changes.

Shown in Fig. 5.4 are the differential HETPs for the top section of the packing. As

can be seen, the packing anisotropy causes the differential HETPs to meander around the differential HETP that is found if the packing would be isotropic. In addition this figure suggests that the initial maldistribution does not disappear completely, as the meandering is still seen in the lower section of the column. When the maldistribution pattern is parallel to the orientation of the sheets in the packing, the HETP is higher than when the orientation is perpendicular. This is in line with our expectations.

The fact that the initial HETP for the perpendicular split is lower than for the equal split is explained by the fact that with the 0.9 perpendicular split, the liquid will spread out much more rapidly than when using an 0.5 split.

5.5 Ternary System 1: Methanol - *iso*-Propanol - Water

In this section we will focus our attention on a non-ideal mixture of methanol, *iso*-propanol and water. This mixture has one binary azeotrope between *iso*-propanol and water. Total reflux calculations were done with this system. The NRTL model was used for evaluation of nonideal thermodynamic behavior.

Column simulations were done for a packed column with a packing height of 4 m,

Component i	Component j	$a_{i,j}$ / $[J \cdot mol^{-1}]$	$a_{j,i}$ / $[J \cdot mol^{-1}]$	$\alpha_{i,j}$ / [-]
methanol	*iso*-propanol	546.323	-746.121	0.3040
methanol	water	-1518.18	4943.753	0.2970
iso-propanol	water	587.483	6062.742	0.2880

Table 5.1: NRTL parameters for mixture methanol - *iso*-propanol - water

consisting of 1 inch Raschig rings. The correlations due to Onda *et al.* (1968) were used for calculation of mass transfer coefficients and vapor/liquid interfacial areas. The packed section was split up into 40 slices of 0.1 m each. The flow rates were chosen such that a column diameter of about 1 m was obtained. For investigating the influence of maldistribution of the reflux flow on column behavior, the radial maldistribution patterns as given in Fig. 5.1 is used. For the given cell layout, a splitting factor of 0.67 is used to obtain a flow pattern that corresponds to the natural flow model. The column internal flows were redistributed according to distribution pattern Radial-0 in Fig. 5.1.

Plotted in Fig. 5.5 are the concentration profiles as obtained with cases Radial-0, Radial-1 and Radial-3. As can be seen, the differences are considerable. In spite of the fact that both the values of C_v and MI for case Radial-3 are lower than for case Radial-1, the effects of maldistribution are more pronounced for case Radial-3.

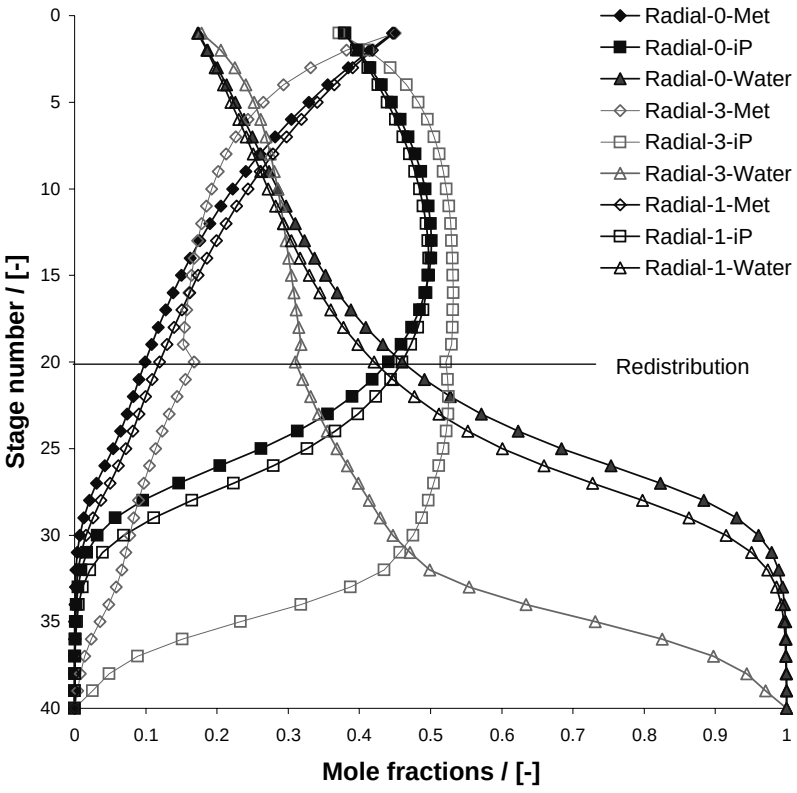

Figure 5.5: Concentration profiles for Methanol - *iso*-Propanol - Water column at various maldistribution patterns

Apparently, the indexes do not completely describe what happens in the column. It should be noted here that in a part of the column under consideration, there is no substantial change in the concentration profiles, and in another section there is a huge jump over just a relatively small number of 'slices'. In these cases, minor differences in the top section of the column may work out to have a substantial influence in the bottom part of the column. Obviously, redistribution cannot prevent this behavior, because most of the 'damage' is done in the top section. The influence of redistribution is visible only in the concentration profiles for Radial-3. This is due to the fact that in the natural flow model, irregularities in the flow profile will be smoothed out along the height of the column and disappear completely if the column is high enough. If the maldistribution is not too severe, the effects will only be felt on a limited number of stages because the natural flow model itself will take care of redistribution.

5.6 Ternary System 2: *iso*-Propanol - Benzene - *n*-Propanol

The *iso*-Propanol - Benzene - *n*-Propanol system also exhibits thermodynamically nonideal behavior. The system has two binary azeotropes, one of which is a low

Component i	Component j	$a_{i,j}$ / $[J \cdot mol^{-1}]$	$a_{j,i}$ / $[J \cdot mol^{-1}]$	$\alpha_{i,j}$ / [-]
iso-propanol	benzene	1386.688	3260.067	0.2913
iso-propanol	*n*-propanol	-2819.03	4150.621	0.2978
benzene	*n*-propanol	4236.07	659.124	0.2888

Table 5.2: NRTL parameters for mixture *iso*-propanol - benzene *n*-propanol

boiling stable node (*iso*-propanol - benzene), the other is a saddle azeotrope between benzene and *n*-propanol. Both azeotropes are connected by a distillation boundary. Total reflux calculations were done for this system, again using the NRTL model.

Column calculations were done for a column with a height of 7 m, packed with 1 inch Raschig rings. The correlations by Onda *et al.* (1968) were used for calculation of mass transfer coefficients and interfacial areas. The packed section was split up into 70 slices of 0.1 m each. The flow rates were chosen such that a column diameter of about 1 m was obtained. A liquid splitting factor of 0.67 was used. The radial maldistribution patterns, as shown in Fig. 5.1 were used for the reflux stream. The internal liquid flows were redistributed over the cross sectional area of the column after 2, 4 and 6 m (at stages 20, 40 and 60).

The observed concentration profiles for cases Radial-0, Radial-1 and Radial-3 are given in Fig. 5.6. Most remarkable here is that for cases Radial-0 and Radial-1,

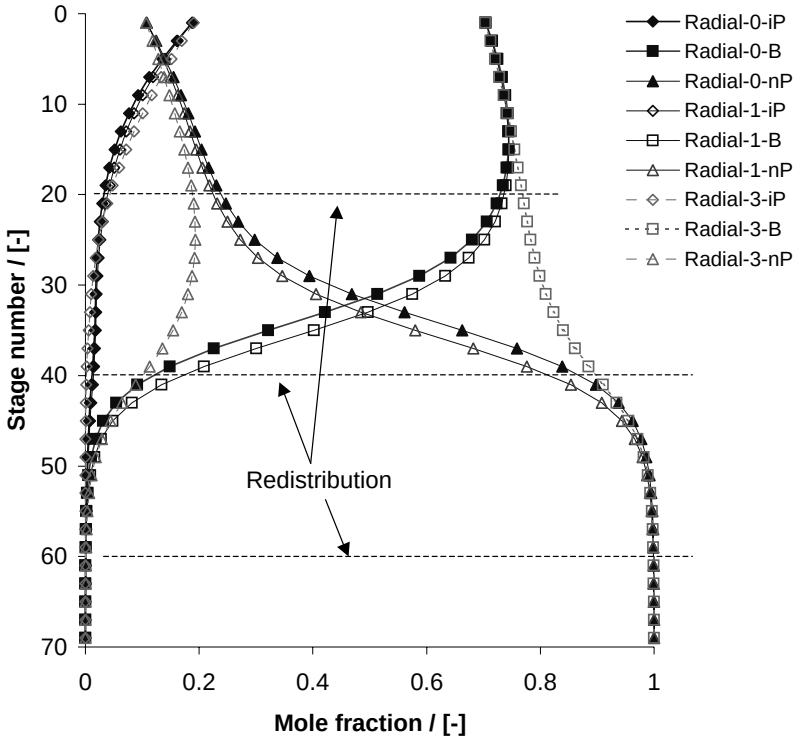

Figure 5.6: Concentration profiles for *iso*-Propanol - Benzene - *n*-Propanol column at various maldistribution patterns

the bottom of the column consists of pure *n*-propanol, whereas for case Radial-3 the bottom product is pure benzene. Depending on how the reflux is maldistributed we can apparently obtain different pure products from one single distillation column.

The reason for the observed behavior can be found in the fact that the maldistribution influences the individual component efficiencies. This is illustrated by the relative efficiency differences between *n*-propanol and *iso*-propanol, given by:

$$\Delta(eff) = \frac{E_{nP}^{MV} - E_{iP}^{MV}}{E_{nP}^{MV}} \tag{5.3}$$

The Murphree vapor phase efficiencies for each slice are calculated from the results of the nonequilibrium model. The results are presented in Fig. 5.7. Shown here are the relative efficiency differences in the top of the column for cases Radial-0, 1 and 3. As can be seen, there are substantial differences between cases Radial-0 and 1 on the one hand and case Radial-3 on the other hand.

Pelkonen *et al.* (1997) have already shown that different models can predict different distillation lines. This is due to the fact that mass transfer interactions may result in changes in the curvature and location of the distillation boundaries. Similar observations are made by Castillo and Towler (1998) who point out that differences between the efficiencies of different components in a ternary mixture can lead to differences in curvature of the distillation lines and boundaries.

In their study, Pelkonen *et al.* (1997) limited themselves to modeling packed column behavior without taking maldistribution into account. As illustrated above, differences in maldistribution may also result in changes in the curvature of the distillation boundaries and lines. This means that distillation lines may start in slightly different directions, and possibly on different sides of the distillation boundary, if the initial

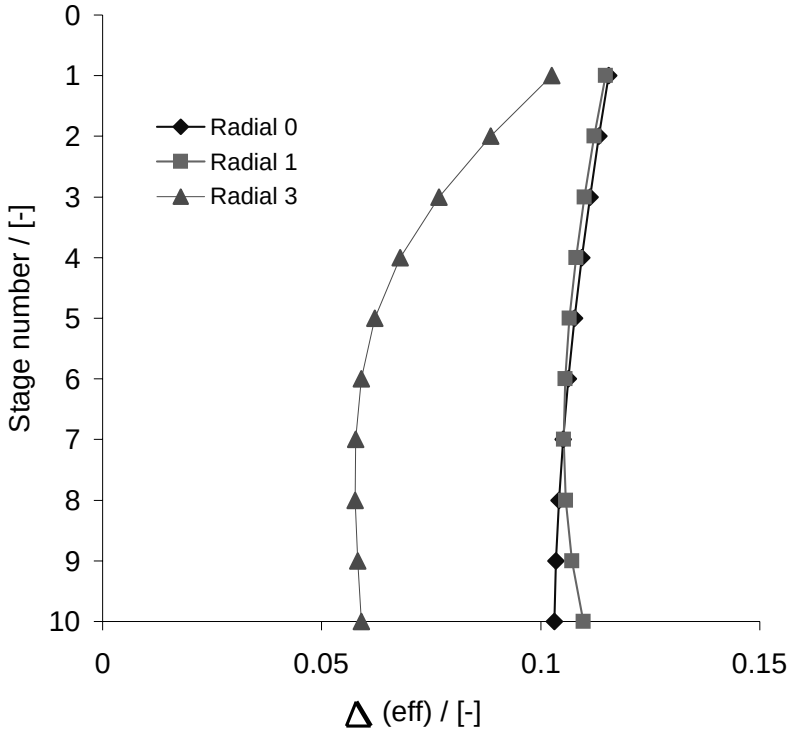

Figure 5.7: Efficiency differences between *iso*-propanol and benzene in top section of column

point is located close to the distillation boundary. This is indeed the case in this example.

To test this conclusion we have done calculations in which all the component efficiencies in a contacting cell were set equal to one another. This was done by neglecting the liquid phase mass transfer resistance and setting all vapor phase diffusivities equal. In this case, there are no relatively large differences in efficiencies in the top part

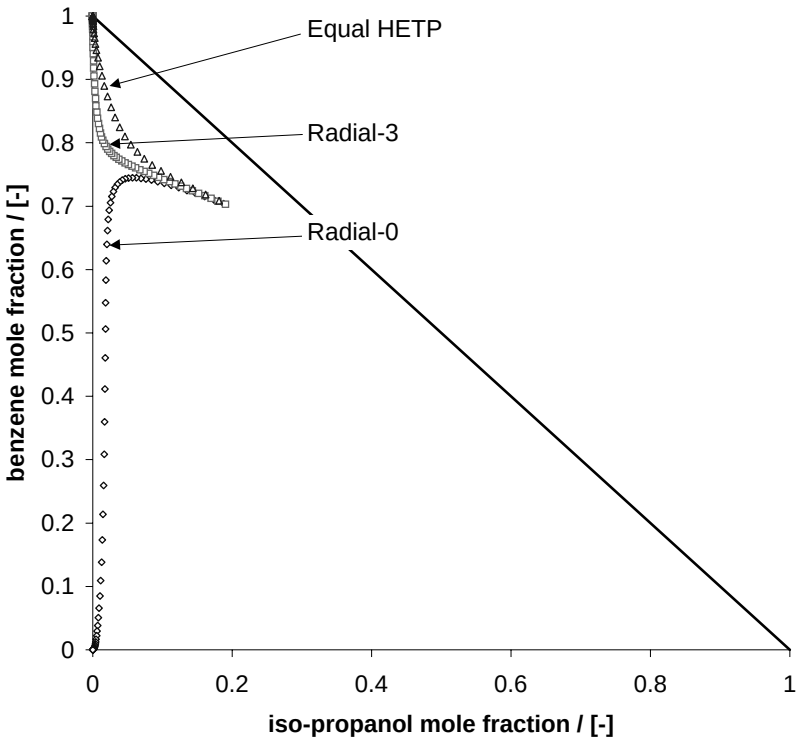

Figure 5.8: Distillation lines for *iso*-Propanol - Benzene - *n*-Propanol system

of the column. As a result, the distillation lines for each individual case will have equal directions at the start, and for all maldistribution cases, that the bottom of the column consists of pure benzene.

The results are summarized in the distillation line map in Fig. 5.8. Plotted here are the distillation lines for case Radial-0, case Radial-3, and the no-maldistribution case with 'equal efficiencies'. All distillation lines originate from the same point, which is

very close to the distillation boundary. From here the no-maldistribution case goes toward the pure *n*-propanol corner. The other two go toward the pure benzene corner.

In addition, we have tested the influence of redistribution by doing the same calculations as described above assuming no redistribution of liquid. The results were very similar to those presented here. Differences in maldistribution patterns lead to distillation lines setting off in slightly different directions. Therefore, redistribution does not have a large impact on the outcome of the calculations, because the important part of the column is just a few stages at the top.

5.7 Reactive System: MTBE Synthesis

As a test case for our nonequilibrium zone stage model we have considered the synthesis of MTBE, using a configuration as presented by Jacobs and Krishna (1993) and shown in Fig. 4.1. In the column under consideration here, packing was used for all sections, rather than a hybrid configuration with both packing and trays that was used in previous works.

We have assumed the nonreactive rectifying and stripping sections are filled with 2 inch Raschig rings, the reactive section with 1/4 inchRaschig rings. Data for the packed section are given in Table 5.3. The rectifying section is taken to be 1 m high,

and is be modeled by means of 10 stages. The reactive section is taken to be 0.7 m high and is modeled by means of 91 stages. Higler *et al.* (1999c) found that this large number of stages was required because of the highly nonlinear interaction between the reaction rates and the temperatures inside the catalytic packing. The stripping section is taken to be 2.5 m and is described by means of 27 stages. The correlations of Onda *et al.*, (1968) are used for the calculation of mass transfer coefficients and interfacial areas. The splitting factors for the individual sections may be calculated using Eq. (2.83). Packing data are supplied in Table 5.3. The reaction was modeled by means of a pseudo homogeneous kinetic expression.

The calculations were limited to maldistributions in the reflux flow. We also assume that maldistributions between the different sections of packing will go straight down to the section below.

5.7.1 Calculations

The first set of calculations considers the influence of the natural flow model on the reactive distillation process. Here we compare calculations done with just one zone per stage and with calculations with 6 zones per stage, assuming that there is no maldistribution of any of the streams supplied to the packing (reflux, feeds and reboil

	Rectifying section	Reactive section	Stripping section
Column diameter (m)	6.0	6.0	6.0
Total column area (m^2)	28.3	28.3	28.3
Packing height (m)	1.0	0.7	2.5
Specific packing surface (m^2)	95	600	95
Packing size (in)	2	1/4	2
Void fraction $(-)$	0.74	0.72	0.74
Nominal size (m)	0.0508	0.00635	0.0508
Critical surface tension $(N \cdot m^{-1})$	0.061	0.061	0.061
Packing Factor $(-)$	213.2	5249.34	213.2
Splitting factor $(\mathcal{K}^L)$ $(-)$	0.995123	0.999953	0.995484

Table 5.3: Packing data for reactive distillation column

streams). The difference between the two calculations is that when using one zone per stage the velocity profile of the liquid flowing down the packing is flat, whereas when using the natural flow model a velocity profile will develop, even if there is no maldistribution. Given in Fig. 5.9 are the conversion of i-butene (top of figure) and mole fraction of MTBE in the bottom product stream (bottom of figure) as a function of the bottom product flowrate. Using one cell per stage (flat flow), we see that there are multiple steady states in the range for the bottom product flowrate between 191 and 196 mol/s. This is similar to the findings presented in the previous chapter. However, when using the natural flow model the multiple steady state range disappears.

This may be due to the fact that in the natural flow model the liquid does not flow uniformly along the packing. In some sections of the packing this will result in loss of interfacial area. The effects of the reduction of the overall facility for mass transfer have already been discussed (see Chapter 4), and we do indeed see similar behavior. The multiple steady state region has disappeared, and for the natural flow model the low production branch is higher than for the uniform flow model. This is because the increased mass transfer resistance reduces the influence of the backward reaction rate, leading to an increased conversion.

In addition, there may be an effect of the different residence times that will 'flatten'

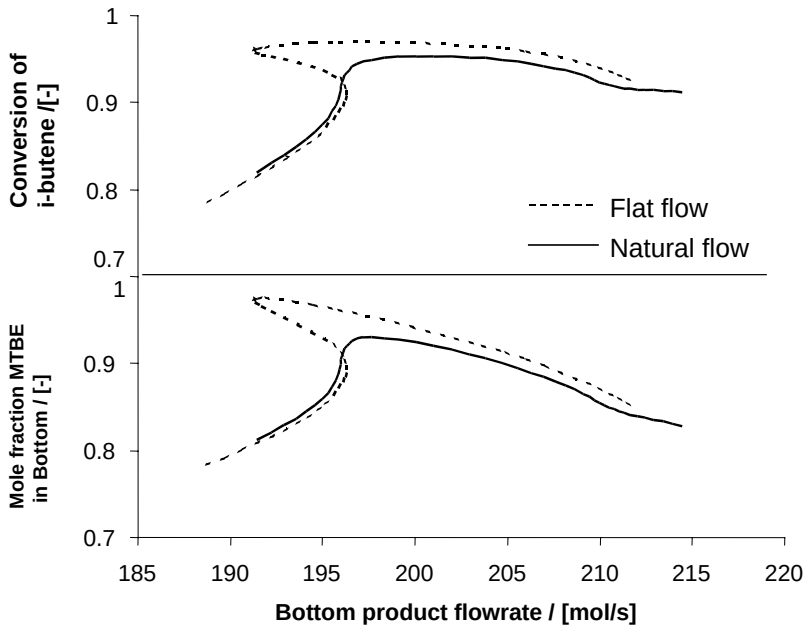

Figure 5.9: Comparison of conversion and bottom product purity for no maldistribution model and natural flow model

temperature and concentration profiles. Gradients in these profiles are much steeper in the low production branch than in the high production branch.

In subsequent calculations the superficial liquid velocity of the reflux stream to the inner three cells of the column was increased by steps of 2% relative to the average flowrate. Fig. 5.10 shows the conversion of *i*-butene as a function of the bottom product flowrate for these cases. It is immediately clear that minor deviations in the flow pattern may have a substantial influence on the conversion in the bottom

product flowrate region between 197 and 207 mol/s.

The reason for this high sensitivity is not so clear. It is not caused only by the loss of interfacial area. In that case, we would not expect the large deviations observed between 195 and 207 mol/s. An explanation for the observed behavior can be found in the production rate profiles shown in Fig. 5.11. These profiles were generated at a bottom product flowrate of 202 mol/s. The result of increasing the flow in the center is clearly visible: the reaction rate profile is 'shifted up' in the catalytic packing, as a result of which, for the highest maldistributed case, part of the catalytic section is used for consumption of MTBE. This undesired effect results in the larger difference in the bottoms flowrate region between 195 and 207 mol/s. The upswing in the conversion that is found between 203 and 207 mol/s for the 4 to 10 % cases may be explained as follows: As the bottom product flowrate increases, the reaction rate profile will be 'flushed' down the packing. As a result, the entire packing will again be used for production of MTBE, resulting in a higher conversion.

Summarizing, we can say that maldistribution does not only have an influence on the interfacial area, but also on the reaction rate profiles. This high sensitivity is quite remarkable since, even in the worst case scenario where the superficial liquid velocity in the center is only 10 % higher than in the outer rings, the C_v value is less than 0.05. Perry *et al.*, (1990) state that a C_v value of less than 0.1 for a distributor is

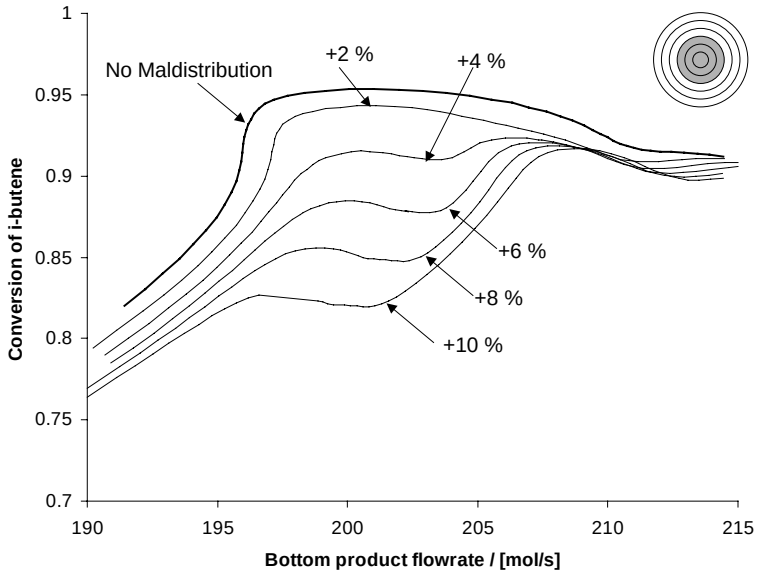

Figure 5.10: Influence of increasing flow down the center of the column on product purity

adequate, provided the maldistributions are randomly dispersed. That this may not be the case is suggested by the value of the maldistribution index $MI = 3$.

In the next set of calculations we have reversed the maldistribution pattern used in the previous calculations and increased the superficial liquid velocity in the three outside rings, up to a maximum of an 8% higher liquid velocity. Shown in Fig. 5.12 is the conversion of i-butene as a function of the bottom product flowrate for the various maldistribution cases obtained with the nonequilibrium cell model. It can

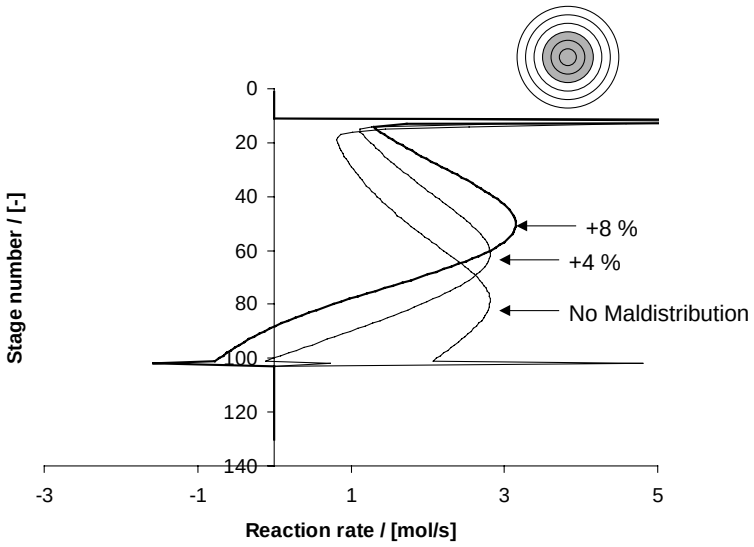

Figure 5.11: production rate profiles obtained at a bottom product flowrate of 202 mol/s for MTBE column at three maldistribution cases

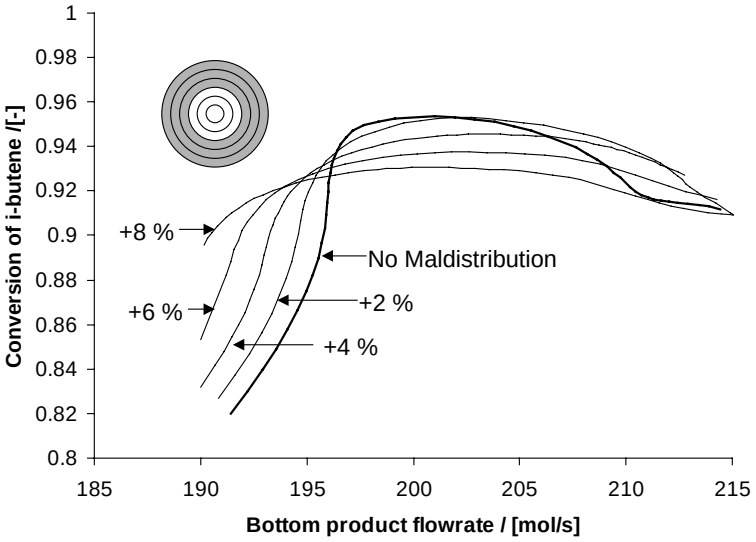

Figure 5.12: Influence of increasing flow close to the wall of the column on i-butene conversion

be seen that the maximum attainable conversion is lowered by the maldistribution. However, below a bottom product flowrate of 195 mol/s the conversion obtained under maldistribution is, in fact, higher than was obtained without maldistribution. In this case, maldistribution actually seems to improve the performance of the column!

The observed behavior may be explained based on the effect of the loss of interfacial area on the reaction rates. Higler *et al.*, (1999) present a parametric study of the influence of the mass transfer coefficient on the overall column conversion. They

concluded that, because in the low conversion branch the reaction is proceeding in the "wrong" direction, the reduced facility for mass transfer will lessen this effect and, therefore, result in a higher conversion.

To test if this reduced facility for mass transfer really causes the observed results, we have done calculations in which we have reduced the interfacial area for the non-maldistributed case by 5%. Fig. 5.13 provides a comparison of three cases: First, the nonmaldistributed case with base case interfacial area, obtained from the Onda *et al.* (1968) correlation. Second the maldistributed case, in which the superficial velocity of the reflux in the outer three cells was increased by 4%, and third the nonmaldistributed case, in which the base case interfacial area was reduced by 5%. In the section of the curve above 195 mol/s there is a good match between the two cases without maldistribution. Here, the differences between the various maldistribution cases are mainly due to combined effects of the reaction and maldistribution and mass transfer. The influence of the interfacial area, and differences of the interfacial area on the process are negligible.

However below a bottom product flowrate of 195 mol/s, there is a close match between the 'reduced-area' case and the 4% maldistributed case. This leads us to believe that, in this region, the observed changes due to maldistribution are mainly due to the loss of interfacial area.

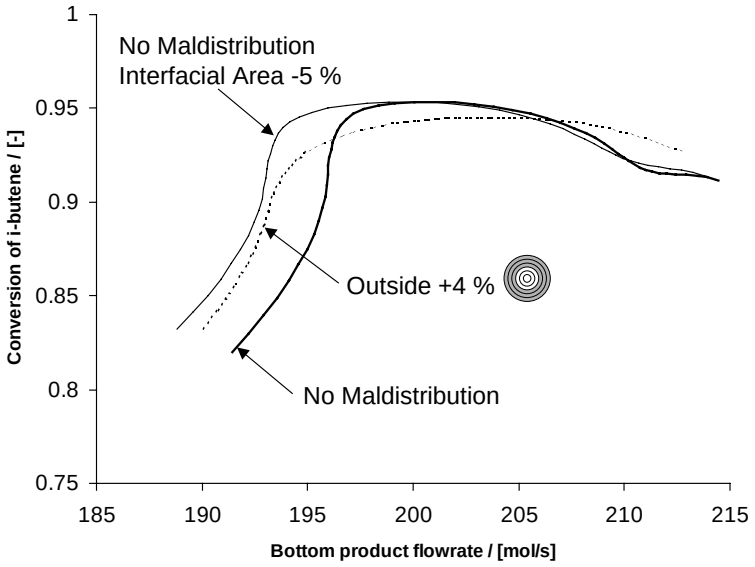

Figure 5.13: Influence of interfacial area on conversion of i-butene

Another important issue that is addressed here is the need for accurate prediction models for interfacial areas and mass transfer coefficients. In this example, a reduction in the interfacial area of 5% results in significantly different steady state behavior. Most prediction models are not within 5% accurate, indicating the need for improvement.

In a final set of calculations we have focussed on supplying more liquid to the single cell next to the wall. Fig. 5.14 shows the conversion of i-butene as a function of the bottom product flowrate for various maldistribution cases. We see an interesting

development in conversion with increasing the liquid flow to the outer ring. Initially, we see an overall increase in conversion (4% curve). A further increase then leads to a drop in conversion and in a shift of the downswing of the conversion to lower bottom product flowrates. The observed behavior is caused by two phenomena. A moderate increase in the flow to the outer ring will cause the flow further down the column to be more evenly distributed than is the case for the natural flow model. The resulting flow model will be in between the natural flow model and the uniform flow model as presented in Fig. 5.9. Further increase of the flow will make the loss of interfacial area due to maldistribution more important leading to the overall lower conversion and the shift of the downswinging curve to the left. This is similar to the behavior illustrated in Fig. 5.12.

5.8 Conclusions

Calculations for some maldistribution cases have indicated that there is some correspondence between the observed deviations of the efficiencies from 'ideal' behavior and the currently available methods for reporting maldistribution, the C_v value and the maldistribution index MI. It should, however, be noted that in some cases, these parameters provide inadequate information. It is generally true that maldistribution

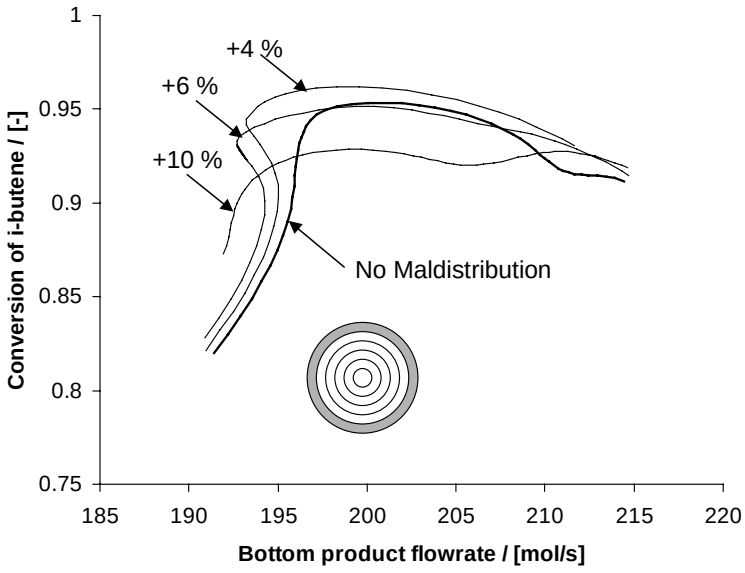

Figure 5.14: Influence of increasing flow close to the wall of the column on product purity

results in loss of efficiency, but poorer maldistribution does not necessarily lead to poorer efficiency. Simulations show that even for binary mixtures, packing HETPs can be a function of the height of the packing.

Efficiencies and HETPs in multicomponent systems tend to be confusing, and the effect of maldistribution on these parameters is ambiguous. We have shown for two ternary systems that different maldistribution patterns can result in substantial differences in column behavior. In some cases, choosing a different maldistribution pattern may lead to a completely different product from a column. To the best of our knowledge, such an observation has not been made before. This observation needs experimental verification.

For reactive systems, have found that in some cases, column behavior due to maldistribution may be explained based on the loss of interfacial area due to liquid and vapor channelling. However, the performance of packed reactive distillation columns appears to be much more sensitive to maldistribution than one would expect, based solely on loss of interfacial area. In these cases, the interaction between maldistribution and the reaction is very important.

This large sensitivity indicates the need for realistic flow models, since small differences can have large effects. It remains, however, unclear as to how the predictive

quality of the nonequilibrium Zone/Stage model presented here depends on the flow model used. In this work we have considered only the simple model for flow as outlined by Zuiderweg *et al.* (1993).

References

- Abufares, A.A. and Douglas, P.L., (1995), Mathematical modeling and simulation of an MTBE catalytic distillation process using SPEEDUP and AspenPlus, *Trans. IChemE.*, **73**, 3 - 12

- Agreda, V.H., Partin, L.R. and Heise, W.H. (1990) High-purity methyl acetate via reactive distillation, *Chem. Eng. Progress*, **2**, 40 - 46.

- AIChE, (1958) Bubble tray design manual, Prediction of fractionation efficiency, AIChE, New York

- Ainsworth, (1991), Booming MTBE demand draws increasing number of producers, *Chem. Eng. News*, 13-16

- Alejski, K. (1991), Computation of the reacting distillation column using a liquid mixing model on the plates, *Comput. Chem. Engng.*, **15**, 313 - 323

- Alejski, K., Szymanowski, J., and Bogacki, M., (1988) The application of a minimization method for solving reactive distillation problems, *Comput. Chem. Engng.*, **12**, 833 - 839

- Backhaus, A.A., (1921), Continuous processes for the manufacture of esters, *US patent 1.400.849*

- Backhaus, A.A., (1922), Apparatus for producing high grade esters, *US patent 1.403.224*

- Backhaus, A.A., (1923a), Process for producing high grade esters, *US patent 1.454.462*

- Backhaus, A.A., (1923b), Process for esterification, *US patent 1.454.463*

- Barbosa, D., and Doherty, M.F., (1988a) The influence of equilibrium chemical reactions on vapor liquid phase diagrams, *Chem. Eng. Sci.*, **43**, 529 - 540

- Barbosa, D., and Doherty, M.F., (1988b) The simple distillation of homogeneous reactive mixtures, *Chem. Eng. Sci.* **43**, 541 - 550

- Barker, P.E. and Self, M.F., (1962), The evaluation of liquid mixing effects on a sieve plate using unsteady and steady state tracer techniques. *Chem. Eng. Sci.* **17**, 541

- Baur, R., Higler, A.P., Taylor, R., and Krishna, R. (1999) Comparison of equilibrium stage and non-equilibrium stage models for reactive distillation, *Chem. Eng. Journal*, submitted for publication.

- Bennett, D.L., Agrawal, R., and Cook, P.J., (1983), New pressure drop correlation for sieve tray distillation columns, *AIChE Journal* **29**, 434 - 442

- Bennett, D.L. and Grimm, H.J. (1991) Eddy diffusivity for distillation sieve trays, *A.I.Ch.E. Journal* **37**, 589 - 596

- Berg, , D.A. and Harris, T.J., (1993), Characterisation of multicomponent diffusion effects in MTBE synthesis. *Ind. Eng. Chem. Res.* **32**, 2147-2158.

- Billingham, J.F., Bonaquist, D.P., and Lockett, M.J., (1997), Characterization of the performance of packed distillation column liquid distributors, *IChemE Symp. Ser.* **142**, 841 - 851

- Bravo, J.L., Pyhalahti, A., and Järvelin, H., (1993) Investigations in a catalytic distillation pilot plant: Vapor/liquid equilibrium, kinetics and mass transfer issues *Ind. Eng. Chem. Res.* **32** 2220 - 2225

- Bravo, J.L., Rocha, J.A., and Fair, J.R., (1992) Distillation columns containing structured packings: A comprehensive model for their performance. 1. Hy-

draulic models. *Ind. Eng. Chem. Res.* **32** 641 - 651

- Carra, S., E. Santacesaria, M. Morbidelli and L. Cavalli (1979a) Synthesis of propylene oxide from propylene-chlorohydrins - I Kinetic aspects of the process, *Chem. Eng. Sci.* **34**, 1123 - 1132

- Carra, S., M. Morbidelli, E. Santacesaria and G. Buzzi (1979b) Synthesis of propylene oxide from propylene chlorohydrins - II. Modeling of the distillation with chemical reaction unit, *Chem. Eng. Sci.* **34**, 1133 - 1140

- Castillo, F.J.L., and Towler, G.P., (1998) Influence of multicomponent mass transfer on homogeneous azeotropic distillation, *Chem. Eng. Sci.*, **53**, 963-976

- Chan, H., and Fair, J.R., (1984) Prediction of point efficiencies on Sieve trays *Ind. Eng. Chem. Res.* **33**, 907 - 913

- Chang, Y.A., and Seader, J.D., (1988), Simulation of continuous reactive distillation by a homotopy continuation method, *Comput. Chem. Eng.* **12**, 1243 - 1255

- Ciric, A.R. and Miao, P., (1994) Steady state multiplicities in an ethylene glycol reactive distillation column, *Ind. Eng. Chem. Res.* **33** 1123-1132

- Ciric, A.R., and Gu. D., (1994), Synthesis of nonequilibrium reactive distillation by MINLP optimization, *A.I.Ch.E.J.* **40**, 1479 - 1487

- Davies, B., Jenkins JD., and Dilfanian, S., (1979) Distillation with chemical reaction - The distillation of formaldehyde solutions in a sieve plate column. *I.Chem.E. symp. ser.*, **56**, 65 - 79

- DeGarmo, J.L., Parulekar, V.N., and Pinjala, V., (1992), Consider Reactive Distillation, *Chem. Eng. Prog.* **88**, 43 - 50

- Deufelhard, P., Hairer, E., and Zugck, J., (1987) One-step and extrapolation methods for differential-algebraic systems, *Numer. Math.* **51**, 501 - 516

- Doherty, M.F. and G. Buzad, (1992), Reactive Distillation by Design, *Trans IChemE*, **70** part A, 448 - 458

- Edwards, D.P., Krishnamurthy, K.R., and Potthoff, R.W., (1998), Development of an improved method to quantify maldistribution and its effect on structured packing column performance, *presented at AIChE annual meeting, Miami Beach, Florida*

- Eldarsi, H.S., and Douglas, P.L., (1998), Methyl-*tert*-butyl-ether catalytic distillation column, Part I: Multiple steady states, *Trans. IChemE.* **70** 448-458

- Evans III, R.B., Watson, G.M., and Mason, E.A., (1961) Gaseous diffusion in porous media at uniform pressure , *J. Chem. Phys.*, **35**, 2076

- Evans III, R.B., Watson, G.M., and Mason, E.A., (1962) Gaseous diffusion in porous media (II) effect of pressure gradients, *J. Chem. Phys.*, **36**, 1894

- Froment, G.F., Bischoff, K.B., (1990) Chemical Reactor Analysis and Design, Second edition, Wiley, New York, 1990

- Gautreaux and O'Connell, (1955), Effect of length of liquid path on tray efficiency ,*Chem. Eng. Prog.* **51**, 232

- Hauan, S., Hertzberg, T., and Lien, K.M., (1995), Why Methyl-tert-butyl-ether production by reactive distillation may yield multiple solutions, *Ind. Eng. Chem. Res.* **34**, 987 - 991

- Higler, A., Taylor, R. and Krishna, R., (1999b) Nonequilibrium Modelling of Reactive Distillation: Multiple steady states in MTBE synthesis, *Chem. Eng. Sci.*, **54**, 1389-1395

- Hoek, P.J., Wesselingh, J.A., and Zuiderweg, F.J. (1986), Small scale and large scale liquid maldistribution in packed columns, *Chem. Eng. Res. Des.*, **64** 431 - 449

- Huang, C., Yang, L., Ng, F.T.T., and Rempel, G.L., (1998) Application of catalytic distillation for the aldol condensation of acetone: a rate-based model in simulating the catalytic distillation performance under steady-state operations, *Chem. Eng. Sci.* **53**, 3489-3499

- Hughes, W.B., (1970) Kinetics and mechanism of homogenous olefin disproportionation reaction. *J. Am. Chem. Soc*, **92**, 532 - 536

- Humphrey, J.L., and Seibert, A.F., (1992) New horizons in distillation, *Chem. Eng.* **12**, 86 - 98

- Jackson, R., (1977), Transport in porous catalysts, Elsevier, Amsterdam

- Jacobs, R., and Krishna, R., (1993) Multiple solutions in reactive distillation for methyl-tert-butyl ether synthesis, *Ind. Eng. Chem. Res.*, **32**, 1706 - 1709

- Keyes, D.B., (1932), Esterification processes and equipment, *Ind. Eng. Chem.* **24**, 1096

- Kirschbaum, E. (1937) Distillation and Rectification. Chemical Publishing Co., New York

- Kooijman, H.A., (1995), Dynamic Nonequilibrium Column Simulation, Ph.D Dissertation, Clarkson University, Potsdam, New York.

- Kooijman, H.A., and Taylor, R. (1995) Modelling mass transfer in multicomponent distillation, *Chem. Eng. Journal* **57** 177 - 188

- Krevelen, D.W. van, and Krekels, J.T.C., (1948) Rate of dissolution of solid substances, *Recl. Trav. Chim. Pays-Bas.* **14**, 1 - 68

- Krishna, R. and Wesselingh, J.A., (1997), The Maxwell-Stefan Approach to Mass Transfer, *Chem. Eng. Sci.* **52**, 861 - 911

- Krishnamurthy, R., and Taylor, R., (1985a), A nonequilibrium stage model of multicomponent separation processes: I. Model description and method of solution, *AIChE Journal* **31**, 449 - 457

- Krishnamurthy, R., and Taylor, R., (1985b), A nonequilibrium stage model of multicomponent separation processes: II. Comparison with experiments *AIChE Journal* **31**, 457-465

- Krishnamurthy, R., and Taylor, R., (1985c), A nonequilibrium stage model of multicomponent separation processes: III. The influence of unequal component efficiencies in process design problems *AIChE Journal* **31**, 1973

- Krishnamurthy, R., and Taylor, R., (1985d), Simulation of packed distillation and absorption columns. *Ind. Eng. Chem. Proc. Des. Dev.* **24**, 513-524

- Krishnamurthy, R., and Taylor, R., (1986), Absorber simulation and design using a nonequilibrium model, *Can. J. Chem. Eng.* **64** 96 - 105

- Kreul, L.U., Gorak, A., and Barton, P.I., (1999), Modeling of homogeneous reactive separation processes in packed columns, *Chem. Eng. Sci.* **54**, 19 - 34

- Kubicek, M., (1976) Algrithm 502, dependence of a solution of nonlinear systems on a parameter, *ACM. Trans. Math. Softw.* **2** 98 - 107

- Landschützer, H. and Bart, H.-J. (1995), Heterogeneous reactive distillation with axial backmixing and nonequilibrium mass transfer, *presented at AIChE Annual meeting, Miami Beach, Fl*, paper 19f.

- Lee, J.H., Dudukovic, M.P., (1998), A comparison of the equilibrium and nonequilibrium models for a multicomponent reactive distillation column, *Comput. Chem. Eng.*, **23**, 159-172

- Lewis, W.K., (1936), Rectification of binary mixtures, *Ind. Eng. Chem* **28**, 399

- Lockett, M.J., (1986) *Distillation tray fundamentals* Cambridge, Cambridge University Press

- Marek, J. (1956), Rectification with a chemical reaction. II. Plant rectification of a water-acetic acid - acetic anhydride mixture. *Coll. Czech. Chem.*

Commun. **21** 1561-1568

- Mason, E.A., Evans III, R.B., and Watson, G.M., (1963), Gaseous diffusion in porous media (III) thermal transpiration, *J. Chem. Phys.*, **38** 1808

- Mason, E.A., and Malinauskas, A.P., (1964), Gaseous diffusion in porous media (IV) thermal diffusion , *J. Chem. Phys.*, **41** 3815

- Mason, E.A., Malinauskas, A.P., and Evans III, R.B. (1967) Flow and diffusion of gasses in porous media, *J. Chem. Phys.* **41** 3199

- Maxwell, JC., (1866), On the dynamical theory of gases *Phil. Trans. Roy. Soc.*, **157** 49-88

- Mohl, K.D., Kienle, A., Gilles. E.D., Rapmund, P., Sundmacher, K., and Hoffmann, U., (1999) Steady state multiplicities in reactive distillation columns for the production of fuel ethers MTBE and TAME: Theoretical analysis and experimental verification. *Chem. Eng. Sci.* **54** 1029 - 1043

- Murphree, E.V., (1925), *Ind. Eng. Chem.* **17**, 605-611

- Nawrocki, P.A., Xu, Z.P., and Chuang, K.T., (1991), Mass transfer in structured corrugated packing, *Can. J. Chem. Eng.* **69**, 1336 - 1343

- Nelson, P.A., (1971), Countercurrent equilibriumstage separation with reaction, *AIChE Journal*, **17**, 1043 - 1049

- Nijhuis, S.A., Kerkhof, F.P.J.M., and Mak, A.N.S., (1993) Multiple steady states during reactive distillation of methyl-tert-butyl ether, *Ind. Eng. Chem. Res.* **32**, 2767 - 2774

- Okasinski, M.J., and Doherty, M.F., (1998), Design method for kinetically controlled, staged reactive distillation columns. *Ind. Eng. Chem. Res.* **37**, 2821 - 2834

- Onda, K., Takeuchi, H. and Okumoto, Y., (1968) Mass transfer coefficients between gas and liquid phases in packed columns, *J. Chem. Eng. Jap.*, **1**, 56 - 62

- Oost, C., and Hoffmann, U., (1995) The synthesis of tertiary amyl ether (TAME): Microkinetics of the reactions *Chem. Eng. Sci.* **51** 329 - 340

- Pelkonen, S., Kaesemann, R., and Gorak, A., (1997) Distillation lines for multicomponent separation in packed columns: Theory and comparison with experiments *Ind. Eng. Chem. Res* **36**, 5392 - 5398

- Perez-Cisneros, E., Gani, R., and Michelsen, M.L., (1997) Reactive separation

systems I. Computation of physical and chemical equilibrium *Chem. Eng. Sci.* **52**, 527-543

- Perry, D., Nutter, D.E., and Hale, A., (1990), Liquid distribution for optimum packing performance, *Chem. Eng. Progr.* **86** 30

- Pinjala, V., DeGarmo, J.L., Ulowetz, M.A., Marker, T.L, and Luebke, C.P., (1996) Rate based modeling of reactive distillation operations, *AIChE Annual meeting*, session 3

- Podrebarac, G.G., Ng, F.T.T., and Rempel, G.L., (1998), The production of diacetone alcohol with catalytic distillation Part II: A rate-based catalytic distillation model for the reaction zone, *Chem. Eng. Sci.* bf 53, 1077-1088

- Porter, K.E., and Jones, M.C., (1963) Theoretical prediction of liquid distribution in a packed column with wall effect, *Trans. IChemE* **41**. 240 - 247

- Powell, M.D.J., (1965) A method for minimizing a sum of squares of nonlinear functions without calculating derivatives. *Comput. J.* **7**, 303

- Raper, J.A., Pinczewski, W.V., and Fell, C.J.D., (1984), Liquid passage on sieve trays operating in the spray regime, *Chem. Eng. Res. Des.* **62** 111

- Rehfinger, A., and Hoffmann, U., (1990) Kinetics of methyl-tert-butyl ether liquid phase synthesis catalyzed by ion exchange resin. I - Intrinsic rate expression in liquid phase activities, *Chem. Eng. Sci.* **45**, 1605 - 1616

- Rehfinger, A., and Hoffmann, U., (1990) Kinetics of methyl-tert-butyl ether liquid phase synthesis catalyzed by ion exchange resin, II - Macropore diffusion of MeOH as rate controlling step. *Chem. Eng. Sci.*, **45**, 1619 - 1626

- Rihko, L.K., Linnekoski, J.A., and Krause, A.O., (1994) Reaction equilibria in the synthesis of TAME and TAEE in the liquid phase *J. Chem. Eng. Data* **39**, 700 - 704

- Rihko, L., and Krause, A.D., (1995), Kinetics of the heterogeneously catalyzed tert-amyl-methyl-ether reactions in the liquid phase *Ind. Eng. Chem. Res.* **34** 1172 - 1180

- Sawistowski, H., and Pilavakis, P.A., (1979), Distillation with chemical reaction in a packed column. *IChemE Symp. Ser.* **56**, 49 - 63.

- Shoemaker, J.D., and Jones, E.D., (1987), Cumene by catalytic distillation, *Hydrocarbon processing*, **6**, 283 - 303

- Siirola, J.J., (1995), An industrial perspective on process synthesis, *AIChE.*

Symp. Ser. no. 304 **Vol 91**, 222 - 233

- Simandl, J. and Svrcek, W.Y., (1991), Extension of the simultaneous solution and inside-outside algorithms to distillation with chemical reactions, *Comput, Chem. Engng.*, **15**, 337 - 348

- Sneesby, M.G., Tadé, M.O., Datta, R., and Smith, T.N., (1997a), ETBE synthesis via reactive distillation. 1. Steady state simulation and design aspects, *Ind. Eng. Chem. Res.*, **36**, 1855 - 1869

- Sneesby, M.G., Tadé, M.O., Datta, R., and Smith, T.N., (1997b), ETBE synthesis via reactive distillation. 2. Dynamic simulation and control aspects, *Ind. Eng. Chem. Res.*, **36**, 1870 - 1881

- Sohlo, J. and Kinnunen S., (1977), Dispersion and flow phenomena on a sieve plate, *Trans IChemE.* **55**, 71

- Spes, (1966), Katalytische Reaktionen in Ionenaustaucherkolonnen unter Verschiebung des chemische Geleichgewichts, *Chemiker Atg/Chem. Apparatur*, **90**, 443-446

- Stikkelman, R.M., (1989) Gas and liquid maldistributions in packed columns, Ph.D Dissertation, Delft Technical University, Delft, the Netherlands

- Stoter, C.F., (1993) Modelling of maldistribution in structured packigns: From detail to column design, Ph.D Dissertation, Delft Technical University, Delft, the Netherlands

- Stoter, C.F., Olujic, Z., and de Graauw, J., (1992), Modelling of hydraulic and separation performance of large diameter columns containing structured packings, *IChemE Symp. Series* **128**, A201 - A210

- Sundmacher, K., and Hoffmann, U., (1992), Importance of irreversible thermodynamics for liquid phase ion exchange catalysis: Experimental verification for MTBE synthesis, *Chem. Eng. Sci.*, **47** 2733 - 2738

- Sundmacher, K., and Hoffmann, U., (1994a), Multicomponent mass and energy transport on different length scales in a packed reactive distillation column for heterogeneously catalysed fuel ether production, *Chem. Eng. Sci.* **49**, 4443-4464

- Sundmacher, K., and Hoffmann, U., (1994b), Macrokinetic analysis of MTBE synthesis in chemical potentials, *Chem. Eng. Sci.*, **49** 3077 - 3089

- Sundmacher, K., (1995) Reaktivdestillation mit katalytischen Füllkör- perpackungen - ein neuer Prozeß zur Herstellung der Kraftstoffkomponente MTBE,

Ph.D. Thesis, Technischen Universität Claustahl, Claustahl Zellerfeld, Germany.

- Sundmacher, K., Uhde, G., and Hoffmann, U., (1999), Multiple reactions in catalytic distillation processes for the production of the fuel oxygenates MTBE and TAME: Analysis by rigorous model and experimental validation. *Chem. Eng. Sci.* **54** 2839-2847

- Suzuki, I., Yagi, H., Komatsu, H., and Hirata, M., (1971) Calculation of multicomponent distillation accompanied by a chemical reaction, *J. Chem. Eng. Jap* **4**, 26 - 33

- Taylor, R., Kooijman, H.A., and Hung. J-S. (1994) A second generation nonequilibrium model for computer simulation of multicomponent separation processes, *Comput. Chem. Engng.* **18**, 205-217

- Taylor, R., Kooijman, H.A., and Woodman, M.R., (1992) Industrial applications of a nonequilibrium model of distillation and absorption operations, *IChemE Symp. Ser.* **128** A415 - A428

- Taylor, R. and Krishna, R. (1993) Multicomponent Mass Transfer, Wiley, New York.

- Taylor, R., Powers, M.F., Lao, M. and Arehole, A., (1987), The development of a nonequilibrium model for computer simulation of multicomponent distillation and absorption operations, *IChemE. Symp. Ser.* **104**, B321 - B342

- Thiel, C., Sundmacher, K., and Hoffmann, U., (1997), Residue curve maps for heterogeneously catalysed reactive distillation of fuel ethers MTBE and TAME, *Chem. Eng. Sci.* **52**, 993 - 1005

- Venkataraman, S., Chan, W.K., and Boston, J.F., (1990), Reactive distillation using AspenPlus, *Chem. Eng. Prog.*, **8**, 45 - 54

- Wayburn T.L., and Seader, J.D., (1987), Homotopy continuation methds for computer aided process design, *Comput. Chem. Eng* **11** 7 - 25

- Wesselingh, J.A., (1997), Nonequilibrium modeling of distillation, *IChemE Symp. Series* **142**, 1 - 21

- Westerterp, K.R., (1992), Multifunctional Reactors, *Chem. Eng. Sci.* **9**, 2195 - 2206

- Wijn, E.F. (1996) The effect of layout pattern on tray efficiency, *Chem Eng Journ*, **63**, 167 - 180

- Xu, X., Zhao, Z., and Tian, S., (1999) Study on catalytic distillation processes,

Part IV: axial dispersion of liquid in catalyst bed of catalytic distillation column, *Trans. IChemE*, **77**, 16 - 20

- Zheng, Y. and Xu, X., (1992a) Study on catalytic distillation processes, Part I: Mass transfer characteristics in catalyst bed within the column, *Trans. IChemE*, **70**, 459 - 464

- Zheng, Y. and Xu, X., (1992b) Study on catalytic distillation processes, Part II: Simulation of catalytic distillation processes, Quasi homogeneous and rate based model, *Trans. IChemE*, **70**, 465 - 470

- Zuiderweg, F.J., Kunesh, J.G., and King, D.W., (1993) A model for the calculation of the effect of maldistribution on the efficiency of a packed column, *Trans. IChemE* **71, part A**, 38 - 44